energies

MDPI

Review

Reactor and Plant Designs for the Solar Photosynthesis of Fuels

Simge Naz Degerli [1], Alice Gramegna [1], Matteo Tommasi [2], Gianguido Ramis [3] and Ilenia Rossetti [1,2,*]

[1] Consorzio Interuniversitario per la Scienza e Tecnologia dei Materiali, INSTM Unit Milano-Università, Dipartimento di Chimica, Università degli Studi di Milano, Via C. Golgi 19, 20133 Milan, Italy
[2] Chemical Plants and Industrial Chemistry Group, Dipartimento di Chimica, Università degli Studi di Milano and CNR-SCITEC, 20133 Milan, Italy
[3] Dipartimento di Ingegneria Chimica, Civile ed Ambientale, Università degli Studi di Genova and INSTM Unit Genova, Via all'Opera Pia 15A, 16145 Genoa, Italy
* Correspondence: ilenia.rossetti@unimi.it

Abstract: Solar-boosted photo-technology stands out as a powerful strategy for photosynthesis and photocatalytic processes due to its minimal energy requirements, cost-effectiveness and operation under milder, environmentally friendly conditions compared to conventional thermocatalytic options. The design and development of photocatalysts have received a great deal of attention, whereas photoreactor development must be studied deeper to enable the design of efficient devices for practical exploitation. Furthermore, scale-up issues are important for this application, since light distribution through the photoreactor is a concurrent factor. This review represents a comprehensive study on the development of photoreactors to be used mainly for the photoreduction of CO_2 to fuels, but with concepts easily transferable to other photosynthetic applications such as ammonia synthesis and water splitting, or wastewater treatment, photovoltaics combined to photoreactors, etc. The primary categories of photoreactors are thoroughly examined. It is also explained which parameters influence the design of a photoreactor and next-generation high-pressure photoreactors are also discussed. Last but not least, current technologies for solar concentrators are recalled, considering their possible integration within the photoreactor. While many reviews deal with photocatalytic materials, in the authors' view, photoreactors with significant scale and their merged devices with solar concentrators are still unexploited solutions. These are the key to boost the efficiency of these processes towards commercial viability; thus, the aim of this review is to summarise the main findings on solar photoreactors for the photoreduction of CO_2 and for related applications.

Keywords: photoreactors; solar photoreactors; concentrating solar systems; solar beam-down photoreactors; reactor design; CO_2 photoreduction; solar fuel production; advanced oxidation processes (AOPs); high-pressure photoreactors

Citation: Degerli, S.N.; Gramegna, A.; Tommasi, M.; Ramis, G.; Rossetti, I. Reactor and Plant Designs for the Solar Photosynthesis of Fuels. *Energies* **2024**, *17*, 3112. https://doi.org/10.3390/en17133112

Academic Editors: Francesco Calise and Raffaele Marotta

Received: 20 April 2024
Revised: 1 June 2024
Accepted: 17 June 2024
Published: 24 June 2024

1. Introduction

Energy is needed for meeting basic demands and maintaining comfortable and enhanced living standards. Energy consumption has accelerated because of the growing world population and people welfare and unregulated industrial growth [1]. This leads to increased fossil fuel usage, which exacerbates the energy crisis and increases CO_2 emissions. In particular, CO_2, as a leading greenhouse gas, significantly contributes to global warming, causing a critical environmental issue [1,2]. Since approximately 30 Gt of CO_2 per year is emitted, primarily from fossil fuels, CO_2 contributes more than 60% to global warming. Conferences such as COP21 and COP26 establish targets for reducing greenhouse gases [3]. Different strategies have been used to minimise the effects of CO_2 emission at the source, such as CO_2 capture, storage and utilisation (CCU) of CO_2 by the production of value-added chemicals [4]. Of all the options, utilising CO_2 to produce renewable fuels is the most attractive pathway; by this way, the dependency on traditional fossil fuels would be decreased. The reutilisation of CO_2 to produce fuels could be achieved through

chemical conversion, electrochemical reduction, biological conversion and reforming processes [4,5]. Figure 1 presents a schematic drawing of solar energy utilisation for fuel production through various chemical processes, delineated into two primary sections: solar thermal and photovoltaic cells.

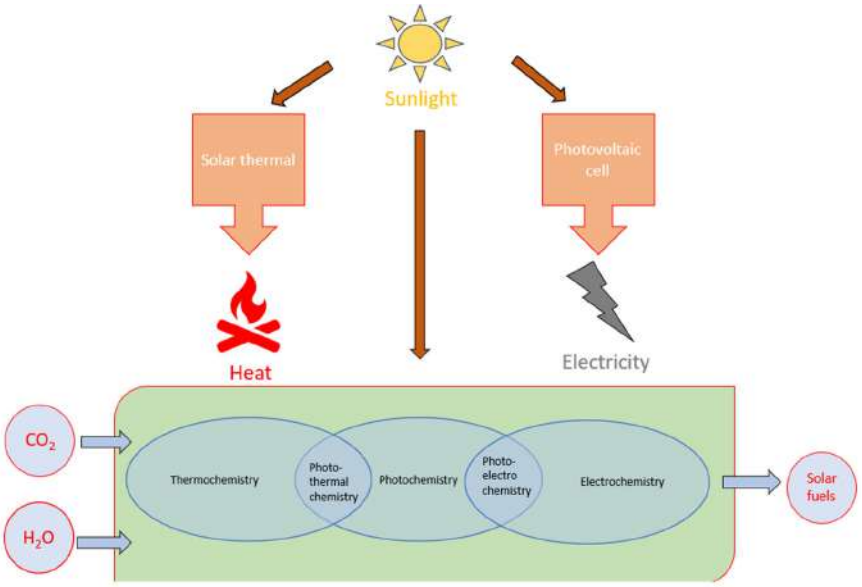

Figure 1. Various methodologies employed in converting solar energy to produce fuels by reduction of CO_2. Readapted from [6,7].

The solar thermal conversion of sunlight into heat can be employed in thermochemical processes to drive reactions that transform carbon dioxide (CO_2) into solar fuels. On the contrary, photovoltaic cells allow the conversion of sunlight into electricity, which can be used to power various electrochemical processes. A third way is photochemistry, which allows us to directly drive chemical reactions through light utilisation. Collectively, these processes contribute to the conversion of CO_2 into solar fuels, exemplifying an integrated approach to harnessing solar energy for sustainable fuel production. Still, these technologies have some drawbacks, including the requirement for high temperatures or electrical voltages to convert stable CO_2 molecules, limited material activity, high operational costs and challenging scale-up.

Photocatalysis using light irradiation gained attention due to low temperature and pressure and small energy input, possibly coming from free solar light [8]. The CO_2 photoconversion would meet the energy demands and overcome environmental issues [9]. However, in the CO_2 photoreduction, the efficiency and selectivity are low and must be improved. There are mainly two parallel strategies to enhance these: (1) development of novel photocatalysts and (2) enhanced design of photoreactors [10]. Much research has been conducted to improve the photocatalyst by designing highly selective and efficient materials for CO_2 photoreduction applications [11]. Various strategies have been applied such as improved visible light harvesting, promoted charge transport and sequestration, the improved adsorption and activation of reduction kinetics and the suppression of parasitic reactions [11–14]. These strategies encompass the methods reported below:

- Use of co-catalyst: It is used to improve the electron–hole separation and to introduce possible visible light absorption through a plasmonic effect [15].
- Use of nanocarbon loading: Nanocarbon materials, such as carbon nanotubes, graphene or carbon dots, can serve as co-catalysts or electron acceptors on the surface of the photocatalyst. This can enhance the photocatalytic activity by promoting efficient charge separation and transfer, leading to improved conversion rates of CO_2 into value-added products. They can also contribute to the photostability of the photocata-

lyst by mitigating photo corrosion or degradation phenomena, thereby extending the lifetime of the catalyst and improving its recyclability in CO_2 photoreduction [16].

- Use of heterojunction construction: An efficient semiconductor should have a wide visible light response, long-term stability, efficient separation of electrons and holes and strong redox capacity in a photocatalytic reaction. Since it is challenging to have all the properties from a single material, a heterojunction uses two different semiconductors, which can be excited at a relatively short wavelength and improve charge separation by an appropriate migration of electrons and holes in the coupled materials [17].
- Use of surface sensitisation: Dyes can be used to absorb light with a broader range of wavelengths compared to the photocatalyst alone. By sensitising the photocatalyst with a dye, the overall light absorption efficiency of the system can be improved, thereby increasing the number of photons available for driving the CO_2 photoreduction [18].
- Use of pore texture tailoring: It influences light scattering and absorption within the photocatalyst. By controlling the pore structure, it is possible to optimise light penetration and distribution throughout the catalyst, maximising photon absorption and utilisation. Also, pore structure modifications can influence the migration and transport of the photogenerated charge carriers within the photocatalyst. Well-designed pore structures can minimise electron–hole recombination and improve the efficiency of CO_2 conversion. Additionally, tailoring the pore texture can influence the accessibility of different sites and pathways on the photocatalyst surface and this can lead to selective CO_2 reduction, favouring the formation of specific target products such as carbon monoxide (CO) or methane (CH_4) over undesired by-products [19].
- Use of dimensionality: It refers to manipulating the structural dimensions of the photocatalyst material, such as its thickness or morphology. The conversion of CO_2 can be improved by changing these properties [20].
- Use of defect control: Defects on the photocatalyst surface can alter its chemical reactivity and interaction with CO_2 molecules. By controlling defect types, it is possible to tailor the surface chemistry [20].
- Use of band-gap engineering: By engineering the band gap of the photocatalyst, it is possible to tailor its light absorption properties to better match the solar spectrum. This allows for a more efficient utilisation of sunlight, maximising photon absorption and providing the energy required for driving the CO_2 photoreduction [21,22].

Although there has been significant progress in ways to increase the efficiency of semiconductor materials, reactor engineering is compulsory to increase the efficiency of photocatalytic systems, at least to allow scale-up. Moreover, for the specific goal of producing solar fuels from CO_2 photoreduction, materials' efficiency is not yet optimised. The photoreactor can be designed by using this approach, including the tuning temperature and reactor pressure, mode of operation, light intensity and configuration, so that products' yield, selectivity and overall efficiency could be enhanced [14].

Generally, photoreactors are vessels in which products are generated through the interaction of the photocatalyst, reactants and photons. This is one of the key points, since the third actor, light, is usually efficiently spread over the catalyst in small-laboratory-scale setups; while providing a real-scale design, its distribution inside the reactor is not at all trivial and should be carefully designed [14].

In CO_2 photoreduction, three main factors determine the type of reaction system: (1) the type of interphase involved (gas–solid, gas–liquid–solid, etc.); (2) operation such as batch, semi-batch or continuous; and (3) type of catalyst bed such as fixed, layers/membrane or fluidised/slurry.

The most widely used arrangement on a lab scale is the slurry photoreactor that uses a three-phase system and agitates the suspended catalyst to promote mass transfer between the catalyst and reacting phases to supply a high surface area to be irradiated. Photocatalysts in fixed-bed photoreactors are immobilised on selected supports such as

plates, beads, fibres, optical fibres, a monolith or other substrates and positioned in the photoreactor close to the irradiation source or directly on the wall of the photoreactor. Even though fixed-bed photoreactors produce high gas output and do not need separation of a catalyst, proper light distribution is an important issue [10].

CO_2 photoreduction, progressively more and more studied in the latest years, is one of the most challenging photocatalytic reactions, which will be considered here as the main-case history, but the same criticalities are common to other very interesting photosynthetic applications (reactions with $\Delta G > 0$), such as H_2 and NH_3 photoproduction and also to photocatalytic down-hill reactions ($\Delta G < 0$).

In membrane photoreactors, two compartments are divided by a membrane, keeping them separate from each other. Although the reaction in membrane photoreactors is well regulated and is not allowed for a backward reaction, the limited charge and mass transfer can be a concern. When employed with direct sunlight, these photoreactors use a reflecting surface to gather and concentrate light into the reactor, thus earning the designation of solar photoreactors [23].

In addition, the annual operating costs of photocatalytic processes are often dominated by the production of photons when artificial light is employed. This is the driver toward the use of photoreactors with natural light harvesting for practical use and large-scale applications. Solar energy can be used in a photoreactor, but specific design is needed to harvest the radiation and solar-sensitive materials, and appropriateness for each designed reaction must be available. For instance, titanium dioxide has been extensively used in CO_2 photoreduction as a photocatalyst. However, a TiO_2 photocatalyst captures radiation with a wavelength below 380 nm and this accounts for ca. 4–5% of total solar energy, making its efficient exploitation challenging under solar irradiation [7].

This review covers a comprehensive study on photoreactors and solar concentrators, predominantly applied to CO_2 photoreduction. It explores the fundamental principles of solar photoreactors and investigates how various parameters can be adjusted to enhance photoactivity and productivity. It also examines different types of reactors used for the solar photoreduction of CO_2, comparing aspects such as catalyst type, irradiation time, irradiated area, light intensity and product yield.

2. Fundamentals of Heterogeneous Photocatalysis and Mechanism

In recent years, research on photocatalysis has intensively increased, especially concerning energy conversion and environment-related applications. Since the discovery of photocatalytic properties of TiO_2 around 1920 [24], many efforts have been dedicated to understand the mechanism, variables and fundamental parameters that have an impact on this process.

Heterogeneous photocatalysis accelerates a photoreaction with the use of a semiconductor, generally in the solid phase, forming a multi-phase system with the reactants (liquid or gas) [25,26]. Heterogeneous photocatalysis begins with the excitation of a semiconductor by a radiant source with energy equal or higher than the bandgap energy ($h\nu \geq EBG$), as shown in Figure 2. The energy gradient between the valence band of the semiconductor (VB) and the conduction band (CB) is indeed defined as the bandgap energy (EBG) [27].

As anticipated, photocatalytic technology may pertain to two main categories. Firstly, the so-called down-hill processes mainly include purification processes such as water and wastewater treatment [28] and air purification [29]. In this case, the photocatalyst acts in kinetic terms, speeding up the oxidation of a compound or driving the selectivity. Possibly, hybrid technology may arise, combining it with other oxidative technologies: this is appealing for boosting the efficiency of a photocatalytic system. Additionally, catalysts can play a role in synthetic pathways by supplying the ΔG of a reaction such as in hydrogen generation through water splitting, CO_2 photoreduction to solar fuels, ammonia photosynthesis or organic synthesis.

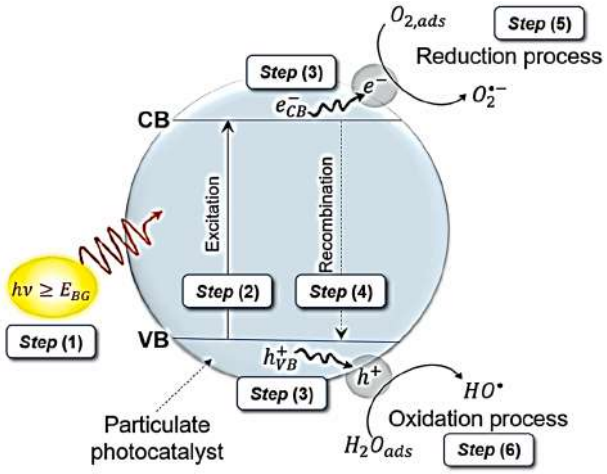

Figure 2. Fundamental mechanism of heterogeneous photocatalytic process. Reproduced by kind permission of Elsevier BV from [27].

So, for instance, during photocatalytic oxidation processes, the photons are absorbed by the photocatalyst in step 1 (Figure 2), and results in step 2 where the electrons are excited from VB to CB. This produces positive holes (h^+) inside the VB, creating an electron–hole couple (e^-/h^+), which can promote the oxidation and reduction of the compounds adsorbed over the surface (step 3). Alternatively, they can recombine restoring the semiconductor in its fundamental state (step 4). For instance, excited electrons in the conduction band facilitate the reduction reaction of oxygen molecules adsorbed on the catalyst, forming the superoxide anion ($O_2{}^{-\bullet}$) (step 5). Photogenerated holes can promote the oxidation of water or of oxydril molecules that have been adsorbed on the surface of the catalyst, which will lead to the production of hydroxyl radicals ($HO^\bullet$) (step 6).

These free radicals are strong oxidisers that can react with organic and inorganic molecules [25,30,31], promoting their photocatalytic degradation.

On the other hand, during photosynthetic reactions, the photogenerated electrons are used by reducible substrates, such as H^+, CO_2 or N_2, to produce reduced species. The holes may either react with water to produce oxygen or with substrates easier to oxidise that may be generically defined as hole scavengers (HSs). Following the former approach (down-hill processes), the formed oxygen-based radical species are strongly oxidising and are directly responsible for the oxidation of the pollutants. Therefore, the requirements on band potentials are quite fixed and predictable. On the contrary, proper band engineering is needed in the second photosynthetic case due to the required matching of band potentials with the redox potentials of the redox couples specifically planned in the reaction. Photosynthetic "up-hill" applications are by far the most challenging and they will be prioritised in the following discussion.

The hole scavengers have a crucial importance to consume the holes present on the valence band of the semiconductor, avoiding the e^-/h^+ recombination. Its presence facilitates the consumption of the holes in the valence band and so that the electron can remain in the excited state. In principle, the consumption of water and the production of oxygen should occur. However, in practice, this reaction proceeds at an exceedingly slow rate, hence the use of a hole scavenger is necessary during photosynthetic reactions. Choosing an appropriate amount of the hole scavenger is fundamental. An excessive quantity poses the risk of overconsumption, while an insufficient amount might cause the beginning of photoreforming earlier than expected. This occurrence initiates when all of the hole scavenger has been consumed.

Various types of hole scavengers can be used for the photoreduction of carbon dioxide such as methanol, ethanol, 2-propanol, triethylamine and sodium sulphite. Sodium sulphite can be chosen as a better hole scavenger than others thanks to the photoactivation of sulphite and the production of highly reactive radicals.

Various photocatalysts were used for the photoreduction of carbon dioxide such as titanium dioxide (TiO_2); tungsten oxide (WO_3); zinc oxide (ZnO); cadmium sulphide (CdS); graphitic carbon nitride (g-C_3N_4); bismuth photocatalysts such as Bi_2O_3, Bi_2S_3 and $BiVO_4$; or Fe_2O_3.

Additionally, metal–organic frameworks (MOFs) are a group of porous crystalline substances characterised by precise structures and adjustable pore sizes, created through the self-assembly of organic ligands and metal ion centres. Notably, altering these frameworks with organic ligands, metal ions and active components can adjust their composition and properties. This versatility has made MOFs extensively utilised as photocatalysts for CO_2 reduction. A MOF from non-porphyrinic photoactive azo-ligands that can integrate functions such as intensive light absorption, CO_2 adsorption and charge separation and transfer was prepared by a hydrothermal method. It showed significant catalytic activity for visible light-driven CO_2 photoreduction in the presence of water vapor. The CH_4 product yield reached 16.32 μmol g^{-1} with 77.57% selectivity [32]. Dye sensitisation has also been carried out in MOFs. The CO evolution rate reached 10.27 μmol g^{-1} in 4 h with a selectivity of over 99% without the need for any organic sacrificial agents or photosensitisers [33]. Heterojunctions between CuO and a Co-based MOF were also explored. The presence of p-n heterojunctions and Schottky barriers in the composite materials inhibited electron–hole pair recombination and enhanced charge migration. The CO production rate was 3.83 μmol g^{-1} h^{-1}, ca. 9.6 times higher than that of pure Cu_2O [34].

These are only examples, since the scope of this review is not a comprehensive discussion of the materials, but a focus on photoreactors. Many different examples of active materials can be found elsewhere for the interested reader [35–37].

In the photoreduction of CO_2, selectivity issues arise due to the generation of different competitive products. The common products of CO_2 photoreduction include carbon monoxide (CO) and methane (CH_4), typically obtained under gas phase operating conditions and/or in the presence of H_2. Methanol (CH_3OH), formic acid (HCOOH) and ethanol (C_2H_5OH) are instead mainly found as products when operating in the liquid phase. The selectivity of these products depends on various factors, including the choice of photocatalyst, reaction conditions and the presence of co-catalysts. The selectivity can be tuned by changing photocatalyst formulation, e.g., adding a co-catalyst (for instance, Cu^{2+} favours the production of methanol, while Au is often reported to favour selectivity to CH_4); changing temperature, pressure or pH; creating oxygen vacancies; or doping with non-metals. By optimising these factors, it is possible to tune the selectivity to favour the production of specific desired products [38]. An efficient way to compare the performances of the photocatalysts can be achieved by calculating the total stored energy [39,40]. The stored energy can be calculated considering the lower heating value (LHV) of the products by using the formulae below:

$$\text{Moles of product i(mol)} = \text{productivity}\left(\frac{\text{mol}}{\text{kg}_{\text{cat}}\text{h}}\right) * \text{time(h)} * \text{m}_{\text{cat}}\text{(kg)} \quad (1)$$

$$\text{Stored energy i(J)} = \text{Moles of product i(mol)} * \text{LHVi}\left(\frac{\text{J}}{\text{mol}}\right) \quad (2)$$

$$\text{Total stored energy(J)} = \sum(\text{Stored energy i}) \quad (3)$$

The total energy can be calculated for all the products obtained to also calculate the overall efficiency of the process, knowing the irradiance or the consumed power. This allows a safe comparison between different catalysts, operating conditions and reactors.

3. General Classification of Photoreactors

The design of a photoreactor has an essential role in the efficiency of the photocatalytic process. There are four main steps to be followed to improve the conversion of reactants. The photoreactor design is based on an in-depth investigation of the variables that influence its performance, including the light source, the geometrical configuration to distribute light,

the material of construction, heat exchange, mixing and, consequently, the flow patterns. An efficiency of capturing photons affects the performance of a photoreactor and it is first correlated to the intrinsic light harvesting ability of the receiving semiconductor, but also to its efficient exposure to light within the reactor. The latter point should be maximised through appropriate reactor engineering [41–43]. To have an efficient photoreactor, the collection of photons should be high and that depends on the geometry of the photoreactor, where the largest active area must be irradiated [10].

The irradiation source dictates the range of wavelengths and intensities used in the photocatalytic process. The type of light source and its accommodation are also important. The need of light transmission limits the choice of materials of construction for the photoreactor [44]. Various materials can be used to build the photoreactor, such as quartz [45,46], Pyrex glass [47] and stainless steel (for external envelope only) [48,49]. Quartz and fused silica are frequently chosen as light transmission material, because of their perfect transparency, especially in the UV range [50].

To regulate the temperature, it is necessary to remove most of the energy supplied by the source inside the reactor through heat exchange. This factor must be considered during the design process [51]. In addition, mixing and flow patterns must also be optimised in a proper way, first to maximise the interaction between the reactants and catalyst, but in addition this affects the light harvesting ability of the catalyst. Additionally, it is crucial to consider the operational mode (batch or continuous), the type of catalyst bed, the number of phases, the selected membrane (if present) and the type of light source [52].

Based on the phases involved, the photocatalytic reactors can also be classified into two categories: (1) two-phase systems, which consist of gas or liquid reactants and a solid catalyst, and (2) three-phase systems, which include solid–liquid–gas interphases.

Based on the catalyst bed, the following additional classification holds for photoreactors: (1) slurry, where the photocatalyst is suspended in the liquid phase; (2) fixed-bed, in which the fluid reactants flow through photocatalyst beads; (3) catalytic layers, where thin films of a catalyst are deposed over transparent inert layers of support and exposed to light; and (4) membrane-type. All of them might be further classified as shown in Figure 3 depending on the light source.

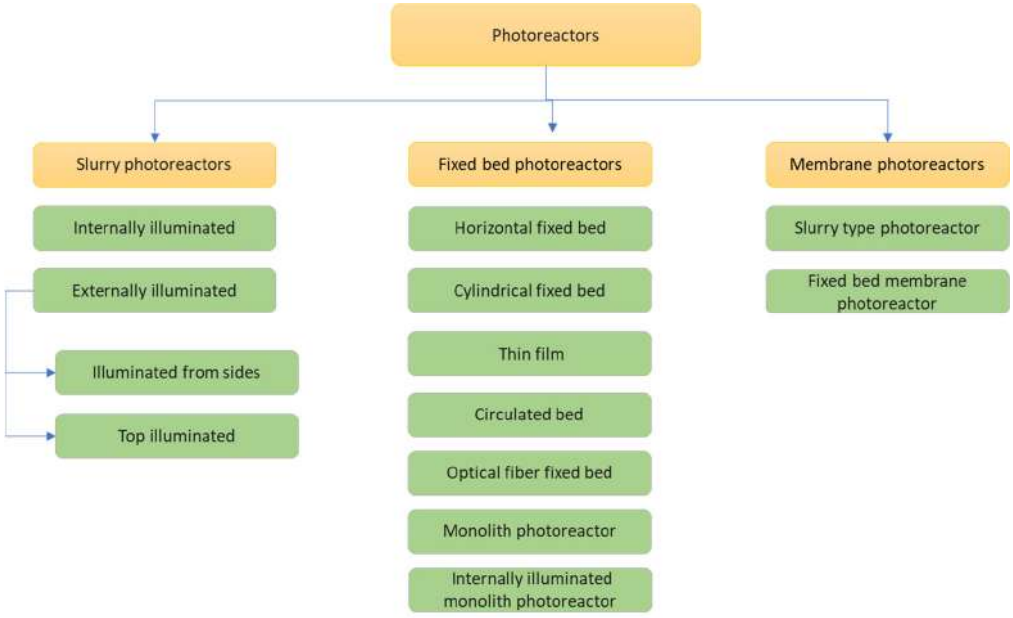

Figure 3. Possible classification of photoreactor design used for CO_2 photoreduction. Readapted from [10].

Based on light locations, the slurry photoreactors have been further divided into externally and internally illuminated photoreactors. On the other hand, fixed-bed photoreactors

have plenty of possible designs. When natural sunlight irradiates any of the previously mentioned photoreactors, they are referred to as solar photoreactors. These reactors are further classified as in Figure 4 based on the type of solar source and the possible presence of a solar concentrator [10].

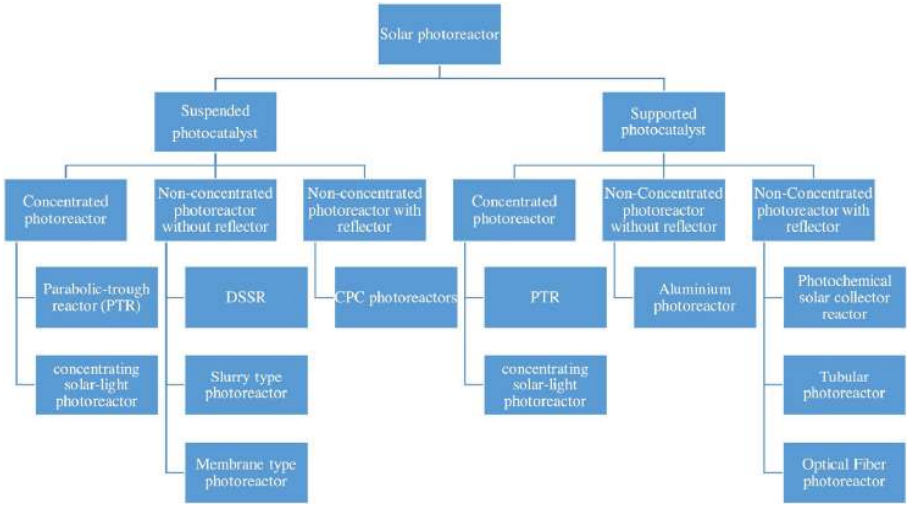

Figure 4. Classification of solar concentrator based on photocatalyst support bed (in this scheme, acronyms stand for the following as indicated: PTR—Parabolic trough reactor; DSSR—Double-skin sheet reactor; CPC—Compound parabolic concentrator) [7].

Details on different arrangements are reported in the next paragraphs.

To have a better understanding of the features of different kinds of photoreactors, a comparative review has been published on different gas–solid photoreactors for the photoreduction of CO_2 and it is partially summarised in Table 1 [53]. In particular, the comparison considers different types of photoreactors and active materials and specifies whenever possible the operating conditions and the main results. The reader is referred to the original review paper for the specific references and detains therein [53], while a short description of its content is reported in the next lines. Finally, a more detailed description of each typology of photoreactor is reported in the next paragraphs.

For instance, In-doped nanoparticles were prepared with a sol–gel method. CO was observed as the main product over TiO_2, while In-TiO_2 increased the methane yield. The CH_4 production rate over 10 wt.% In-doped TiO_2 was 7.9-fold higher than the bare TiO_2 at 100 °C and the CO_2/H_2O ratio of 1.43. A technique based on the adsorption of ions onto the surface of two-dimensional (2D) nanosheets has been devised for the photocatalytic reduction of CO_2. Isolated Bi ions, confined within the surface of TiO_2 nanosheets with the aid of simple ion adsorption, enables the formation of a built-in electric field that enhances the separation of charge carriers. Consequently, this contributed to an improved performance of the photocatalytic CO_2 reduction with favoured selectivity to CH_4 [54].

A method utilising the adsorption of ions on the surface of two-dimensional (2D) nanosheets has been developed for the photocatalytic CO_2 reduction. Isolated Bi ions, confined on the surface of TiO_2 nanosheets through a straightforward ionic adsorption technique, aided in creating a built-in electric field that efficiently enhanced charge carrier separation. This resulted in improved performance of the photocatalytic CO_2 reduction process, favouring the conversion to CH_4. It was observed that the TiO_2-Bi provided 6.38 μmol g^{-1} CO and 153.08 μmol g^{-1} CH_4, while the blank TiO_2 provided 3.74 μmol g^{-1} CO and 34.86 μmol g^{-1} CH_4 in 14 h. It is worth mentioning that TiO_2-Bi exhibited a 1.7-fold increase in CO conversion performance. However, it demonstrated even more significant enhancement in CH_4 conversion, achieving a 4.4-fold increase compared to the blank TiO_2 [55].

Table 1. Comparative examples of CO_2 reduction performance of gas–solid phase photoreactors reported in the literature. Readapted from [53].

Photoreactor	Photocatalyst	Reference	Light Source	Condition	Main Products
Tiles or "carpet type"	In-TiO_2	[54]	500 W Hg lamp	0.25 g, 0.20 bars reactor pressure, 373 K reaction temperature and CO_2/H_2O feed ratio of 1.43	CH_4 243.75 μmol g^{-1} h^{-1}, CO 81.25 μmol g^{-1} h^{-1}
	TiO_2-Bi	[55]	300 W Xe lamp	100 mg, photocatalyst powder was put in a glass reactor filled with CO_2, followed by an injection of 2 mL H_2O in the reactor for 14 h	CH_4 153.08 μmol g^{-1} h^{-1}, CO 6.38 μmol g^{-1} h^{-1}
	ZnO	[56]	125 W Hg lamp	50 mg, 0.5 mL deionised water at 473 K	CO 406.77 μmol g^{-1} h^{-1}, CH_4 20.16 μmol g^{-1} h^{-1}
	Pt-TiO_2	[57]	8 W Hg lamp	Photocatalyst was suspended in 10 mL of distilled water and this suspension was applied to the foam	CH_4 22.04 μmol g^{-1} h^{-1}
Thin film	HN-TiO	[58]	300 W Xe lamp with a 400 nm cut-on filter attached in front of AM 1.5 G filter	CO_2 and water vapor at 343 K	CO 12.67 μmol g^{-1}, CH_3OH 1.79 μmol g^{-1}
	rGO-TiO_2 NP	[59]	100 W Xenon solar simulator	A 2.0 × 2.0 cm^2 film, a mixture of CO_2 and H_2O vapor	CH_4 5.67 ppm cm^{-2} h^{-1}
	NiMgGaAl	[60]	300 W Xenon lamp with fitted IR blocking filter	Drop-casted (15 mL of 25 mg mL^{-1} aqueous solution) thin film on 1 cm by 1 cm glass	CO ca. 55 μmol g^{-1}
	CdS/Mn_2O_3 nanocomposites	[61]	Sunlight	25 cm^2 photocatalyst film	C_2H_5OH 52.2 μmol g^{-1} h^{-1}, HCOOH 1392.3 μmol g^{-1} h^{-1}
	Vs-$CuIn_5S_8$	[62]	Simulated visible light	CO_2 and H_2O vapor at 101.1 kPa	CH_4 8.7 μmol g^{-1} h^{-1}
Optical fibre	Cu-Fe/TiO_2	[63]	150 W Hg lamp	The space velocity of CO_2 gas and H_2O vapor was maintained at 0.72 h^{-1}	CH_4 0.91 μmol g^{-1} h^{-1}, C_2H_4 0.58 μmol g^{-1} h^{-1}
	Cu-Fe/TiO_2-SiO_2-acac	[64]	150 W Hg lamp	The space velocity of CO_2 gas and H_2O vapor was maintained at 0.72 h^{-1}	CH_4 0.279 μmol g^{-1} h^{-1}
	Cu-TiO_2	[65]	365 W Hg lamp	The flow rate of CO_2 was almost 3 mL min^{-1} and the pressure of CO_2 was in the range of 1.05–1.4 bar	CH_3OH 0.46 μmol g^{-1} h^{-1}
Monolithic	Fe-MMT/TiO_2	[66]	200 W Hg lamp	Fed flow rate was 20 mL min^{-1} at 100 °C	CO 166 μmol g^{-1} h^{-1}
	(MMT)/TiO_2	[67]	200 W Hg lamp	The nanocatalysts (about 50 mg) were coated uniformly as a thin film inside the microchannels of the monolith	CH_4 139 μmol g^{-1} h^{-1}, C_2H_4 52 μmol g^{-1} h^{-1}
	NiO/$InTaO_4$	[68]	Xenon lamps	CO_2 and water vapor flows into the monolith inlet	CH_3OH 1.85 10^{-4} mol m^{-3}
Plate microreactors	Cu^{2+}-TiO_2	[69]	UV LED 365 nm	H_2O and CO_2 with a ratio of 1:10 at 333 K	CH_3OH 36.18 μmol g^{-1} h^{-1}, C_2H_5OH 79.13 μmol g^{-1} h^{-1}
	CdS-Cu^{2+}/TiO_2	[70]	300 W Xe lamp	H_2O and CO_2 with a ratio of 1:10 at 333 K	C_2H_5OH 109.12 μmol g^{-1} h^{-1}
	Cu_1P25	[71]	1 W UV LED	40 mg, water vapor was incorporated in the pure CO_2 stream using a water bubbler to saturate the stream	CH_4 117 μmol g^{-1} h^{-1}

The efficiency in separating electron–hole pairs and the adsorption capacity of photocatalysts towards CO_2 represent the pivotal factors influencing the performance of photocatalytic CO_2 reduction. In order to improve these points, the surface structure of the semiconductor was tuned. Three ZnO samples with different morphologies, surface area and defect content were fabricated by varying the preparation methods. The results demonstrated that the prepared porous ZnO nanoparticles and nanorods were characterised by more defect sites, and these are zinc and oxygen vacancies. These defects would decrease the combination rate of the electron–hole pair together with the promotion of the formation of basic zinc carbonate by Lewis acid–base interaction, which is the active intermediate species for the photoreduction of CO_2. ZnO nanoparticles and ZnO nanorods with few defects exhibited limited CO_2 adsorption, resulting in inferior photocatalytic performance [56].

Pt/TiO_2 (0.5–3.0 wt.%) samples were prepared by deposition–precipitation then deposited on a commercial Al_2O_3 foam. It was observed that the main reaction product was

methane, but hydrogen and carbon monoxide were also detected. The highest yields of CH_4, H_2 and CO were achieved in the presence of 1.5 wt.% Pt/TiO_2. It was seen that higher yields of CO_2 photocatalytic reduction were achieved in the presence of photocatalysts deposited on the commercial support compared to the powder photocatalysts [57].

A core–shell metal oxide with their shell having nitrogen and hydrogen coordinated to a metal atom provides energy states for visible light absorption and efficient electron–hole separation. Nanocrystals for a visible light sensitising core–shell metal oxide of titanium oxide (HN-TiO_2) were fabricated and its energy states were determined by integrating experimental measurements with density functional theory (DFT) calculations. Additionally, photoelectrochemical measurements were performed to observe the photocatalytic activity of the visible light sensitising core–shell metal oxide photocatalyst. The efficiency of solar-to-fuel conversion has also been assessed, demonstrating that the conversion rate to C1 chemical fuels such as methanol and carbon monoxide was significantly improved using a Cu co-catalyst (HN-TiO_2:Cu), which is approximately 25-fold higher than that of the bare TiO_2 loaded with a Pt co-catalyst (bare TiO_2:Pt) and 8-fold higher than that for a Pt co-catalyst (HN-TiO_2:Pt). Also, the method used to fabricate a visible light sensitising core–shell structure of TiO_2 has been applied to fabricate other similar structures, such as HN-ZnO and HN-CuO, which enabled efficient charge separation from other wide-bandgap metal oxides like ZnO and CuO [58].

TiO_2 nanotube arrays were covered with reduced graphene oxide (rGO) plates containing embedded TiO_2 nanoparticles. It was observed that methane yield was enhanced, attributed to the graphene providing enhanced light absorption and effective separation of the photogenerated charges. It was observed that the rGO-TNTNP evolution rate, 5.67 ppm cm^{-2} h^{-1}, was 4.4 times higher than the pure TNT sample, 1.28 ppm cm^{-2} h^{-1} [59].

Metal-based layered structures were promising as photocatalysts. For instance, a quadruple metal-based layered structure, composed of aluminium (Al), gallium (Ga), magnesium (Mg) and nickel (Ni), has been reported, which allows the photocatalytic conversion of CO_2 into CO with a high selectivity close to 100% in the presence of water. The shifted oxidation states of the Ni and Mg ions, compared to their usual bivalent states, resulted in increased electronegativity for the adjacent oxygen (O) atoms, while the Ga and Al ions retained their trivalent states. This adjustment allowed the oxygen atoms to adsorb a higher amount of CO_2. Additionally, the quadruple metal-based layered structure, even without the use of scavengers, demonstrated nearly double the photocatalytic activity compared to bi- or triple-metal-based structures [60].

The photoreduction of CO_2 was accomplished by using CdS and CdS/Mn_2O_3 nanocomposites as a photocatalyst supported on porous anodic alumina (PAA) support. An incomplete anodisation of an aluminium film substrate left a thin layer of aluminium in the middle that enhanced mechanical integrity and retained electrical conductivity of the support. The rod-shaped crystals of CdS, grown on the support's pore surface, formed a crumpled sheet-like structure that enhanced the trapping of light energy incident on the catalyst surface. The photocatalytic reduction of CO_2 was carried out under direct sunlight, using reflectors such as flat mirrors, compound parabolas and concentrating Fresnel lenses to focus the solar radiation onto the catalytic surface. The combination of a Fresnel lens as a concentrator and a CdS/Mn_2O_3 nanocomposite as the catalyst significantly improved the photocatalytic activity compared to CdS alone. The CO_2 conversion efficiency (CCE) (%) determines the ability of the photocatalyst in converting CO_2 to useful organic compounds and the CCE (%) obtained using CdS/Mn_2O_3 nanocomposites as a photocatalyst was exceptionally high with Fresnel lens giving 23.2% of CO_2 conversion [61].

Atomically thin layers of sulphur-deficient $CuIn_5S_8$ that contained charge-enriched Cu-In dual sites were highly selective towards the photocatalytic production of CH_4 from CO_2. The formation of highly stable Cu-C-O-In dual sites was the key feature determining selectivity. This configuration lowered the overall activation energy barrier and also converted the endoergonic protonation step to an exoergonic reaction process, changing the reaction pathway to form CH_4 instead of CO. Near 100% selectivity was achieved for

visible light-driven CO_2 reduction to CH_4 over CO, with a rate of 8.7 μmol g^{-1} h^{-1} by using $CuIn_5S_8$ [62].

The photocatalytic reduction of CO_2 with H_2O in the gaseous phase was studied by using a Cu-Fe/TiO_2 catalyst coated on optical fibres under UVA and UVC irradiation. Catalyst-coated optical fibres were assembled in the reactor such that the UV light can enter along the fibres to conduct the photocatalytic reaction on its surface. Methane and ethylene were observed as main products. The presence of Fe as a co-dopant in the Cu/TiO_2 catalyst synergistically enhanced the reduction of CO_2 with H_2O to produce ethylene, achieving a quantum yield of 0.024% and a total energy efficiency of 0.016% [63].

A montmorillonite (MMT)-dispersed Fe-doped titanium dioxide (Fe/TiO_2) nanocomposite was tested for dynamic photo-induced CO_2 reduction by H_2 to fuels. Cordierite monolithic support was used in order to enhance the photoactivity and reusability of the Fe-MMT/TiO_2 nanocomposite. MMT-supported Fe/TiO_2 samples were prepared by a direct sol–gel method and were dip-coated over the monolith microchannels. The efficiency of Fe-loaded MMT/TiO_2 for CO_2 photoreduction by H_2 towards CO was investigated using a monolith photoreactor under UV light. The maximum CO yield over the 3 wt.% Fe-10 wt.% MMT-loaded TiO_2 catalyst reached 166 μmol g^{-1} h^{-1} at a selectivity of 99.70%, which was higher than the amount of CO produced over the MMT/TiO_2 (16,166 μmol g^{-1} h^{-1}) and the bare TiO_2 (5 μmol g^{-1} h^{-1}) [66].

An optical fibre reactor was used for the photoreduction of CO_2 with H_2O to fuels under UVA artificial light and concentrated natural light. The optical fibres were coated with gel-derived TiO_2-SiO_2 mixed oxide-based photocatalysts. During the sol–gel process, Fe atoms were incorporated into the TiO_2-SiO_2 lattice, leading to complete visible light absorption and influencing the product selectivity of the resulting catalyst. Under UVA, ethylene was mainly produced on a Cu-Fe/TiO_2 catalyst with the quantum yield of 0.0235% whereas a Cu-Fe/TiO_2-SiO_2 catalyst was observed to favour methane production with the quantum yield of 0.05%. It was found that only methane evolved over both bare TiO_2-SiO_2 and Cu-Fe/TiO_2-SiO_2 catalysts under natural sunlight with production rates of 0.177 and 0.279 μmol g^{-1} h^{-1} [64].

An optical fibre photoreactor, consisting of approximately 120 fibres coated with Cu/TiO_2, was designed and assembled to uniformly distribute light within the reactor. The TiO_2 film was applied to the optical fibres using a dip-coating technique. Cu-loaded titania solutions were prepared through thermal hydrolysis. The obtained Cu/TiO_2 film had a thickness of 53 nm and was composed of very fine spherical particles with diameters around 14 nm. The most active Cu species on the TiO_2 surface were Cu_2O clusters, which played a crucial role in methanol formation. The methanol yield increased with the intensity of UV irradiation. The maximum methanol rate was 0.45 μmol $g_{cat}{}^{-1}$ h^{-1} using a 1.2 wt.% Cu/TiO_2 catalyst at 1.29 bar of CO_2, 0.0026 bar of H_2O and a mean of 5000 s under 16 W cm^{-2} UV irradiation. Higher Cu loading than 1.2 wt.% resulted in a lower methanol yield rate due to the masking effect of Cu_2O clusters on the TiO_2 surface [65].

The performance of a montmorillonite (MMT)/TiO_2-coated monolith photoreactor was tested for the photoreduction of CO_2. The main products were obtained as CH_4 and CO with productivity of 139 and 52 μmol g^{-1} h^{-1}, respectively. The higher rates in the monolith photoreactor were due to the higher illuminated surface area and efficient light utilisation [67].

An optical fibre monolith reactor (OFMR) for $InTaO_4$-based CO_2 photoreduction was used as a photoreactor. OFMR was coupled with a parabolic trough concentrator (PTC) to increase the daylighting area without raising the cost of photocatalysts. Using the Monte Carlo ray tracing (MCRT) approach and the finite volume method (FVM), a computational model of the reaction module was developed to optimise the fibre honeycomb reactor coupled with the PTC, considering the light, heat and mass transfer. As a result, the volume-averaged product concentration reached $1.85 \cdot 10^{-4}$ mol m^{-3}, significantly higher than the traditional OFMR concentration of $9.61 \cdot 10^{-6}$ mol m^{-3} under the same conditions.

Optimised monolith structure for improved photocatalytic performance was identified, showing that gas channel diameters between 1.5 and 2 mm enhance reaction efficiency [68].

Cu^{2+}-TiO_2 nanorod thin-film photocatalysts were applied in optofluidic planar reactors under UV light. These Cu^{2+}-deposited TiO_2 nanorod thin films were fabricated through a combination of the hydrothermal method and an ultrasonic-assisted sequential cation adsorption method. Their photocatalytic activities were assessed through the reduction of gas-phase CO_2, producing primarily methanol and ethanol. The experimental results indicated that with a Cu^{2+} dopant concentration of 0.02 M, the yield of products reached the maximum, with methanol and ethanol yields of 36.18 μmol g^{-1} h^{-1} and 79.13 μmol g^{-1} h^{-1} at a flow rate of 2 mL min^{-1} and a reaction system temperature of 80 °C. The high photocatalytic efficiency of Cu^{2+}-TiO_2 nanorod thin films in CO_2 reduction was attributed to the incorporation of Cu^{2+} ions and the one-dimensional nanostructure, which enhanced photon transmission limitations [69].

CdS-Cu^{2+}/TiO_2 nanorods were used for the photoreduction of CO_2 under visible light. They were prepared by the hydrothermal method, after which Cu^{2+} ions and CdS quantum dots (QDs) were deposited on the TiO_2 nanorod arrays using an ultrasonic-assisted sequential cation adsorption method and successive ionic layer adsorption and reaction (SILAR) method. The experimental results demonstrated that when the SILAR method cycle deposition was repeated twice, the ethanol yield reached the maximum [70].

Various photocatalysts were prepared based on the combination of TiO_2 and Cu_xO. The synthesised systems were applied in the photoreduction of CO_2 to yield CH_4 inside a two-dimensional flow reactor where the gas stream was passed over a thin layer of the catalyst under UV irradiation. The combination of core-level and valence-band-level spectroscopies enabled the authors to have a Z-scheme-structured photocatalyst. A significant formation rate of CH_4 was reached (100 μmol g^{-1} h^{-1}) using low-power led irradiation [71].

3.1. Slurry Photoreactors

The most popular type of reactor in a two- or three-phase system is a slurry photoreactor. For instance, in the case of CO_2 photoreduction, CO_2 is fed in the gaseous phase, and the reductant (in general, H_2O) is often in the liquid phase with or without additional compounds such as sacrificial agents, HSs or pH tuners (e.g., NaOH, Na_2SO_3, etc.). Nonaqueous solvents (e.g., acetonitrile, dimethyl sulfoxide, dimethylformamide, etc.) or ionic liquids are sometimes used in place of water. The photocatalyst is suspended through a stirrer, usually magnetic in small-size devices, or mixed by injecting the gas by bubbling it through the reactor without sedimentation. Slurry photoreactors are also named as fluidised bed photoreactors, usually when gas–solid reactions take place, due to the mobilisation of the catalyst bed [72]. For the selected application, a mixture of steam and CO_2 is fed from the photoreactor bottom to suspend the fine catalyst particles.

Slurry photoreactors are operated in a batch or continuous mode, where the process begins with the injection of CO_2 into the sealed reactor (the first step could be removing air by vacuum or outgassing) and the reaction starts upon exposure to light. Depending on the operating mode, there can also be an accumulation of gaseous or liquid products, even if liquid product collection is often performed in batch mode. In a batch process, CO_2 is bubbled through the photoreactor for a specific duration. The reaction is started by switching on the light irradiation and stopping the CO_2 feed; in contrast, in continuous photoreactors, CO_2 is continuously bubbled into the reactor through the liquid solution, while the gaseous products (such as CH_4, CO or H_2) are taken continuously to be analysed.

The main characteristics in slurry photoreactors can be summarised as below:

1. Liquid-suspended particles enable a high surface-area-to-volume ratio for the exposed photocatalyst.
2. Inorganic salts have been reported to have a remarkable effect on the photoreduction of CO_2. The addition of NaOH increases the solubility of CO_2 with respect to pure H_2O because OH^- ions react with the CO_2 to produce CO_3^{2-} and HCO_3^-. It has

been proposed that a high concentration of HCO_3^- in the system can accelerate the photoreduction reaction, improving its performance [38,72].

3. Liquid-suspended particles remain inside the liquid stream and should be removed after the reaction. This creates substantial cost and complexity for separation and recycling.
4. The progressive consumption of HS might cause the increment of the recombination rate of the electron–hole pairs. In continuous systems, the accumulation of spent HS is an issue.

In slurry photoreactors, the reaction rate depends on several factors: (1) the intensity of the light on the photocatalyst's surface, (2) semiconductor light harvesting properties, (3) the adsorption properties of the reacting and non-reacting components in the solution and (4) the photocatalyst intrinsic (quantum) efficiency [73,74].

Advantages of slurry photoreactors are related to the easy construction that implies low investment cost. Furthermore, if the particles' size of catalyst is small and the mixing is properly conducted, the whole surface illumination of the solid occurs, with increased effectiveness of the catalyst.

Drawbacks include a limited penetration depth due to light absorption or scattering by liquid and solid catalyst particles, causing ineffective usage of part of the surface area of the catalyst. Vigorous agitation is needed to maximise the homogeneity of suspension and improve mass transfer. This leads to the drawback of catalyst particle erosion and attrition. This may further decrease the particle size of the catalyst, changing the optical properties and activity, and again affecting the scattering effect [75].

The particle size has an essential role because it affects the electron–hole recombination, surface area and possibly to a certain extent the band gap, so that optimum size must be chosen to reach the maximum efficiency for photocatalytic conversion. Nevertheless, the particle size should be selected for optimising the use of light irradiation vs. scattering/absorbing effects [10].

To have the best conversion results in a photochemical reaction, light should be absorbed as much as possible by the photocatalyst. Considering this, slurry photoreactors have potential to be the ideal choice for the photocatalysts that have small particles. The other possible option that can be conducted to enhance the light capture and reduce the irradiation losses due to reflection is optimising the lamp position through careful modelling of light dispersion across the reactor volume, as exemplified in [76,77] and references therein.

According to lamp position, they can be further classified into externally illuminated, either from sides or from the top, or internally illuminated.

3.1.1. Externally Side-Illuminated Slurry Photoreactors

In this type of photoreactor, light is utilised inefficiently because, falling along the curved face of the cylinder constituting the reactor envelope, it is partially reflected and this causes the loss of photonic energy. In addition, the irradiation should be conducted from different sides; otherwise, inhomogeneous exposure of the material is achieved. This causes a higher consumption of energy, making the process uneconomical. Based on particle size and mixing efficiency, if no segregation of phases occurs, the whole external surface exposure may be reached, but in any case not simultaneously decreasing the effectiveness of the catalyst on a mass basis. In the worst cases, the penetration depth might be decreased, leading to large inactive surface area. As an example, Ola et al. [78] used a stirred batch annular reactor for CO_2 conversion, depicted in Figure 5. In this design, two irradiation sources were put next to the photoreactor, located on two sides. To measure the light intensity, a UVA digital radiometer was placed inside the reactor. CH_4 productivity of 0.03 μmol g_{cat}^{-1} h^{-1} was achieved. This result was also compared with an internally illuminated monolith reactor by the same group and in this configuration, a productivity of methanol equal to 0.10 μmol g_{cat}^{-1} h^{-1} and of acetaldehyde equal to 0.21 μmol g_{cat}^{-1} h^{-1} was obtained. Still, it is possible to have further improvement by altering the location of the light and expanding the irradiation area, which has been found to be quite limited.

Figure 5B provides a schematic of another photoreactor arrangement where the light source was located on one side. A bed of powdered samples was spread uniformly on the photoreactor surface. CO_2 was flown into the reactor diluted with H_2 or N_2 and saturated with water.

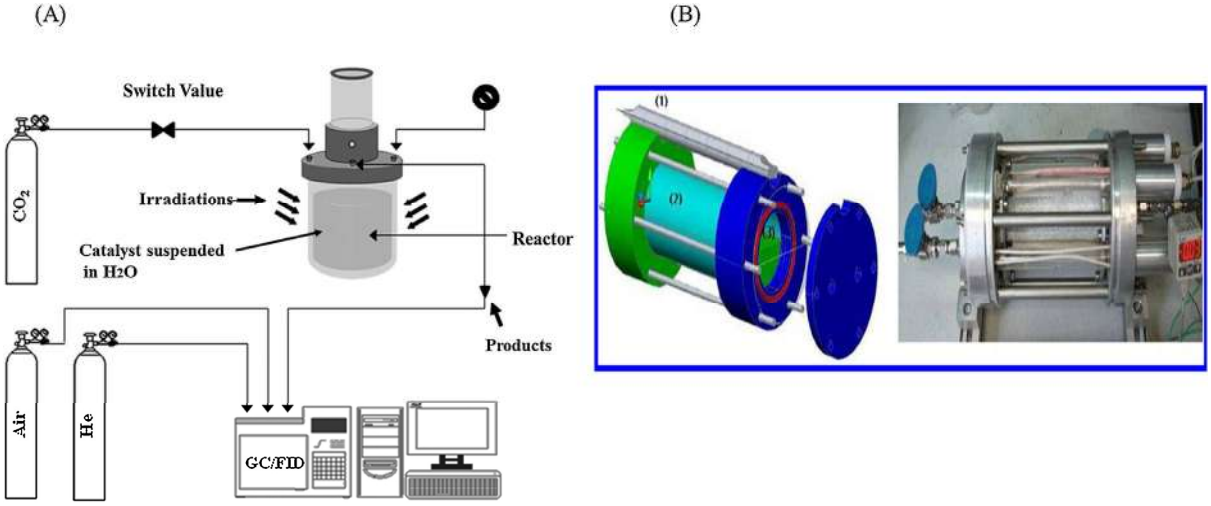

Figure 5. (**A**) Schematics of a slurry photoreactor externally illuminated from side [10,78]. (**B**) **Left**: photoreactor consisting of Hg lamp (1), synthetic quartz windows (2) and gas chamber, (3). **Right**: Top view displaying shallow bed of material situated in photoreactor [10,79]. Reproduced by kind permission of Elsevier BV from [10].

This type of photoreactor is generally preferred in the case of having a photocatalyst with a small particle size, a bright colour and water, which does not have any organic impurities, used as a reducing agent so that maximum penetration depth can be reached. However, the external irradiation limits the energy efficiency of this solution.

Further issues may arise in case refrigeration or heating are needed. Common positioning of a heat exchange device is on the shell of the reactor, at least up to ca. 10 L sizing, since internal heat exchange devices cannot be easily allocated, which would interfere with light distribution from an external light source.

Another study conducted by Tahir et al. [80] worked with a novel externally reflected photoreactor for photocatalytic CO_2 conversion in the liquid phase by the use of the functionalised carbon nitride (f-C_3N_4) modified with ZnV_2O_6 nanosheets and then compared with the solar photoreactor. The maximum production rate of CH_3OH was 4.7 mole kg_{cat}^{-1}, which was 1.25 times higher than the solar photoreactor (3.7 mole kg_{cat}^{-1}). This photoreactor demonstrated exceptional efficiency in converting CO_2 through photocatalysis, attributed to its superior light capture compared to the solar photoreactor. As a reason of that, it was given that the externally reflected photoreactor reached enhanced rates because the reflector provides greater photon flux for dynamic CO_2 reduction.

3.1.2. Top-Illuminated Slurry Photoreactors

In this configuration, irradiation is placed directly from the top of the reactor vessel. Particle size and irradiation energy, again, have an important role for designing the photoreactor [81]. Light hits over the surface of the particles in the slurry and some passes through, the rest being reflected. The advantage of this configuration is that reflection may occur from the bottom of the vessel with a possibly higher utilisation of photons. Nonetheless, it has some cons. One is that the area directly illuminated is limited, and in addition to this, when the solution is dark, then it becomes challenging for the light to pass through the slurry and to reach or be reflected from the bottom. To achieve better performance, the slurry solution must be distant from the optical window to prevent the photocatalyst powder sticking to the surface of the window, obstructing the incoming light. For example, a study reported in [48] used a cylindrical slurry reactor for the photoreduction of CO_2 to

fuel, having CH_4 as the major product, along with methanol and ethanol. The reactor was irradiated from the top using a Xe lamp. Similarly, in other papers [82–85], the photoreduction of CO_2 was accomplished in a stainless steel slurry photoreactor, where irradiation was passed from the top through a quartz window. The main products were CH_4, CO and H_2. In another study [82], platinum- and copper-doped photocatalysts with 0.5–2 wt.% of Pt, 0.5–2 wt.% of Cu and 1 wt.% of Pt combined with 1 wt.% of Cu prepared and tested them for the photocatalytic reduction of CO_2 in a stirred batch reactor. A 2wt.% Cu/TiO_2 photocatalyst demonstrated the highest photocatalytic performance in the production of methane, 35 μmol g^{-1}, which was nine times higher than in the case of the commercial TiO_2 photocatalyst. In addition, its higher specific surface area, S_{BET} 112 m^2g^{-1}, supported its higher performance. The schematic representation is demonstrated in Figure 6 [10,82].

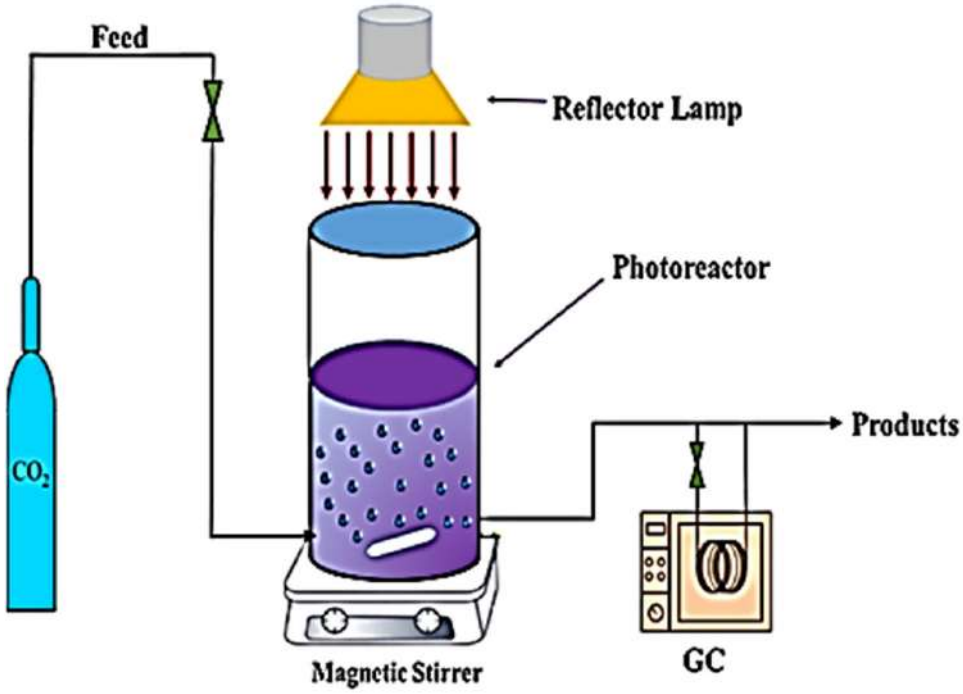

Figure 6. Schematic diagram of photocatalytic CO_2 reduction system irradiated from top. Readapted from [10].

3.1.3. Internally Illuminated Slurry (IIS) Photoreactors

In this type of reactor, the lamp is placed inside the reactor vessel. This type of photoreactor uses the irradiation quite efficiently. First, the direct contact area of light with the reacting solution is larger than externally illuminated reactors. In addition, since the reactor is annular-shaped, the optical path of light radiation is shorter and easier to reflect from the wall. So, among the others, this configuration could be the most attractive one for photocatalytic and photosynthetic applications on a small scale. Possible issues may arise for scale-up. For instance, Tseng et al. [72] carried out the photoreduction of CO_2 for producing methanol with 254 nm UV irradiation. The lamp irradiated inside the reactor, as illustrated in Figure 7. The catalyst powder was suspended in 300 mL of a 0.2 N NaOH aqueous solution. The concentration of the TiO_2 photocatalyst was maintained as lower than 1 g dm^{-3} for avoiding light scattering, which would hinder the light in reaching the surface of the particles.

However, internally illuminated photoreactors also have some disadvantages as follows: (1) The holy grail in photocatalysis is to use free solar light as a source of energy, but in this configuration, it is not easy to exploit it efficiently, since the light source should be conveyed in the axial optical guide. (2) The volume of IIS photoreactors is limited and hard to increase because of the fast decreasing light intensity with an increasing optical

path from the axis to the periphery while there is an increasing reactor volume. (3) There might not be homogeneous photocatalyst distribution because of the presence of the inner tube, which requires efficient and optimised mixing. The latter is quite easy to achieve on a lab scale both for the reduced size and the suitable proportion with the capability of a conventional stirrer. The typical mixer configuration for large-scale reactors is instead axially mixed through vertical stirrers moved by a top motor, which conflicts with the same location of the immersion lamp. (4) There might be some photocatalyst impingement onto the wall of the inner tube if the particle size is very small and this decreases the light passage across the solution [10].

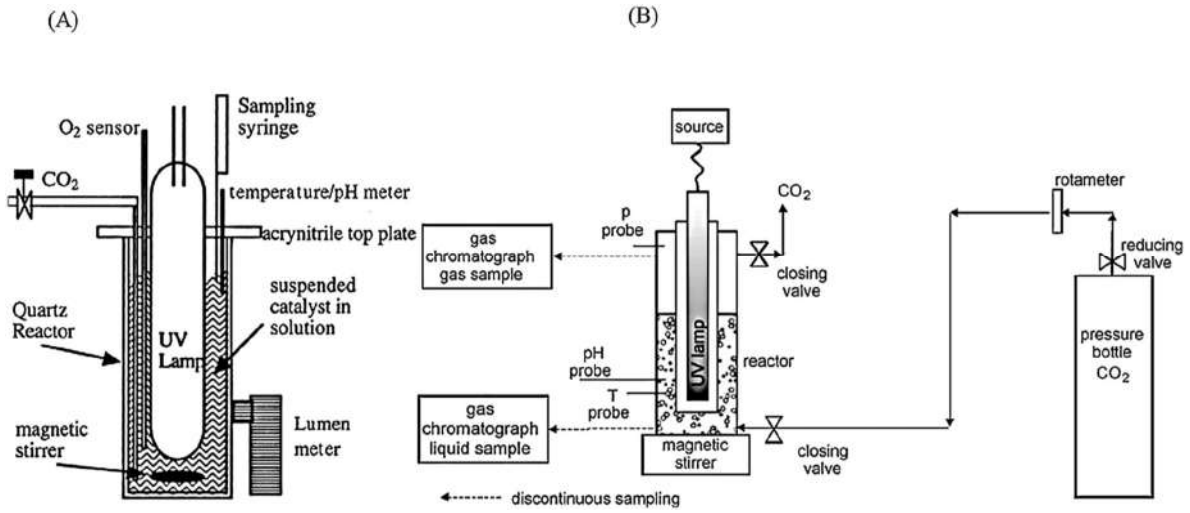

Figure 7. (**A**) Schematics of annular photocatalytic photoreactor irradiation source positioned internally (reproduced by kind permission of Elsevier BV from [72]). (**B**) Block scheme of internally illuminated annular photoreactor for CO_2 photocatalytic reduction (reproduced by kind permission of Elsevier BV from [10,76]).

Another study conducted by Asadi et al. [86] also employed the bubble slurry photoreactor but the focus was on the modelling and simulation of photocatalytic CO_2 reduction into methanol. A 2D axisymmetric geometry was utilised considering different parameters such as the number of spargers, inlet gas flux, average bubble diameter and light intensity.

In addition, Olivo et al. [87] investigated the effect of CO_2 photoreduction parameters, irradiance and reaction time to produce methane in a cylindrical Pyrex glass reactor. It was achieved through a design of experiments (DOE), which evaluated how experimental conditions varied across different setups. The usage of a low light intensity (40–60 W m^{-2}), reaction time and temperature showed a significant effect on methane productivity, with a maximum value of 28.50 µmol $g_{cat}{}^{-1}$ (40 W m^{-2}, 4 h). Meanwhile, with the use of high irradiance (60–2400 W m^{-2}), the maximum production of methane was 0.19 µmol $g_{cat}{}^{-1}$ (1240 W m^{-2}, 2 h). It was found that irradiance was the main parameter with a significant effect on the production of methane. The impact of varying input was evaluated using a DOE approach, which considered experimental parameters influencing photon input, irradiance and reaction time. The relationship between product formation and irradiance remains poorly understood, requiring comparisons with more established photooxidative processes. It was observed that at low irradiance levels where the surface has not been saturated by the photons, both reaction time and irradiance influence the production of methane, suggesting that photoexcitation limits overall process efficiency. Conversely, at high levels, where the surface has been saturated by the photons, increasing irradiance does not affect photocatalytic performance, but extending the reaction time is crucial for increasing methane yield. It is not sufficient to have a single irradiance condition for evaluating material activity. To have better understanding, low- and high-irradiance tests should be combined to observe how efficiently the catalyst interacts with the reagents.

3.2. Fixed-Bed Photoreactors

Slurry reactors have been used for many years to perform bench-scale photocatalytic reactions. However, their utility is constrained by the small catalyst particle size that may foul the light source. Furthermore, there will be an additional cost for removal/recovery of photocatalysts, and catalyst separation may be hard and not feasible for continuous application. Due to these restrictions, a new class of photoreactors was developed, fixed-bed photoreactors, taking advantage of the experience in thermocatalytic processes for which this is the simplest and most common arrangement.

The photocatalyst is often fixed on supports, allowing for continuous operation without the requirement for catalyst separation. These photoreactors are employed mostly in the gas–solid phase where CO_2 and other gaseous substances may be directly fed. The design of materials, especially the small particle size and reduced grain boundaries of photocatalysts, may be a key factor for exposing the photocatalytic sites. In this type of photoreactor, photons directly reach the exposed photocatalyst surface, which should be maximised. Additionally, the low-penetration-depth issue can be overcome by using a thin-film layer of a photocatalyst, which will result in a larger exposed surface area for improved photon usage in CO_2 reduction. Large grain size can be used in fixed-bed photoreactors to increase external mass transfer and reduce pressure drop. Light distribution becomes a limiting factor in this system considering the geometry of the irradiation source and spatial distance between the light source and photocatalyst. Furthermore, depending on the transparency of the support and thickness of the catalyst layer, the optical path through the reactor can be more or less effective [88].

The catalytic bed and the photoreactor vessel (shell) are the two primary components of a fixed-bed photoreactor. Different types of materials, mainly glass or stainless steel, are used to construct the photoreactor vessel. In this type of reactor, the photoactive material can be either fixed in powder form at the bottom of the reactor [89] (very inefficient arrangement) or coated over different kinds of support such as glass beads or tiles [90,91], optical fibres, monoliths or plane or curved surfaces, thus avoiding catalyst separation cost. These supports can have a variety of shapes, including spheres [90], cylinders [92], fibres and tiles [64]. In a photocatalytic reactor, variables such as the thickness of the photocatalyst active film and the transparency and the size and shape of the supporting particles affect how much radiant energy will be absorbed by the catalytic bed. Thin catalytic films and small sizes of support enable deeper light penetration into the photocatalyst active sites, increasing conversion efficiency. However, continuous light irradiation may harm the photocatalyst due to the increased temperature, which would cause less reactants to adsorb on the photocatalyst surface, reducing the productivity. Conversely, a thick layer of a photocatalyst or large particle size might cause a shallow penetration depth and poorly activated sites. Additionally, the selecting of optimum thickness and particle size of a photocatalyst is crucial when designing a fixed-bed photoreactor.

3.2.1. Horizontal Photoreactors

The geometry of a photoreactor is closely tied to the irradiation source, aiming to maximise light collection while minimising the energy losses and investment costs. Fixed-bed photoreactors can be both vertically and horizontally oriented. Horizontal fixed-bed photoreactors are commonly used in batch processes, and the maximum area to be exposed to photocatalyst light irradiation is obtained either by spreading in the bottom of a photoreactor or by coating/dispersing the catalyst on a plate. In this configuration, the shell of the reactor is placed horizontally, the catalyst bed is fixed in the reactor and the irradiation source is placed either inside or outside of the reactor.

For instance, Tahir et al. [93] used a rectangular photoreactor; the photocatalyst was homogeneously dispersed in powder form at the bottom to have a well-distributed light over the catalyst surface, as can be seen in Figure 8A. A Hg vapor lamp was used as an irradiation source. The productivity of methane by the photoreduction of CO_2 was found to be 0.208 mmol kg_{cat}^{-1} h^{-1}. In another study [92], a horizontal quartz tube reactor

was used and the light source was put inside the tube as illustrated in Figure 8B. In total, 0.12 mmol kg_{cat}^{-1} h^{-1} of methane was produced after 6h of UV irradiation on the catalyst, constituting TiO_2 pellets. Also, a flat tray was used to hold the catalyst pellets. In a related study by Zhang [94], a cylindrical quartz tube photoreactor such as the one in Figure 8C was utilised, and a flat quartz glass held a Pt-loaded TiO_2 catalyst used for the photocatalytic reduction of CO_2. The light source was located inside the tube. As the temperature rose, it was found that the CH_4 yield increased. Additionally, an increase in temperature was noted to enhance the desorption process of the formed products and increase the likelihood of effective collisions. The productivity of CH_4 was found to be approximately 1.5 µmol g_{cat}^{-1} at 323 K while with the increased temperature at 343 K, the maximum productivity reached 5.5 µmol g_{cat}^{-1}. A similar cylindrical quartz tube photoreactor was utilised in a different study by Park et al. [95], but the light source was fixed outside of the cell, as illustrated in Figure 8D. A Pyrex glass plate was coated with double-layer film of catalysts TiO_2/Cu-TiO_2 as compared to TiO_2 and inserted as shown in the reactor. It was found that adding Cu to TiO_2 improved the double layers' photocatalytic activity. The improved photocatalytic activity resulted from two factors. First, the photocatalyst demonstrated a red-shift in UV-Vis absorption with the increase in Cu concentration. Additionally, improving charge separation and the prevention of the recombination of the photogenerated electron–hole (e^-/h^+) pairs was demonstrated thanks to interfacial transfer between TiO_2 and Cu-TiO_2. The maximum methane yield was 0.175 mmol kg_{cat}^{-1} h^{-1} over TiO_2/5.0 mol% Cu-TiO_2 after 8h compared to the 0.08 mmol kg_{cat}^{-1} h^{-1} accomplished over the TiO_2/TiO_2 double-layered film.

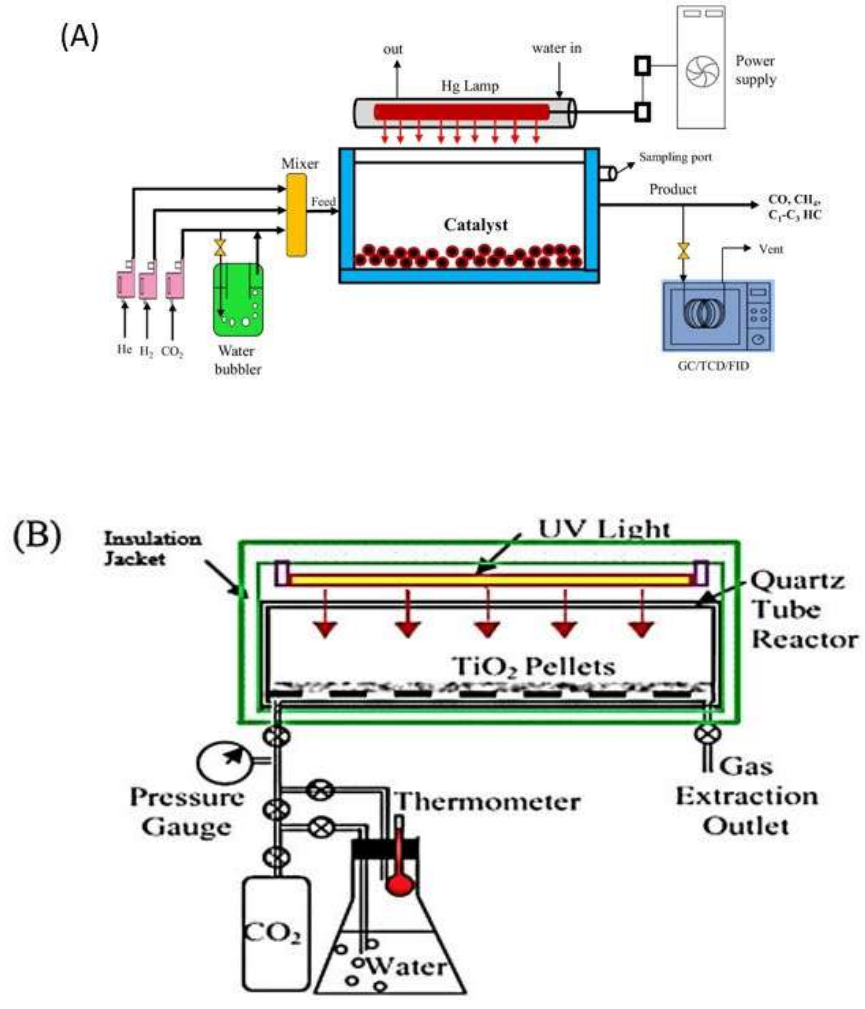

Figure 8. *Cont.*

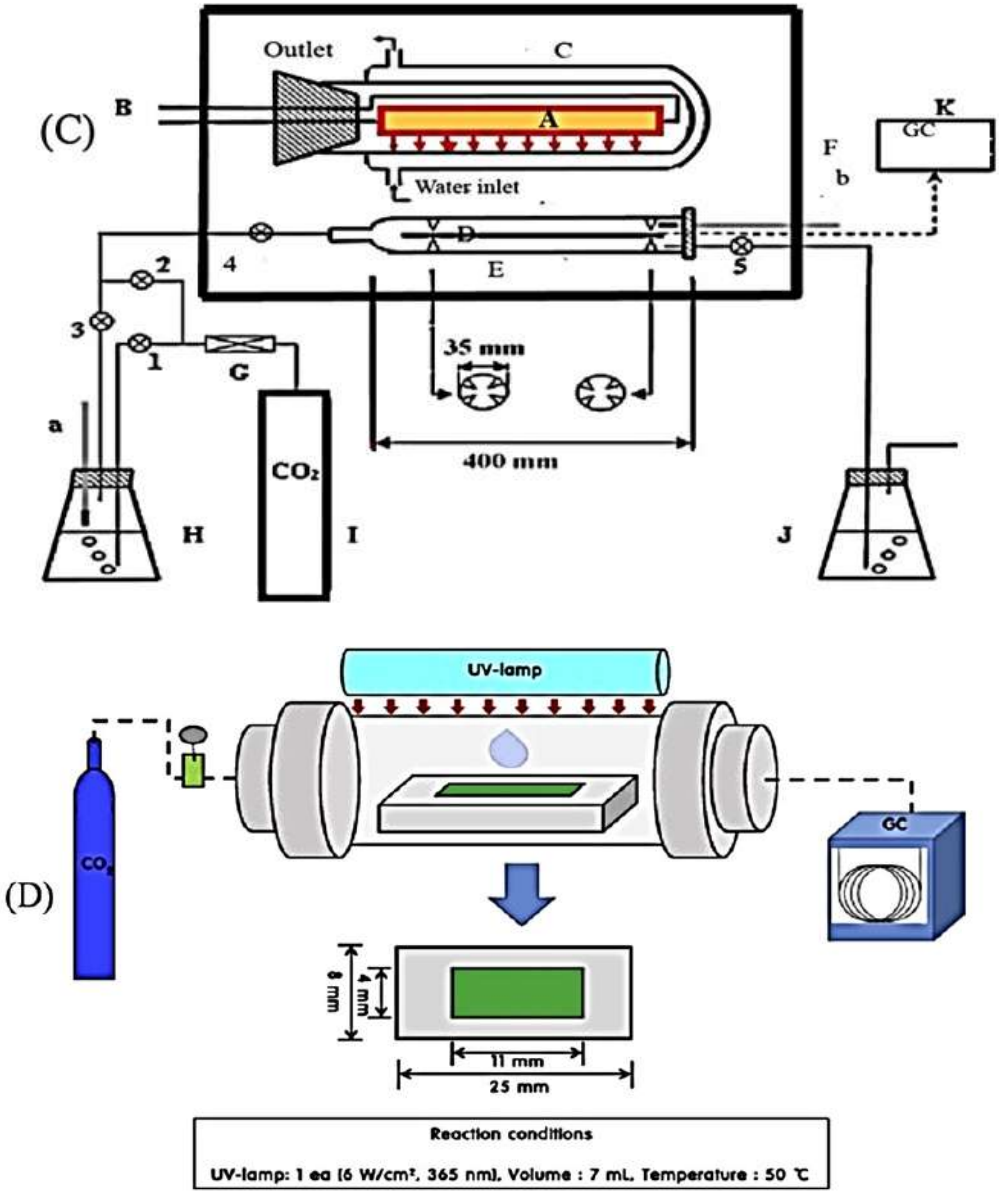

Figure 8. (**A**) Schematic of experimental setup of horizontal fixed-bed photoreactor for photocatalytic CO_2 reduction with H_2O and/or H_2 (reproduced by kind permission of Elsevier BV from [93]). (**B**) Schematic drawing of cylindrical quartz tube reactor (reproduced by kind permission of Elsevier BV from [92]). (**C**) Setup of fixed-bed photocatalysis reactor. A—UV/visible light; B—electrical wire; C—U-type terrarium; D—quartz glass plate; E—quartz glass reactor; F—insulating chest; G—gas flowmeter; H—conical flask for deionised water; I—CO_2 gas; J—absorption flask; K—gas chromatograph; 1–5—valve; a,b—thermometer (reproduced by kind permission of Elsevier BV from [94,96]). (**D**) Horizontal tubular photoreactor with double-layer film catalyst coated on glass plate (reproduced by kind permission of Elsevier BV from [95]).

3.2.2. Cylindrical Photoreactors

This reactor design includes a cylindrical tube that can be placed vertically or horizontally. Based on where the irradiation source is located, these reactors can be classified into three different configurations: (1) illuminated from the top; (2) illuminated from the sides where the catalyst bed is placed in the middle of the photoreactor and the light source is installed on the wall of the cylindrical tube; and (3) illuminated from the centre where the light source is placed axially and the catalyst is coated on a support having an annular shape with respect to the reactor. To achieve the highest photocatalytic efficiency, massive

usage of photonic energy must be considered, while maximising the interaction between the photocatalyst and reactants (CO_2 and H_2O).

Configurations where the photocatalyst bed is placed at the bottom or in the centre of the photoreactor are illustrated in Figure 9. A study reported in [67] dispersed the catalyst in powder form in a stainless steel cylindrical tank that was 150 cm^3 in volume and had a length of 5.5 cm. A 200 W mercury reflector lamp served as the UV irradiation source. This arrangement fits gas–solid phase reactions and it is suitable for small reactors only.

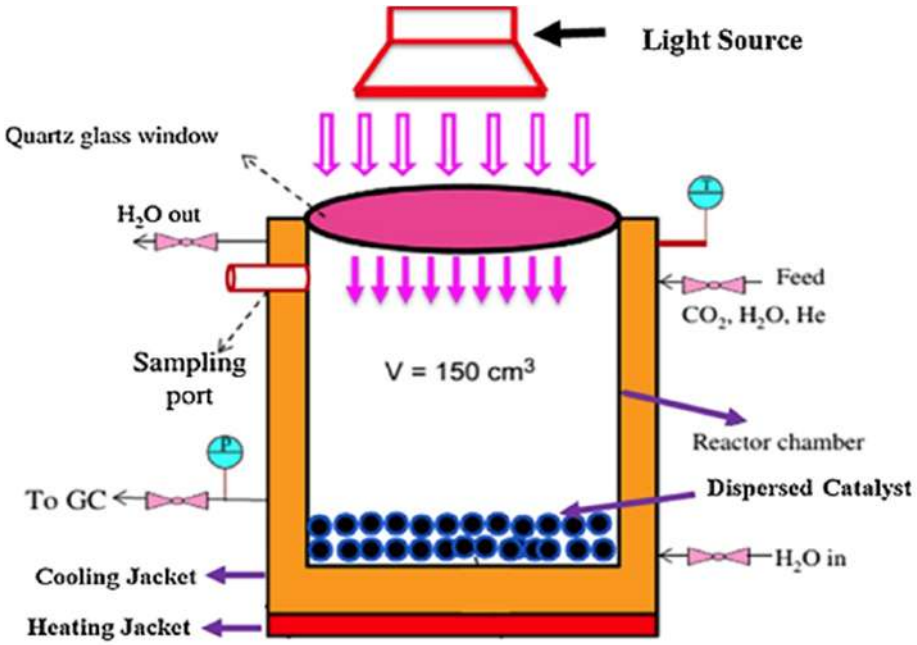

Figure 9. Vertical tubular fixed-bed photoreactor with catalyst dispersed in powder form in bottom of vessel. Readapted from [67]).

The results demonstrated that the photocatalyst bed was spread at the bottom of the photoreactor in such a way that the flow was occurring over the bed and not through the bed, resulting in poor contact and low CH_4 yield, concomitantly caused by inefficient light distribution and mass transfer.

The most widely used fixed-bed photoreactors are those in which reactant flow occurs cross-sectionally through the bed to optimise the interaction between the photocatalyst and reactants. The photocatalyst bed is spread out over supports in this instance, most frequently fibre glass filters, which have great strength, good stability and low cost. Stainless steel mesh is also occasionally employed. However, to keep saturated water vapor in the reactor, glass wool is also used. However, if this arrangement improves the contact between the catalyst and the reactants, it is less efficient for irradiation.

In another study [97], a cylindrical photoreactor was employed, with the light sources positioned on the walls of the reactor in opposite directions as depicted in Figure 10. A UV lamp and Xe lamps, which emit ultraviolet and visible light, were the sources of light. In the same way, a nanocomposite of nickel-loaded TiO_2 photocatalysts was fixed on activated carbon fibres (ACFs), and NiO-TiO_2/ACF (3 cm × 3 cm) was spread on a Teflon surface dispersed in the centre of the photoreactor. The porous structure and large surface area improved the conversion of CO_2 to methanol by providing more surface-active sites. The photocatalytic conversion of CO_2 to fuels under visible light irradiation was enhanced through catalyst immobilisation, which boosted light absorption and improved the formation and survival of electron–hole pairs.

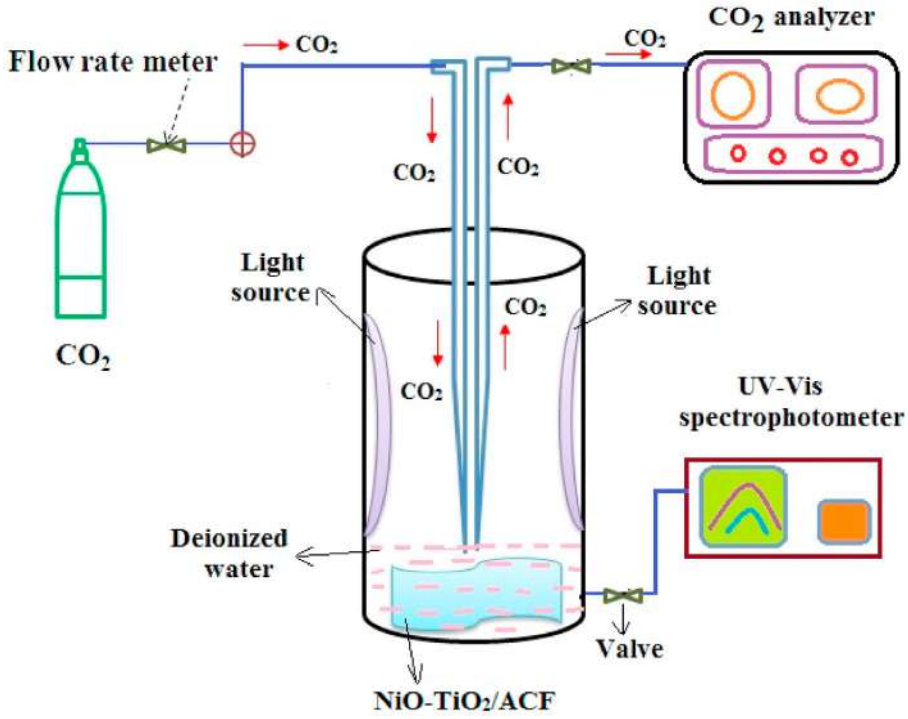

Figure 10. Schematic drawing of cylindrical quartz tube reactor [97].

3.2.3. Thin-Film Photoreactors

Typically, only a small percentage of the photocatalyst in fixed-bed photoreactors gets activated by light, which lowers the efficiency of the entire process. The impregnation of the photocatalyst on a moist quartz wool can be a desirable alternative, but the amount of water is not checked, so there might be some differences in the calculations of the CO_2/H_2O ratio. So, film reactors have been designed to increase the efficiency of the photocatalyst in the CO_2 conversion. For instance, in the work by Olivo et al. [87], the TiO_2, CuO-TiO_2 and Au-TiO_2 photocatalysts were deposited on the reactor surface exposed to radiation, preventing light absorption from the reaction medium, which has been observed to occur in thin-film reactors in previous studies. This enabled reducing the catalyst amount from 400 mg to 10 mg and, significantly, almost complete exposure of the catalyst to incident light. The small amount of catalyst and the use of thin film promoted the adsorption of reagents. Light harvesting was more efficient on the thin film-deposited catalyst. It was observed that methane formation increased significantly from 0.03 mmol kg_{cat}^{-1} to 14.00 mmol kg_{cat}^{-1}, changing the reactor from a fixed-bed to thin-film reactor. The presence of CuO and Au promoters influenced the activity together with the selectivity in CO_2 photoreduction. When they are compared with the undoped TiO_2 sample, the promotion by CuO slightly enhanced the photocatalytic activity toward the formation of methane (from 20 to 23 $mmol_{CH4} \cdot kg^{-1}$); indeed, the selectivity to methane enhanced from 95% for the undoped TiO_2 sample to 98% for the Cu-TiO_2 sample while the sample containing Au nanoparticles resulted in the lowest methane production (15 $mmol_{CH4} \cdot kg^{-1}$), leading to 60% selectivity to methane. The reaction was illuminated under a 125 W mercury UVA lamp while the temperature was kept at 40 °C.

In addition, Rossetti [98] developed a simple and scalable method for immobilising TiO_2 P25 on glass slide surfaces using an organic-based surfactant by using the dip-coating technique. By this way, improved adhesion properties and the homogeneous dispersion of catalyst nanoparticles were achieved. To have a uniform and homogeneous deposition, a six-slide holder was designed by using 3D printing technology that can be dipped into the suspension or solution of the target materials. Then, photocatalytic tests were performed by using synthesised catalysts for two major applications, hydrogen production through the photoreforming of glucose and the photoreduction of CO_2 into various solar fuels. The

latter experiments were conducted in a high-pressure reactor using Ag/P25-supported catalysts, showing significant results with formic acid productivity three times higher (around 20 mol kg^{-1} h^{-1}) than that of dispersed catalysts, along with enhanced stability and recoverability. No weight loss was observed for the coated tiles.

3.2.4. Packed-Bed Photoreactors

Utilising a circulating packed-bed assembly enhanced the efficiency of photocatalytic reactors. The selected photoreactor allowed larger surface area, and a uniform concentration distribution has occurred and thanks to this, the reaction time has been reduced. In this configuration, the photoreduction of CO_2 with H_2 and H_2O was carried out in a circulated batch photocatalytic reactor as illustrated in Figure 11. The temperature was kept at 43 ± 2 °C. Four UV light sources were placed around the photoreactor, which was used to immobilise the TiO_2 and ZrO_2 catalysts on glass pellets independently. Glass beads were coated with photocatalyst powder to create homogeneous layers, and the layer thickness was easily adjusted by changing the coating time. An ideal coating thickness must be selected because thicker coatings have lower optical transparency, which lowers their photocatalytic activity, while thinner coatings might have a negative impact on stability. The productivity of methane was 4.11 mmol kg_{cat}^{-1} h^{-1} while that of carbon monoxide was 0.14 mmol kg_{cat}^{-1} h^{-1} and that of ethane was 0.10 mmol kg_{cat}^{-1} h^{-1}. The photoreduction of CO_2 to CO, CH_4 and C_2H_6 at room temperature has been proven as feasible, despite the low product yield [99], but this type of photoreactor is unable to efficiently irradiate the catalyst because the catalyst-coated glass pellets inside the tube cannot be reached. In addition, the use of four irradiation sources results in additional costs and inefficient power use.

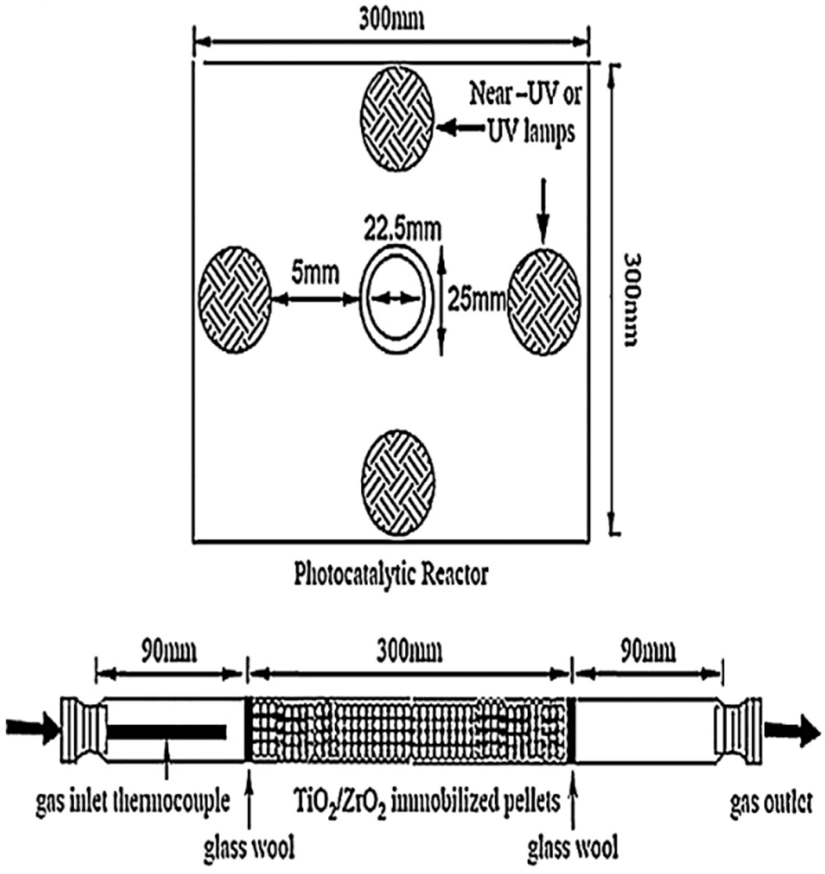

(**A**)

Figure 11. *Cont.*

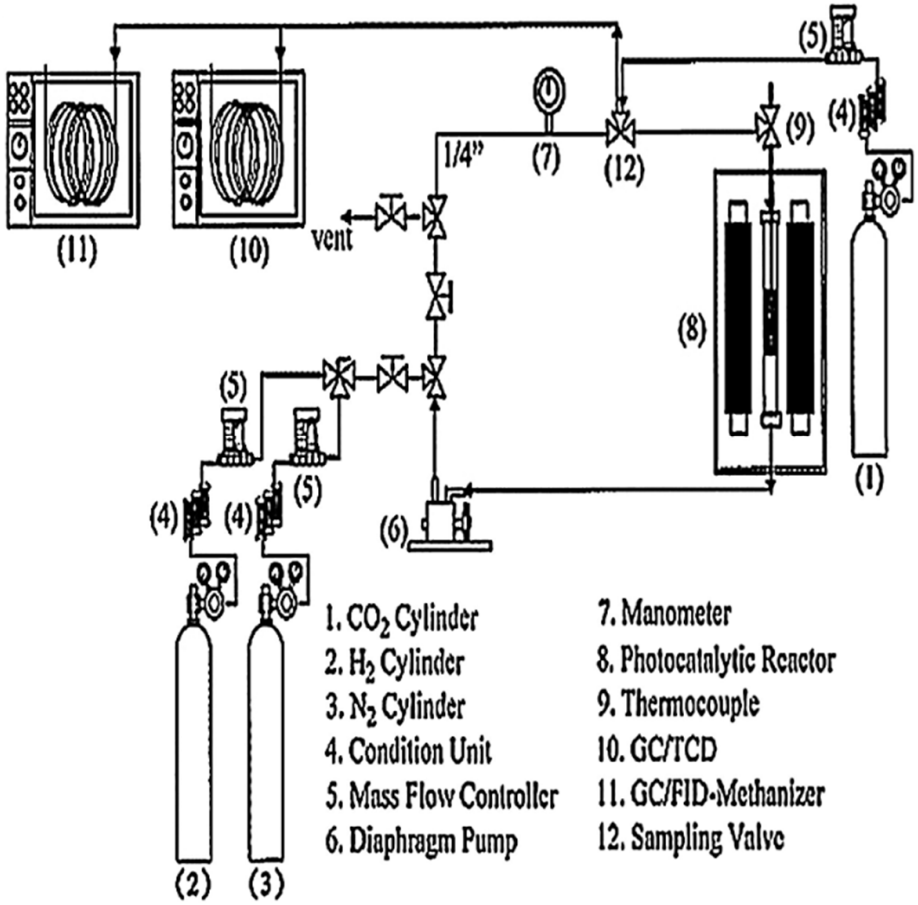

(**B**)

Figure 11. Schematic of experimental setup: (**A**) photoreactor and lamps; (**B**) plant scheme. Reproduced by kind permission of Elsevier BV from [100].

A study in the literature conducted by Rastgaran et al. [101] worked on a 3D model for the photoreduction of CO_2 to CH_4, H_2 and CO in a packed-bed reactor. The study was divided into two parts: designing the geometry of the reactor using a new method in a "blender" and using computational fluid dynamics (CFD) to study and analyse the reaction, transport phenomena and light intensity through the reactor. To provide a quantitative comparison, the average rates of surface reactions were calculated for CH_4, CO and H_2, resulting in values of 533.70 μmol m^{-2} h^{-1}, 876.16 μmol m^{-2} h^{-1} and 48.79 μmol m^{-2} h^{-1}, respectively. Creating the geometry of a 3D packed-bed reactor was crucial for optical modelling, as a large number of rays needed to be traced. Using the blender's rigid body physics, all the pellets were considered to simulate realistic conditions. This was the first time that rays were traced through a photocatalytic packed-bed reactor, known to be the most challenging geometry. This technique can be combined with other models including optical modelling to overcome the challenge. As an example, in packed-bed reactors, as the cross-sectional area and the number of particles increase, the number of secondary rays will exponentially enhance too, increasing the calculation cost. The authors suggested reducing the time and cost of calculation by using a GPU instead of a central processing unit (CPU), as ray tracing calculations are parallel. Still, common CFD software does not utilise a graphics processing unit (GPU) for ray tracing yet.

3.2.5. Optical Fibre Photoreactors

In comparison to conventional fixed-bed reactor designs, optical fibre photocatalytic reactors have been employed to enhance the distribution of light inside a reaction. The photoreactor is commonly constructed from a cylindrical glass vessel with a quartz window

to allow light to enter. To increase contact between the catalyst and CO_2, catalyst-coated optical fibres are set in a way to occupy a large volume of the reactor. One of the best advantages of this type of reactor is that unlike traditional reactors, this reactor overcomes the challenge of photon energy supply nearby the photoactive material and may therefore have applications for large-scale design [99]. Figure 12 displays a schematic and images of optical fibre photoreactors.

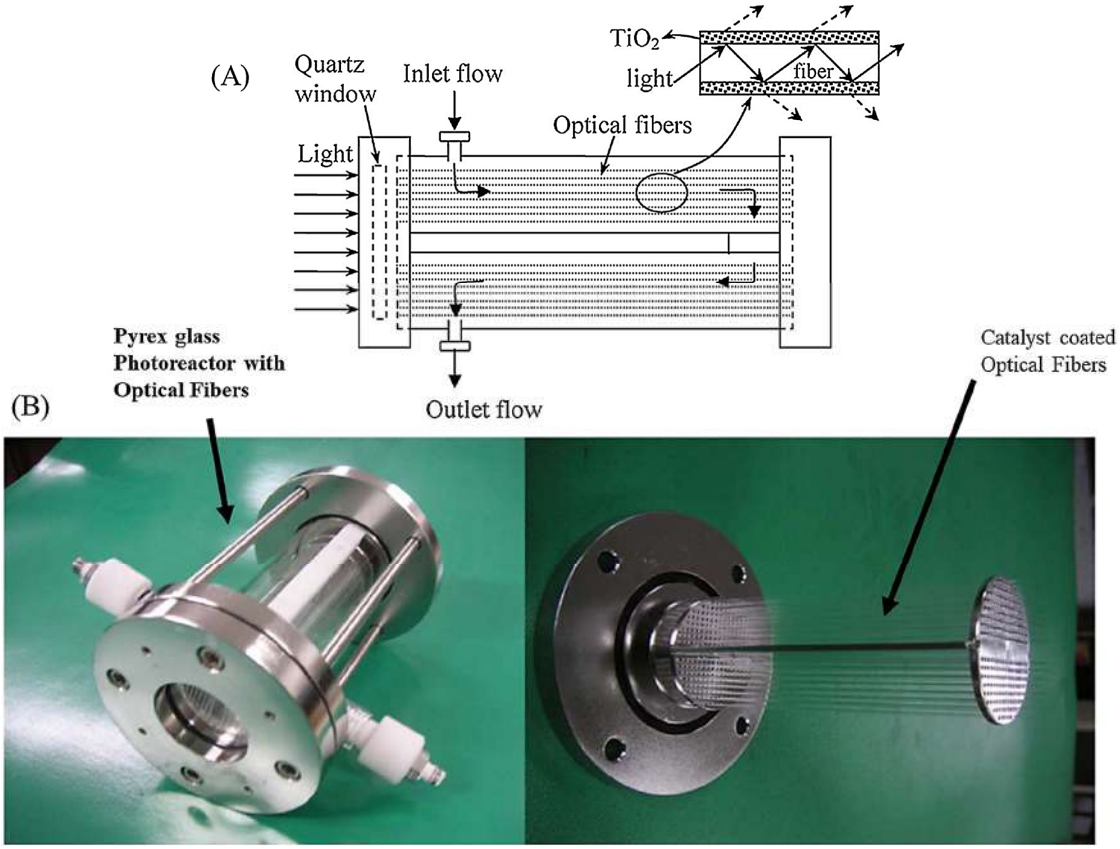

Figure 12. Schematic diagram (**A**) and images (**B**) of photoreactor with catalyst-coated optical fibres. Reproduced by kind permission of Elsevier BV from [63].

Wang et al. [99] carried out the photoreduction of aqueous CO_2 using an optical fibre reactor and achieved quantum efficiencies of 0.0045 and 0.063% in two reactor types, respectively. It is observed that the quantum efficiency was enhanced due to the higher light-energy utilisation of NiO/ $InTaO_4$ thin film in the optical fibre photoreactor. To boost the activity, various catalysts were coated on optical fibres. For instance, to enhance the yield of fuel from CO_2, many materials such as TiO_2 [63], NiO/$InTaO_4$ [99], Cu-Fe/TiO_2 [65], a TiO_2-iO_2 mixed oxide [64], inverse opal titania [102] and many more have been coated on optical fibres. Most of the techniques for the conversion of CO_2 to fuels have been discovered to produce a significant amount of methanol and formic acid as primary products. The incoming light hits the inner surface of the fibre; then, two beams are divided because of the difference in the refractive index between the coating film and the silica core. Some of the light is reflected and transmitted through the fibre, while some photons penetrate then excite the film at the interface. When it is compared with the traditional packed-bed photoreactor, light is uniformly transmitted through the optical fibre reactor, with the photocatalyst dispersed on the optical fibres with large surface area per unit reactor volume [99]. However, the drawback of this photoreactor is the low usage of the volume because the coated catalysts on the fibres are quite thin, thus occupying minimal volume within the reactor (utilisation of just 20–30% of the effective total reactor volume). Additionally, the thickness of the catalyst layer and its adhesion strength on the

fibres may impact its durability and performance. The use of an optical fibre photoreactor has boosted the efficiency of photoreactors; however, more development is required to make them commercially applicable.

In addition to this, Walko et al. [103] also studied scalable optical fibre reactors for the photocatalytic H_2 production. They utilised optical fibres coated with 5 wt.% CuO supported on TiO_2 for photocatalytic H_2 production from water–methanol mixtures. In a CuO/TiO_2 photocatalyst, Cu species are known to act as sensitisers that induce visible light activity. The study demonstrated the scalability of optical fibre-based systems and their potential use in non-potable turbid water media. In particular, the device used included 10,000 optical fibres, partially etched with HF. The maximum activity observed was 22 moles of H_2 in 8 h with 50 mg of a catalyst quantity coated on optical fibres, which increased linearly with an increase in the number of fibres. In contrast, a drastic reduction in activity was observed in the powder catalyst with an increased quantity of the catalyst. Furthermore, a direct comparison of 700 mg of the catalyst in powder form and coated on optical fibres revealed more than a one-order improvement in activity in the optical fibre-based system.

3.2.6. Monolith Photoreactors

A monolith is one of the structured photoreactors that has been utilised to convert CO_2 into fuels [104,105]. The schematic representation is shown in Figure 13. Some of the benefits of the monolith in the photoreactor are as follows: (1) its unique structure, (2) low-pressure drop and (3) efficient light harvesting and photon flux. Additionally, the large number of channels coated with a catalyst provides high contact time with reactants and light irradiation, and the surface area given by the monolith substrate can be 10–100 times higher when it is compared to other catalyst supports [106,107]. As an example, CO_2 was photoreduced with H_2 to CH_4, CO and many other hydrocarbons. It was discovered that the CH_4 produced by the monolith reactor was six times higher than that attained in a slurry photoreactor. In addition, a monolith photoreactor for the synthesis of CH_4 returned a quantum efficiency 12 times higher than a slurry-type photoreactor [108].

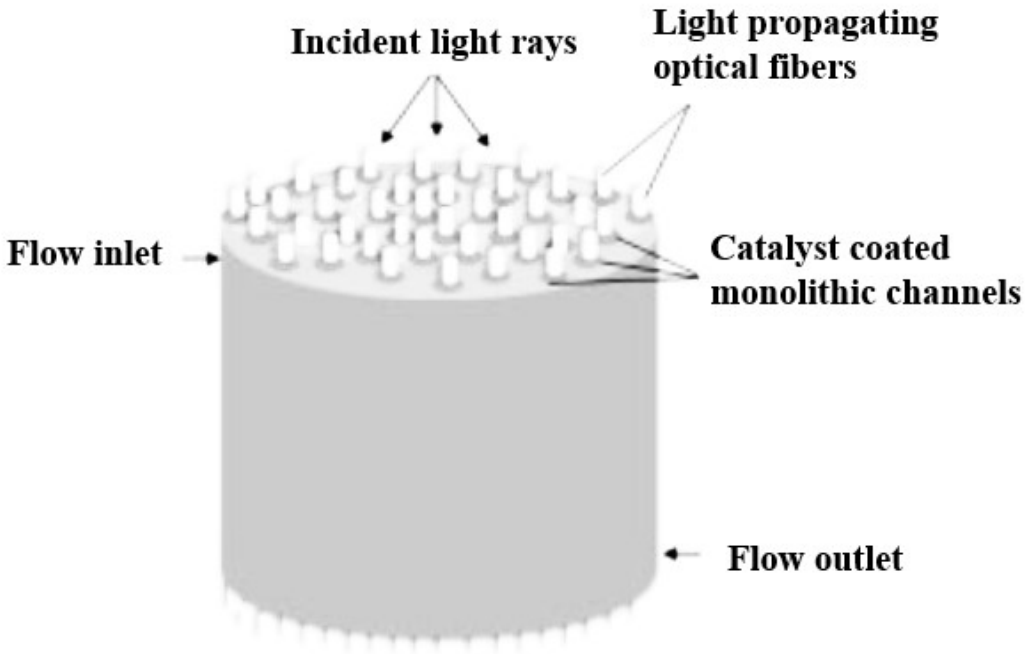

Figure 13. Internally illuminated reactor with top illumination. Readapted from [14].

3.2.7. Internally Illuminated Honeycomb Photoreactors

The efficiency of photon conversion is enhanced by the ability of optical fibres to evenly distribute light to the photocatalyst surface. However, because of the small surface-

to-volume ratio of the reactor, the optical configuration is unable to fully utilise the reactor volume. The drawbacks of optical reactors can be solved by monolith photoreactors with honeycomb structures because they can supply a high surface-area-to-volume ratio. However, a monolith's efficiency is compromised since limited light can get through the cells of the honeycomb substrate. Tahir et al. [67] (Figure 14) worked on a montmorillonite (MMT)/TiO_2-loaded monolith photoreactor for the photoreduction of CO_2. CH_4 and CO were the main products, yielding rates of 139 and 52 μmol g_{cat}^{-1} h^{-1}, respectively. The reactor performance for CH_4 formation followed the order of MMT–TiO_2–monolith (139 μmol g_{cat}^{-1} h^{-1}) > TiO_2–monolith (82 μmol g_{cat}^{-1} h^{-1}) > MMT–TiO_2–cell (43 μmol g_{cat}^{-1} h^{-1}) > TiO_2–cell (7.7 μmol g_{cat}^{-1} h^{-1}). The higher yields in the monolith photoreactor were attributed to the larger illuminated area and more efficient light employment.

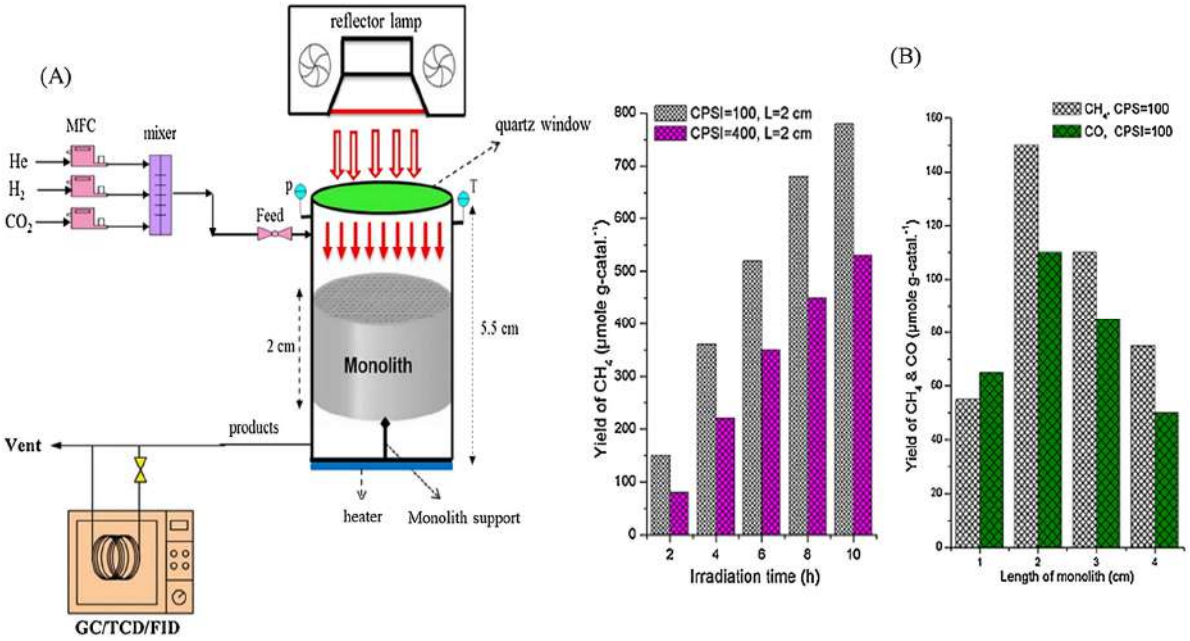

Figure 14. (A) Schematic representation of experimental setup of monolith photoreactor for photocatalytic CO_2 reduction with H_2; (**B**) Effects of channel density and length on performance of the monolithic photoreactor. Reproduced by kind permission of Elsevier BV from [67].

The internally illuminated honeycomb photoreactor by Wu et al. [109] incorporated a honeycomb structure of the monolith with optical fibres, to get over the difficulty of limited light penetration. A uniform NiO/$InTaO_4$ layer was deposited on a pre-coated SiO_2 layer on the internal cells of the monolith. The polymethylmethacrylate (PMMA) optical fibres could transmit and scatter light effectively to illuminate the catalyst within the monolith's channel. Gaseous CO_2 was photocatalytically reduced with H_2O to hydrocarbons under Vis or UV irradiation under flowing conditions. The maximum methanol production rate was 0.16 mmol kg_{cat}^{-1} h^{-1} with Vis light at 25 °C. The observation indicated a significant enhancement in quantum efficiency, suggesting the efficient utilisation of photon energy in the monolith reactor.

Another study conducted by Xiong et al. [110] has proven that the rate of CO_2 photoreduction in a honeycomb reactor was remarkably higher than in a conventional reactor, attributed to the high surface area and efficient light utilisation. The schematic representation is shown in Figure 15.

To overcome the challenge of limited light penetration, Wu et al. [109] incorporated an optical fibre-inserted honeycomb structure into the monolith, as shown in Figure 16. The integration of optical fibres and the monolith was given significant enhancement for the photoreduction of CO_2.

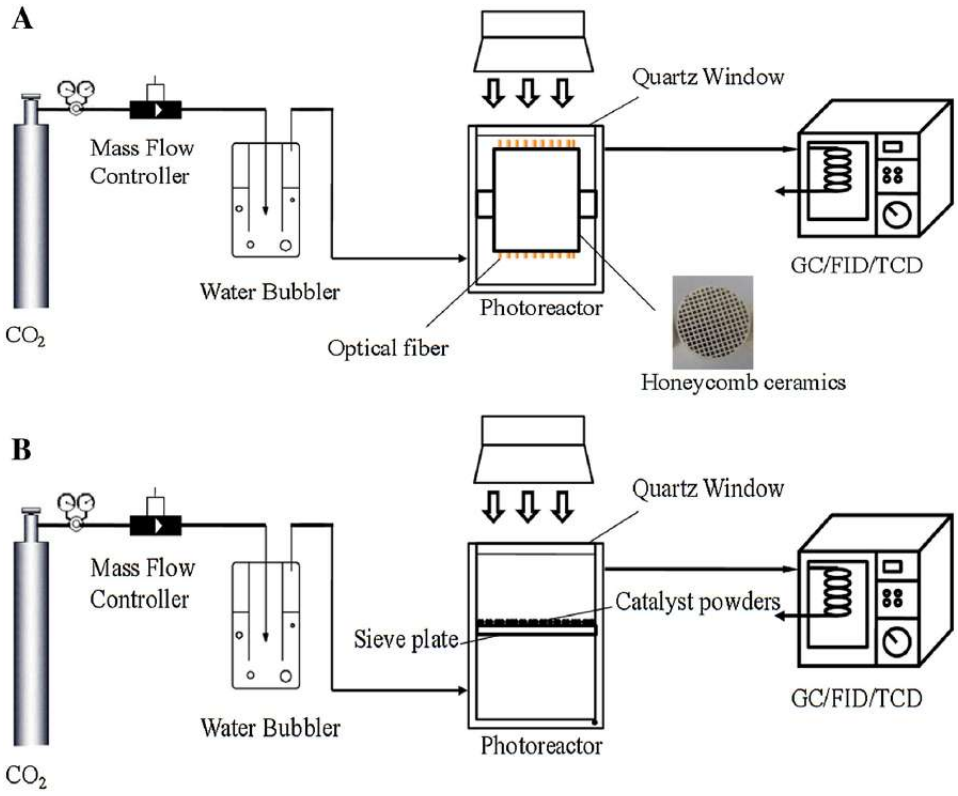

Figure 15. Schematic representation of internal-illuminated honeycomb reactor (**A**) and conventional powder reactor (**B**). Reproduced by kind permission of Elsevier BV from [110].

Figure 16. Internally illuminated monolith photoreactor: optical fibres are embedded within the monolith to improve light penetration through the solid support. Reproduced by kind permission of RSC from [109].

In addition, Zheng et al. [111] worked on a sunlight-driven honeycomb photoreactor, which is prepared by swelling poly(ionic liquid)s with polymeric carbon nitrides for wastewater treatment. Ionic liquids containing polymerizable groups polymerised in situ with crosslinkers in a system dispersed in polymeric carbon nitride (PCN) to realise a photoreactor. The resulting photoreactor exhibited improved photoelectric properties attributed to a 3D honeycomb structure, which improved the contact between the active centres in the reactor and the reaction substrate. This enhancement in the electron–hole separation efficiency of PCN was achieved by efficient electron transfer ability of poly(ionic liquid)s. This developed photoreactor demonstrated the ability to degrade anionic dyes such as methyl orange and acid blue 93 using a metal halide lamp or natural sunlight.

3.3. Membrane Photoreactors

Membrane reactors have a membrane, a photocatalyst or, in some cases, an electrocatalyst. This design has been particularly advocated for integrating water splitting and CO_2 photo-hydrogenation in a twin photoreactor. Additionally, they could be categorised as fixed-bed and slurry photoreactors based on the type of photocatalytic bed arrangement. In general, they perform controlled reactions separately, so the blending of products or reactants and solutions are blocked. Electrons, protons and holes are transferred between the chambers, as well as reactants. A membrane is inserted between the chambers and the transfer of electrons may take place internally through the reactor or externally through a wire connected to it. Sometimes, a potentiostat is inserted in the external wire to assist the electron flow by supplying a biased voltage [112]. Those photoreactors function similarly to reverse fuel cells, with each compartment acting as a half-cell. This method combines, for instance, water splitting with CO_2 reduction to produce hydrocarbons. As a result of charge separation under light irradiation, photocatalytic water splitting occurs in one of the chambers, while CO_2 reduction is carried out in another to convert it to fuels [113]. In comparison to other photocatalytic reactors, the membrane photoreactors have the following benefits: (1) a backward reaction is not allowed because hydrogen and oxygen are produced in divided chambers. (2) Since oxidation and reduction take place in different chambers, therefore, the reaction takes place and is easy to control and the selectivity of products is quite high. However, the efficiency is still very low. Low efficiency is due to a number of factors, including (1) the mass transfer limitations of reactants to the surface of a catalyst; (2) loss of photocatalytic efficiency due to a low illuminated-area-to-weight ratio; (3) the distance for electrons, protons and holes to travel across the membrane is quite high from a microscopic view, so side reactions may occur, leading to undesired reactions; (4) additionally, membrane fouling is a significant issue that lowers the efficiency of membrane reactors [114].

3.3.1. Slurry-Type Membrane Photoreactors

This type of photoreactor is characterised by the presence of three phases where the photocatalyst (solid phase) is suspended in the liquid phase, while CO_2 is in the gaseous phase, dissolved in the liquid–solid suspension. The photoreactor comprises two chambers separated by the membrane to facilitate the separation of oxidation and reduction reactions. Slurry membrane photoreactors can also be divided into stirred membrane photoreactors (generally magnetically stirred) and fluidised photoreactors, in which fluidisation is accomplished by either bubbling or pumping CO_2 through the reactor with overpressure. In a slurry-type photoreactor, protons may be formed in a chamber in which water is photocatalytically oxidised and transferred across a membrane to form fuels through the reduction of CO_2 in another compartment [115–117]. Twin-tower photoreactors have been found to be more effective than single-tower photoreactors because O_2 is isolated from the reduction reaction, thereby blocking the reverse oxidation of H_2 and hydrocarbons [115]. Twin-tower photoreactors have more than double efficiency than a single-tower photocatalytic reactor system. Additionally, the rise in temperature and

pressure leads to improved mass transfer, which enhances the conversion efficiency of CO_2 into fuel.

In order to improve mass transfer between the liquid and gas phases, Chu et al. [116] demonstrated a new bubbling twin-tower reactor. This reactor produced 9.75% higher ethanol in comparison to traditional twin reactors. Compared to fixed-bed photoreactors, membrane photoreactors, which involve suspending a photocatalyst in a solution, are more efficient, versatile and adaptable for practical applications. However, challenges such as CO_2 diffusion and electrical conductivity limit their practical applications. In order to enhance the performance, sacrificial agents, such as NaOH and Na_2CO_3, are able to boost the photocatalytic reduction of CO_2 to fuels, and improve the performance of slurry-type membrane photoreactors: (1) the sacrificial agents increase the dissolution of CO_2 in the liquid phase, leading to an enhanced concentration of CO_2 in liquid; (2) by scavenging the photogenerated holes, the use of sacrificial agents can considerably reduce the charge recombination; (3) there might be an improved electrical conductivity for simple charge transport [10].

Qin et al. [118] designed an H-type photoreactor with electrodes immersed in two separate solutions as illustrated in Figure 17. The photocathode featured a bi-functionalised TiO_2 film, aiding in the separation, transfer and renewal of photoexcited electrons involved in the photocatalytic reduction of CO_2. Also, external electrical power was applied to enhance the production of value-added fuels.

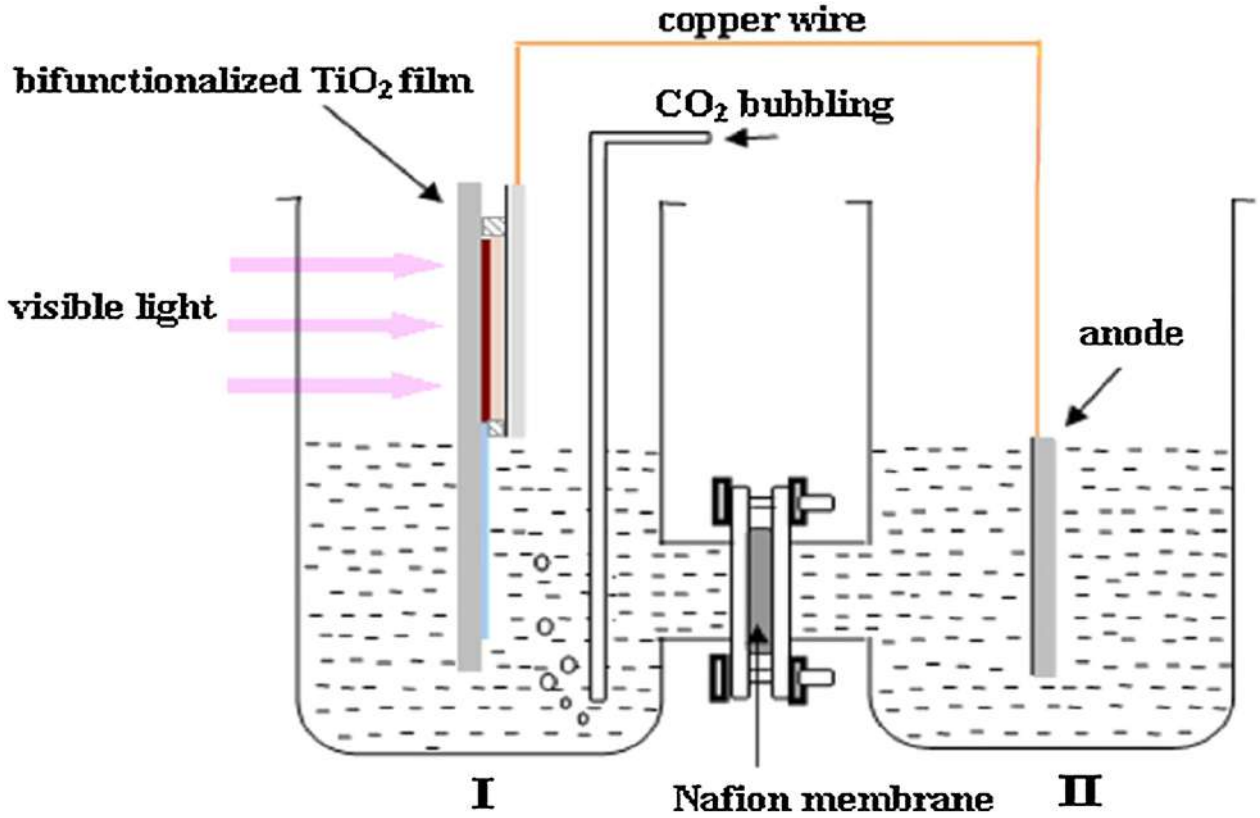

Figure 17. Photocatalytic reduction of carbon dioxide in H-type reactor. Distilled water is used as medium for both solutions I and II. The catalyst is inserted into solution I, while a Pt/FTO electrode is inserted into solution II. Reproduced by kind permission of Elsevier BV from [118].

3.3.2. Fixed-Bed Membrane Photoreactors

Catalysts are fixed on the surface of electrodes in fixed-bed reactors. Light is irradiated onto a cathode, anode or both by rotating the electrodes to operate as a photocathode and/or photoanode, depending on the reaction that must be carried out. Then, electrons, holes and protons might participate in various reactions for generating several compounds.

However, to obtain the advantages of the aforementioned three products, electrons and/or protons generated in the water splitting chamber are transferred to the other part across a membrane in order to reduce CO_2 and form hydrocarbons. The internal transmission of electrons between the chambers may occur with the use of a quite thin composite material sheet or it may occur externally using an electric connection, converting the photoreactor into a photoelectrochemical reactor [112]. Again, to keep the flow of electrons, a potentiostat may be put outside of the reactor supplying an electrical bias and it was found that the CO_2 photocatalytic conversion significantly enhanced when external power was used.

In contrast, Arai et al. [119] asserted in their experiments that a wireless system is more efficient than one that uses an external wire when there is no electrical bias.

3.4. High-Pressure Photoreactors

As mentioned previously, the high stability of a CO_2 molecule makes the conversion options difficult, but additional elements contribute to its scarce conversion. To increase the photocatalytic efficiency of CO_2 photoreduction, an innovative high-pressure photoreactor has been designed, which newly opens the route for high-pressure photocatalysis [120,121]. The photoreactor operates at a high CO_2 pressure up to 20 bar; by this way, it enhances the availability of carbon dioxide in the aqueous reaction medium when operating in the three-phase mode, which demonstrates more efficiency than gas–solid phase reactors. Operating at high pressure improves the photocatalytic performance by also increasing the CO_2 surface adsorption over the photocatalyst surface.

Photoreactors generally operate at atmospheric pressure since transparent windows are required, typically fragile materials. Furthermore, ambient temperature is typically used in water-based media and a moderate increase in temperature has been explored up to ca. 60 °C, showing decreasing activity with increasing temperature. However, the high-pressure operation also makes it possible to reach relatively high temperatures in the liquid phase (up to 100–110 °C). These conditions were utilised for the photoreduction of CO_2, speeding up kinetics and mass transfer, while also keeping as significantly higher the gas solubility and surface adsorption of the reactants. Indeed, CO_2 solubility dependence on T and P has been quantified elsewhere (Figure 18) [114] and confirms the predominantly positive effect of raising P compared to the negative one of raising T. According to the finest literature data, exceptionally high productivities have been attained with this strategy.

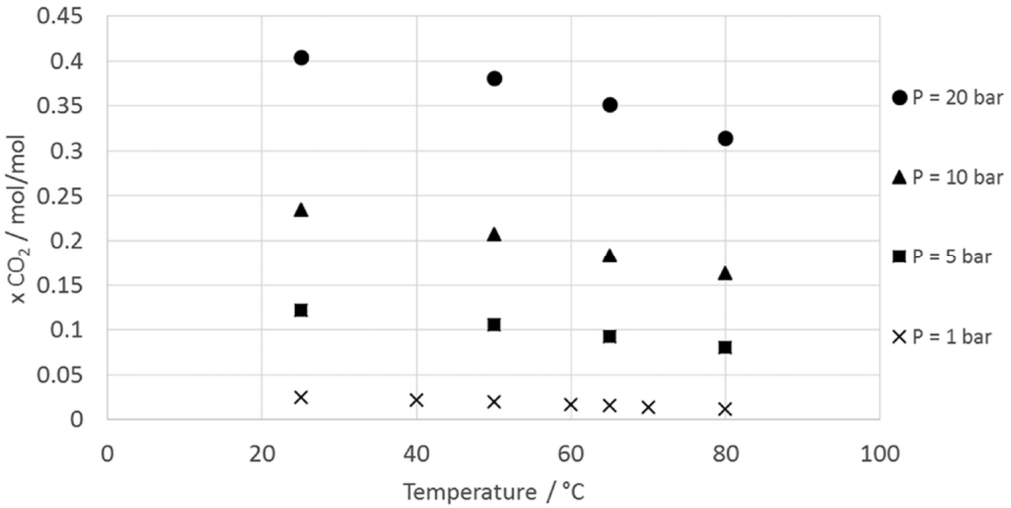

Figure 18. Effect of saturation temperature and pressure on equilibrium CO_2 molar fraction in water. Reprinted by kind permission of RSC from [114].

Titania-based samples were used to first illustrate the concept. The configuration is set up at two different pressures, at 8 and 18 bar, to understand the effect of pressure to convert CO_2. Since water oxidation was too slow, Na_2SO_3 was used as a hole scavenger. The results

showed that the increasing pressure favours the productivity of formic acid, which reached 7.0 mol h^{-1} $kg_{cat}{}^{-1}$ at 8 bar and further enhanced by 64% when CO_2 pressure of 18 bar was reached.

Another study [122] used a g-C_3N_4 photocatalyst and results demonstrated that the productivity has increased significantly at high pressure. The productivity of HCOOH was found to be 8 mol h^{-1} $kg_{cat}{}^{-1}$ at 8 bar and 80 °C. In another study [40], enhancing the pressure has favoured the accumulation of organic reduced products in the liquid phase such as HCOOH with 7 mol $kg_{cat}{}^{-1}$ h^{-1}, whereas productivity of compounds in the gas phase was favoured at intermediate pressure in the presence of a 0.2 wt.% Au/P25 photocatalyst. This high-pressure process was demonstrated for CO_2 conversion to high-value products such as methane, methanol, formaldehyde or formic acid [38,123–125].

Significantly high methanol productivity was also obtained at ca. 1.4 mol $kg_{cat}{}^{-1}$ h^{-1}, which is incomparably higher than other results in the literature. Overall, the highest productivity and energy storage efficiency was achieved by maximising formic acid production and a feasibility assessment for the possible exploitation of solar light has been undertaken in [39,40].

The sketch of the high-pressure photoreactor can be seen in Figure 19. The operated reactor is made of AISI 316 stainless steel having an internal capacity of 1.7 L. It is equipped with a magnetic stirrer providing appropriate liquid mixing and a double-walled thermostatic system.

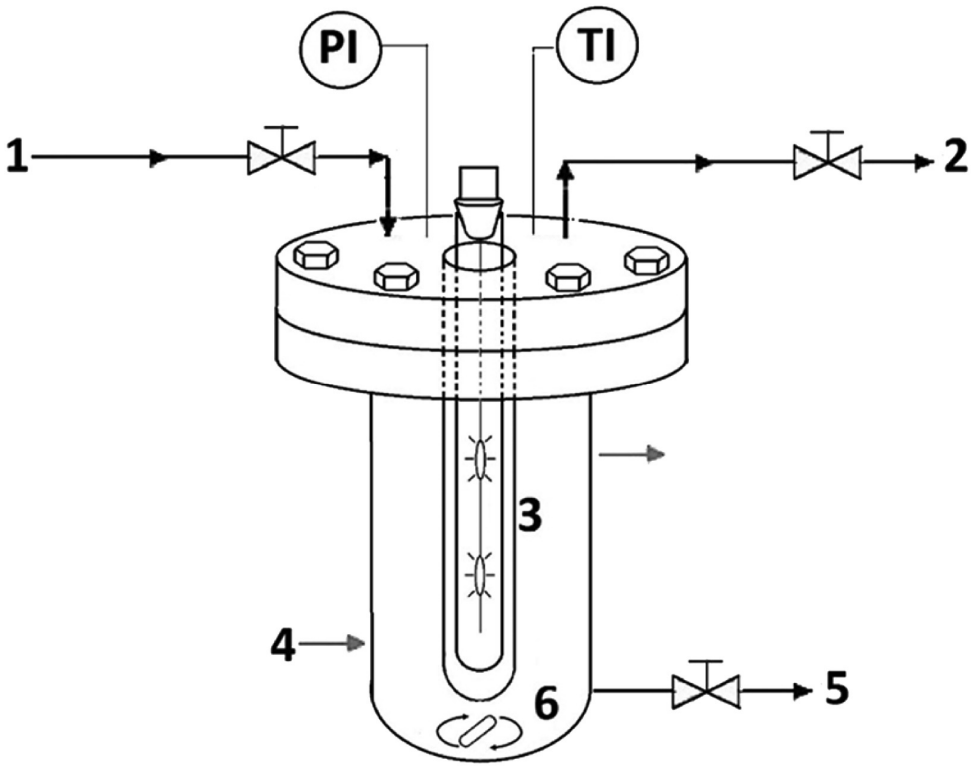

Figure 19. Sketch of high-pressure photoreactor. 1: Pressure reducer, 2: Sample valve for gas phase, 3: Lamp, 4: Double-walled thermostatic system, 5: Sample valve for liquid phase, 6: Magnetic stirrer, PI: Pressure indicator, TI: Temperature indicator. Reproduced by kind permission of Elsevier BV from [126,127].

A 125 W medium-pressure Hg vapor lamp with emission wavelengths from 254 nm to 364 nm was utilised as the source of radiation and was inserted vertically into the reactor axis. The pressure and temperature inside the reactor were measured using a pressure transducer and a thermocouple, respectively. Continuous heat removal from the lamp bulb was achieved with the aid of an air circulation system surrounding it, which also

assisted in maintaining the temperature of the solution at a constant value, measured by the thermocouple located 1 cm away from the centre of the quartz candle [126].

Although the results were promising, the configuration as a slurry three-phase reactor prevented the easy separation of the catalyst and made a continuous mode reaction quite challenging. A further study in the literature [98] proposes a new layout in order to overcome these issues. A simple and scalable method has been developed for immobilising TiO_2 P25 over the surface of glass slides using an organic-based surfactant that imparts good adhesion properties.

A holder was designed with 3D printing technology (Figures 20 and 21) so that it can hold catalyst-coated glass tiles in a precise position near the lamp. Photocatalytic tests were performed in a high-pressure reactor with Ag/P25-supported catalysts since it was demonstrated that very high formic acid productivity (ca. 20 mol kg_{cat}^{-1} h^{-1}) comparable to the one achieved in the slurry phase with the dispersed catalyst is feasible, with the further advantage of improved stability and recoverability [98].

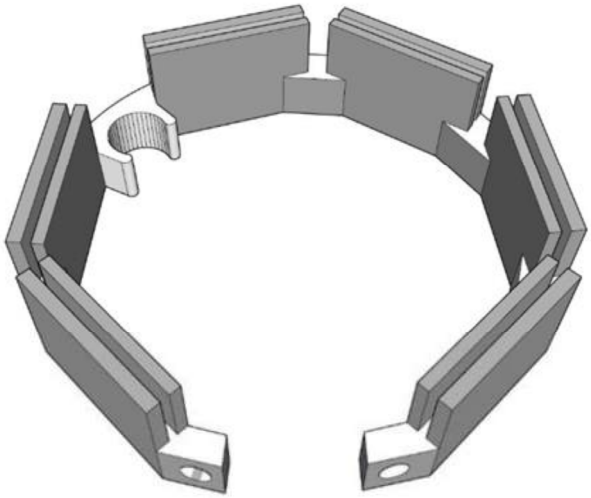

Figure 20. Optimised design of the glass tile holder. Reproduced under the Creative Commons licence from [98].

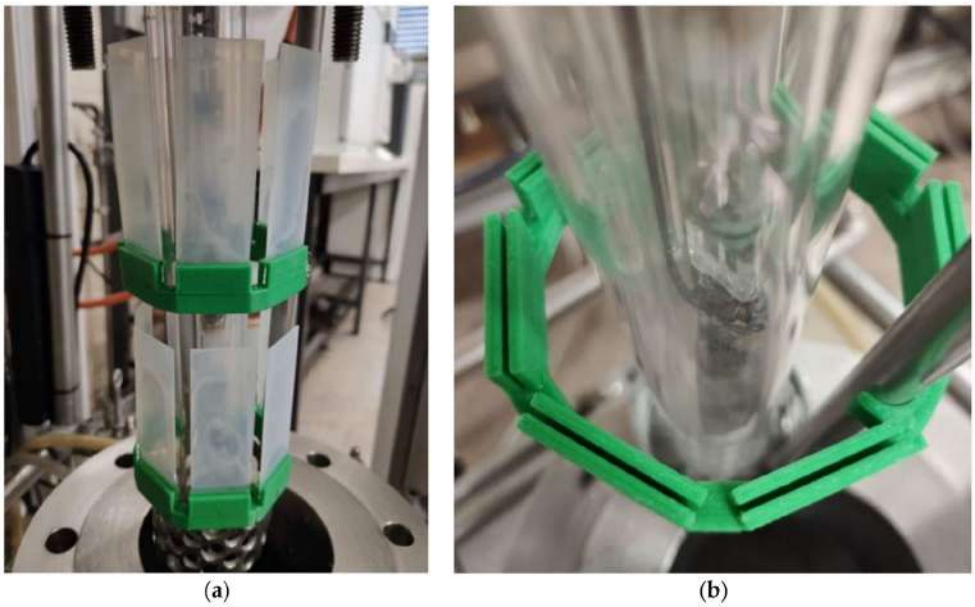

Figure 21. (**a**) The final version of the holder supported, printed and set up in ABS. (**b**) Details of the sample holder. Reproduced under the Creative Commons licence from [98].

3.5. Solar Photoreactors

The benefits and drawbacks of different solar photoreactors along with their specific characteristics are shown in Table 2.

Table 2. Benefits and drawbacks of different solar photoreactors along with their specific characteristics. Readapted from [7].

Solar Photoreactor	Reactor Characteristics	Advantages	Disadvantages
Slurry photoreactor	→ Light illumination can be directed from the top or sides → The photocatalyst is suspended in the liquid phase → Agitation methods: Mechanical stirring or gas agitation	→ Simple construction Possibility to scale up to the large photoreactor → Higher surface-area-to-volume ratio of illuminated catalyst → A lower amount of photocatalyst required	→ Limited possibility for catalyst recycling → Excessive stirring could result in erosion of photocatalyst → Issues of low active surface area due to inefficacious light distribution
Optical fibre photoreactor	→ Photocatalyst-coated optical fibre triggers the photocatalytic reaction → There is good contact between the photocatalyst and carbon dioxide	→ Even distribution of solar light transmission on the catalyst surface → High conversion rates	→ Lower surface area for coating support → Non-efficient utilisation of the entire reactor volume → Durability issues
Monolith photoreactor	→ Comprises a network of channels impregnated with the photocatalyst on its walls → Operation mode: Batch, continuous	→ Low-pressure drop → High surface area	→ Lower conversion to solar fuels → Low penetration of light under solar irradiation
Twin reactor (membrane photoreactor)	→ The reactor system is separated by a membrane, which enables the redox process to occur in a separate compartment	→ Higher diffusion and mass transfer among gas as well as liquid phases → Higher conversion efficiency → Higher selectivity → Prevent backward reaction	→ Difficulty with CO_2 diffusion and electrical conductivity

More or less, the same configurations already described are also used to exploit solar light. The critical issue in this case is the need for efficient light harvesting and to focus the captured light into the photoreactor.

The solar/energy efficiency of various photoreactors is examined in Table 3.

Table 3. Solar efficiency obtained with various solar photoreactors. Readapted from [7].

Solar Photoreactor	Solar Energy Efficiency
Concentrated reactor system	0.087–0.15%
Slurry photoreactor	1%
Optical fibre photoreactor	0.0182%
Membrane reactor	0.08–10%

The conversion of photon to chemical energy is an aspect of solar-to-energy efficiency. Solar concentrated photoreactors enable us to have maximum efficiency thanks to a better utilisation of solar radiation.

Nguyen et al. [64] employed an optical fibre photoreactor coated with gel-derived TiO_2-SiO_2 mixed oxide-based photocatalysts for the photoreduction of CO_2. The overall energy efficiency for CH_4 as well as C_2H_4 formation was significantly higher on Cu-Fe/TiO_2-SiO_2 (0.0182%) compared to its Cu-Fe/TiO_2 counterpart (0.0159%).

3.5.1. The Effect of Parameters on the Performance of Solar Photoreactors

Solar Photoreactor Geometry and Configuration

The geometry of solar photoreactors has strong influence on the efficiency of the collection of photons, choosing the construction of the solar photoreactor in a way that enables efficient light transmittance and reflection. A desirable photoreactor design ought to have the capacity to enhance the photons absorbed and to enable the efficient usage of electron–hole pairs. The larger the area that can be illuminated by the solar light with a uniform transmission enhances the performance of solar photoreduction [14,42]. A critical parameter is the thickness of the reactor. The use of glass reactors provides better light transmittance; however, there is still the risk of breaking and a restriction in reactor size.

Physical geometry of the reactor has a crucial effect on the light distribution and physical parameters. For instance, a cylindrical photoreactor is mainly employed at the laboratory scale since it allows for good mixing of reacting particles inside the reactor. Mixing can be achieved through magnetic stirring in small-scale batch photoreactors.

In the first configuration of Figure 22, the catalyst inside the reactor can stick to the windows of the reactor and this could shield the light irradiation, decreasing the efficiency. In the second example, thanks to generated turbulence, which prevents the photocatalyst particles from settling outside the photoreactor, the photocatalyst particles remain suspended. It is observed that the H_2 productivity is higher in the latter assembly [128].

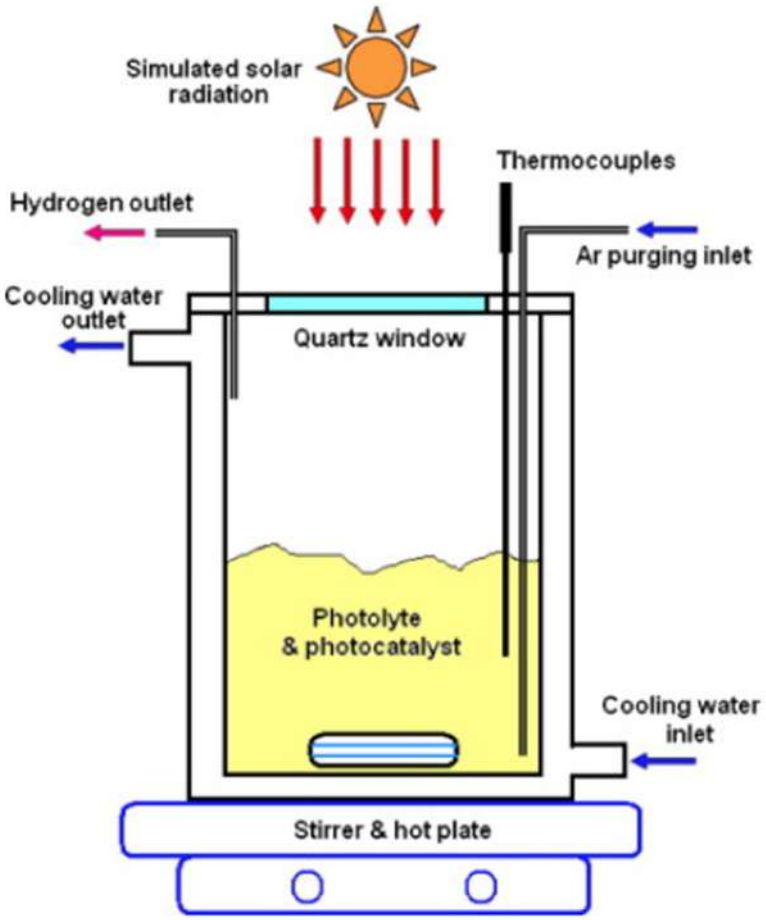

(A)

Figure 22. *Cont.*

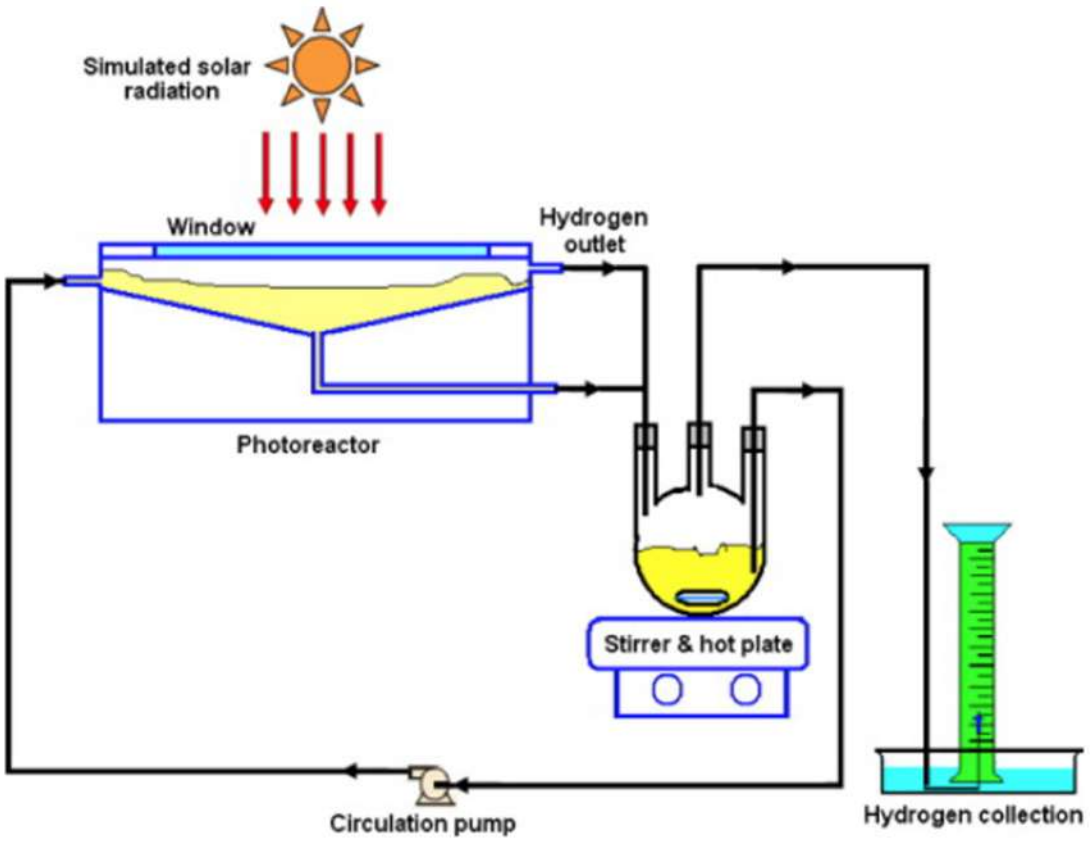

(**B**)

Figure 22. (**A**) Batch photoreactor under solar radiation for H_2 production. (**B**) Modified batch photoreactor set up for passive mixing. Reproduced by kind permission of Elsevier BV from [128].

The reactor can be shaped as annular, tubular or cylindrical. The dimension and the shape of the selected light source have a crucial effect on the geometry of a photocatalytic reactor. Its geometry should enable us to increase the collection of the emitted light from the selected sources. Photoirradiation can be occurring from outside of the reactor, called external illumination, as seen in Figure 23a, or from inside by the lamps immersed in the liquid, called internal illumination, in Figure 23b. External illumination can be occurring through one or more lamps and/or LEDs' strip placed inside the reactor in Figure 23a,b. In the case of packed-bed reactors, they generally have an annular geometry and they are illuminated by a central lamp to allow the harvesting of all the light released by the source (as in Figure 23c). However, it might have a limitation of having an incomplete irradiation of the photocatalyst because of the annular thickness. In addition to this, nonuniform liquid flow distribution might restrict the contact between the volume of water and the surface of a photocatalyst and as a consequence, the performances of the photoreactor are decreased. Compared to annular ones, photocatalytic reactors having flat plate geometry (Figure 23d–f) are easily scalable and they are able to be employed with the direct solar light. Therefore, they are very attractive for practical application [129].

Operating Conditions

Providing optimum temperature and pressure is an important criterion for a solar photoreactor. Heater tape is used for heating purposes. The solubility of CO_2 in water is really low, i.e., 1650 ppm at 25 °C in pure water [130]. Recirculating cooling water through the photoreactor setup to keep the reactor temperature at 0° C can enhance the solubility of CO_2.

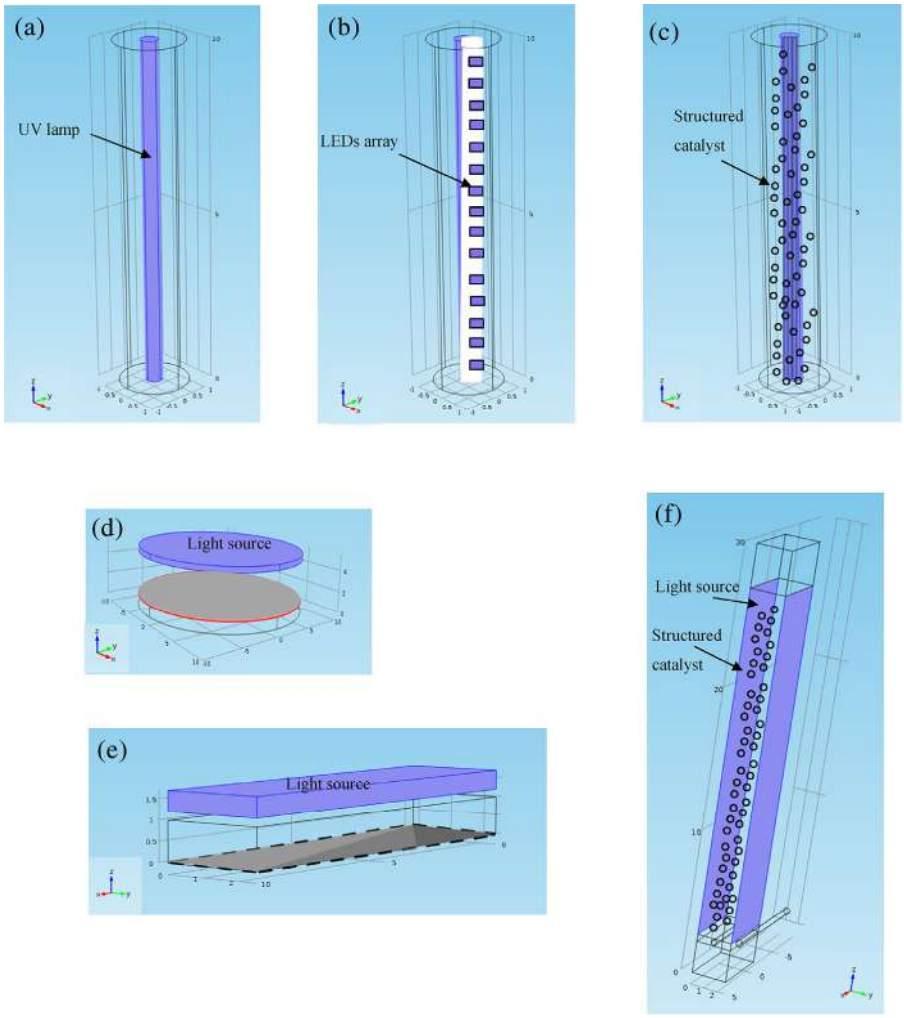

Figure 23. Examples of different photoreactor geometries: (**a**) Annular geometry irradiated by central lamp, (**b**) annular geometry irradiated by central light emitting diodes (LEDs), (**c**) annular packed-bed photocatalytic reactor, (**d**) parallel plate disk photoreactor, (**e**) flat plate photoreactor and (**f**) flat plate photocatalytic reactor filled with structured catalyst. Reproduced by kind permission of John Wiley and Sons from [129].

Even at the considerably higher temperature of 85 °C, the solubility of CO_2 can be addressed by having a high-pressure photoreactor in which the pressure is set to 7–20 bar in the liquid phase, as demonstrated in Figure 18 [97,98]. High productivity rates of products, such as H_2 at 51.2 mmol h^{-1} $kg_{cat}{}^{-1}$, CH_4 at 1.73 mmol h^{-1} $kg_{cat}{}^{-1}$ and organic compounds (in either liquid or gas phase) at 110 g C h^{-1} $kg_{cat}{}^{-1}$, have been recorded employing a Ag/TiO_2 photocatalyst [114]. Another work has demonstrated that the formation of liquid compounds was favoured by an increase in pressure. In the case of gaseous products, the initial formation rate is high because CO_2 is more soluble, but during the process of the reaction, this production rate is slowed down due to thermodynamic limitations [131].

Sanju et al. [132] demonstrated that the yield of the product is affected by relative humidity. Thin wafers composed of P-25 TiO_2, promoted with Cu or Pt nanoparticles, have been investigated for the gas-phase photoreduction of CO_2. Sputtered layers of Cu and Pt co-catalysts were applied to the wafer surface for increasing reaction rates, which were negligible in the absence of co-catalysts. The optimum loading of co-catalysts on the wafer surface was found to be approximately 9.6 at % of Cu and 8.7 at % Pt, whereas the presence of both co-catalysts enhanced the overall reaction rates. The influence of relative humidity (RH) on CO_2 reduction indicated that the maximum production of reduction products occurred at about RH of 55%. In these conditions, the yield was 20 ppm cm^{-2} h^{-1}

for methane and 9 ppm cm^{-2} h^{-1} for carbon monoxide for Cu-coated samples, and in the case of Pt-coated samples, the yield of methane was 32 ppm cm^{-2} h^{-1} under solar simulator AM 1.5 G irradiation, 100 mW cm^{-2}. The pressure was maintained close to the atmospheric pressure to carry out the photocatalytic reaction under ambient conditions.

3.6. Current Technologies for Concentrating Solar Systems

Concentrated solar power (CSP) is an electricity generation technology that focuses solar irradiance using heliostats onto a small area, known as the receiver. A heat transfer medium (currently a fluid) carries heat to the heat storage and power block. For the past decade, CSP has been highlighted as one of the promising and potential renewable and sustainable energy technologies. A review on recent opportunities from this point of view can be found in [133].

Solar concentrators can be a useful tool to increase the photons' flow inside the photoreactors, boosting productivity. The concentrating ratio significantly impacts the efficiency performance of solar photoreactors. In concentrating solar light photoreactors, it was observed that when increasing the concentrating ratio, the CH_4 yield increased at first and then lowered.

There are many different types of solar concentrating power plants, and most of them are found in solar fields. Existing solar concentrating devices can produce substantial heat at medium to high temperatures, which can be utilised to feed power blocks. The fundamental concept behind all the designs is to employ mirrors to effectively reflect and focus solar radiation in a specific area, which is called the receiver, and so high photon flow and/or high temperature could be reached in the focal area. A working fluid flows from the receiver, absorbing heat that could be used in the power production plant.

The concentration ratio (CR), which is a crucial parameter of solar concentrating technologies, is defined as the ratio of the solar field aperture (A_{field}, i.e., total effective area through which sunlight is captured in a solar field) to the receiver area ($A_{receiver}$), as shown below [134]:

$$CR = \frac{A_{field}}{A_{receiver}} \quad (4)$$

The concentration ratio plays a crucial role in determining the overall system performance, as it establishes the global system efficiency (η_{glob}). The optimal operating temperature of the receiver ($T_{r,opt}$) for the ideal scenario of a solar concentrating system incorporated with an ideal power engine (Carnot Cycle) can be found below [135]:

$$T_{r_{,opt}} = T_{am} \sqrt{1 + \frac{CRG_b\eta_{opt}}{U_L T_{am}}} \quad (5)$$

In this equation, the ambient temperature (T_{am}), the direct beam irradiation (G_b) and the collector thermal loss coefficient (U_L), which is considered as constant, are used for calculations. Equation (2) indicates that a higher concentration ratio results in a higher optimum receiver temperature and a study showed that [136] increasing the optimum receiver temperature enhances the global system efficiency. As a result, the concentration ratio is an important parameter, associated with the design of the solar concentrating systems. According to the concentrating image geometry, there are primarily two broad categories for solar concentrating technologies.

- Linear concentrating systems: The primary field of the mirrors has a linear pattern, and solar irradiation is concentrated within a narrow, linear region. The parabolic trough collector (PTC) and the linear Fresnel reflector (LFR) are the most representative solar concentrating technologies with linear configuration.
- Focal point concentrating systems: To maximise the concentration ratio and the operating temperature levels, the solar irradiation concentrates in a small area in comparison to the solar field. The primary reflectors generally have a circular pattern, and the solar

towers (STs) and solar dishes (SDs) are the most representative technologies. Some common designs couple dishes with Stirling engines.

The most common solar concentrating technologies are depicted in Figure 24. They are separated as the linear systems and the focal point systems. It is essential to point out that concentrating technologies greater than CR > 5 [137] are essentially imaging solar systems that utilise only direct solar beam irradiation. This value for linear technologies is generally within 10–50 [138], whereas in the focal point systems, it reaches up to 1000 [139]. Considering the working temperature, linear technologies are able to function at up to 400 °C using thermal oil as the working fluid [138], and up to 600 °C using molten salts [140]. However, focal point systems, particularly solar towers, could function up to 900 °C or even higher [141].

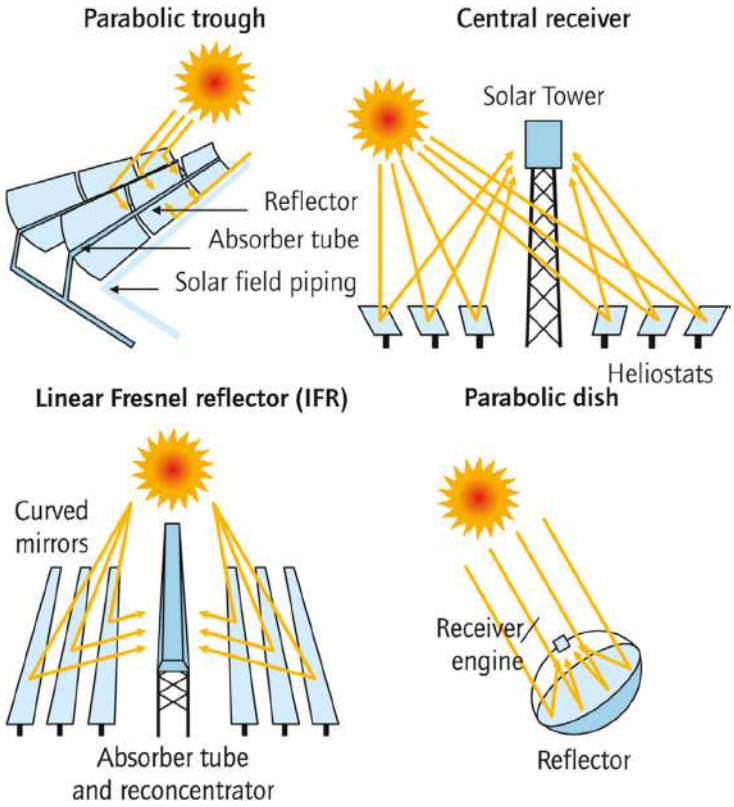

Figure 24. Conventional solar concentrating technologies. Reproduced by kind permission of Elsevier from [142,143].

A tracking mechanism must be used for the concentrating systems to operate effectively in order to accurately follow the "apparent path" of the sun. The linear technologies require a single-axis tracking system, whereas the focal point requires a two-axis tracking mechanism, which makes these technologies complex and expensive to realise and adapt to centralised facilities.

3.6.1. Basic Index Definitions for the Concentrating Solar Power Systems

From a more modelling-oriented point of view, it is worth mentioning the study by Faez Ali et al. [144] that focuses on the optical analysis of solar systems with secondary concentrators, compound parabolic concentrators (CPCs), and they evaluated designs both in the presence and absence of tracking mechanisms. A separate study reported in [145] worked on the two-stage concentrating systems by considering various geometries. The characterisation of the CSP systems and subsystems is dependent on some specific performance indexes, which are outlined in the present part.

The collector optical efficiency (η_{opt}) can be calculated as the proportion of the absorbed solar irradiation (Q_{abs}) by the receiver to the solar beam irradiation in the solar field (Q_{sol}):

$$\eta_{opt} = \frac{Q_{abs}}{Q_{sol}} \quad (6)$$

The optical efficiency (η_{opt}) can be computed based on several factors, typically expressed for a collector with two reflectors, a cover glass and a receiver, and is

$$\eta_{opt} = K\gamma r_1 r_2 \gamma a \quad (7)$$

in which the intercept factor (γ), the reflectance of the first reflector (ρ_1), the reflectance of the second reflector (ρ_2), the transmittance of the cover (τ) and the absorbance of the receiver (a) are considered in this equation.

The intercept factor is the proportion of the solar energy reaching the receiver opening (prior to the cover) to that reflected from the last mirror. The parameter K represents the collector's incident angle modifier, which accounts for the impact of solar rays' angles on the collector aperture [146].

The collector solar thermal efficiency (η_{th}) is described as the proportion of the heat production (Q_u) to the solar beam irradiation in the solar field (Q_{sol}):

$$\eta_{th} = \frac{Q_u}{Q_{sol}} \quad (8)$$

The thermodynamic cycle efficiency (η_{cycle}) that uses the useful heat from the solar system is calculated as the proportion of the produced electricity (P_{el}) to the heat input from the solar field in the system (Q_{in}), specifically in cases where a power unit is incorporated with the receiver.

$$\eta_{cycle} = \frac{P_{el}}{Q_{in}} = \frac{P_{chem}}{Q_{in}} \quad (9)$$

In the case analysed here in which a solar concentrator is coupled to a photochemical or photocatalytic transformation, P_{chem} can be defined as the amount of energy stored in the chemical compounds produced through the transformation in the receiver (chemical reactor). In turn, this can be calculated, e.g., from the lower heating values (LHVs) of the products, or by using a similar definition of the energy content of the products. Examples of such calculation are reported in [39,40].

$$P_{chem} = \sum_{i=1}^{n} \left(\text{mass of product i obtained from the reaction(kg)} \times LHV_i \left(\frac{kJ}{kg} \right) \right) \quad (10)$$

The storage system might have some thermal losses to the system. With the neglection of the storage capacity, the storage efficiency (η_{st}) could be calculated as follows:

$$\eta_{st} = \frac{Q_{in}}{Q_u} \quad (11)$$

The system efficiency (η_{sys}) can be defined as the produced electricity (P_{el}) to the solar irradiation in the solar field (Q_{sol}):

$$\eta_{sys} = \frac{P_{el}}{Q_{sol}} \quad (12)$$

3.6.2. Parabolic Trough Collector (PTC)

Among the developed solar concentrating technologies, a parabolic trough solar collector is quite common [147], for power production [148], solar cooling [149], desalination [150], industrial processes [151] and chemical processes [152]. The collector design features a bent reflector in a linear parabolic shape, whereas the receiver is typically an evacuated tube positioned in the focal point of the parabola. Convection thermal losses

between the absorber tube and the glass cover are reduced by evacuating the tube envelope and that provides high performance for operation at medium and high temperatures. Safe operation can be conducted by using, as a receiver thermo-vector fluid, a thermal oil (e.g., Therminol VP-1) up to 400 °C [153], or molten salts up to 550–600 °C [140]. Additionally, combining molten salts with the appropriate thermal storage system often consists of two storage tanks, one cold and one hot tank.

A PTC uses a single direction tracking system that follows the sun axially. Integrating the concentrating solar systems, particularly the trough concentrators, with the photoreactors is a possible strategy to increase the overall irradiation input. As an example, a study in the literature [154] constructed a large-scale photoreactor integrated with the parabolic trough concentrators (PTCs) for the pentachlorophenol degradation, accomplishing superior photocatalytic activity compared to a laboratorial scale [155]. Meanwhile, another study [64] used an optical fibre photoreactor under the concentrated solar light occurring by the dual-axis tracking Fresnel concentrators for the photoreduction of CO_2 since inserted fibre illuminating structure increases quantum efficiency [9]. Integrating the OFMR with a relatively high reaction density [14] and the trough concentrators, being a mature solar concentrating technique, holds promise for large-scale photocatalysis under solar light [156].

Nevertheless, some challenges remain in coupling concentrators with photoreactors, as mentioned below.

1. In a standard continuous photoreactor incorporated with a trough concentrator, the flow of reactants is perpendicular to the incoming irradiation, as illustrated in Figure 25a. Conversely, in the OFMR, both the flow direction and incident rays align parallel to the reaction channels with the internal fibres, illustrated in Figure 25b. The introduction of a monolith into a transparent tube-like concentrated solar photoreactor vertically may cause an increased pressure drop along with the flow direction and the decrement in mass transfer efficiency. Because of these reasons, the requirement of concentrated irradiative flux distribution for OFMR is different. In an OFMR, the orientation of the optical fibres is uniform; by this way, incident rays become more appropriate for the configuration while the compound parabolic concentrators (CPCs) and surface uniform concentrators (SUCs) are structured to give a uniform irradiative flux distribution around the surface of the tubular vessels [157].
2. The properties of the material for optical fibre restrict the use of the dish concentrators. The overheating of optical fibres with a dish concentrator creates a huge issue because of a high concentration ratio, as depicted in Figure 25, and the low melting point of the organic fibres in Figure 25d [158].
3. Another challenging issue for a dish concentrator irradiated system is to enhance the reaction capacity due to the shadowing effect of the monolith. Therefore, the concentrated flux of a high concentrating ratio needs long reacting channels. However, this leads to an increase in installation costs in high altitude for large monoliths.

Hence, photoreactor design is tailored to align with the geometrical and physical characteristics of the commercial ceramic monoliths and the PTC systems. Gas channels are incorporated along the gas flow direction, intersecting the reaction channels to minimise the pressure loss and enhance the mass transfer efficiency. As indicated in the literature [159], the reaction efficiency is directly related to the flow velocity within the reaction channels, leading to an unavoidable efficiency loss because of the side flow structure.

The fundamental configuration of the PTC combined with the OFMR resembles a standard PTC system used for thermal power generation, with the tubular receiver being replaced by honeycomb monoliths containing fibres as depicted in Figure 26. This photocatalytic reaction model includes various items such as light transmission, mass transfer and a photoreaction. The light transmission process is illustrated in Figure 27. The red rays, upon striking the parabolic trough concentrator, get reflected and concentrated onto the fibre ends. Then, they travel through the fibres (shown in pink) and exit from the sides for illuminating the monolith's internal surface coated with the photocatalyst uniformly.

The configuration is detailed and the fundamental elements are demonstrated in Figure 28. The photocatalytic reaction occurs on the internal walls, known as the reaction walls. The mass transfer driven by the creeping flow and species diffusion decreases the products' concentration, which makes the reversible reaction possible. The gas channels within the glass vessel are parallel to the main flow and penetrate the ceramic monolith, improve mass transfer efficiency and decrease the pressure drop without the need for catalyst coating. The mixture of reactants and products exits from the outlet after the reaction. The blocking effects of the optical fibres enable the air flow to the vertical directions, ensuring that the reaction surface is fully utilised to maximise the reaction capacity. The photocatalytic kinetic model was developed based on the outcomes of the OFMR experiments using $NiO/InTaO_4$ as a catalyst from a study [109]. Methanol was found as the major product when the photoreduction of CO_2 took place at room temperature with mercury lamps as a light source. However, when a Xenon lamp was used as a light source and the reaction temperature was increased to 70 °C, acetaldehyde was observed as a main product and high selectivity was reached. Xenon lamps' emission spectrum closely resembles sunlight and when coupled with a solar concentrator, the reaction temperature increases.

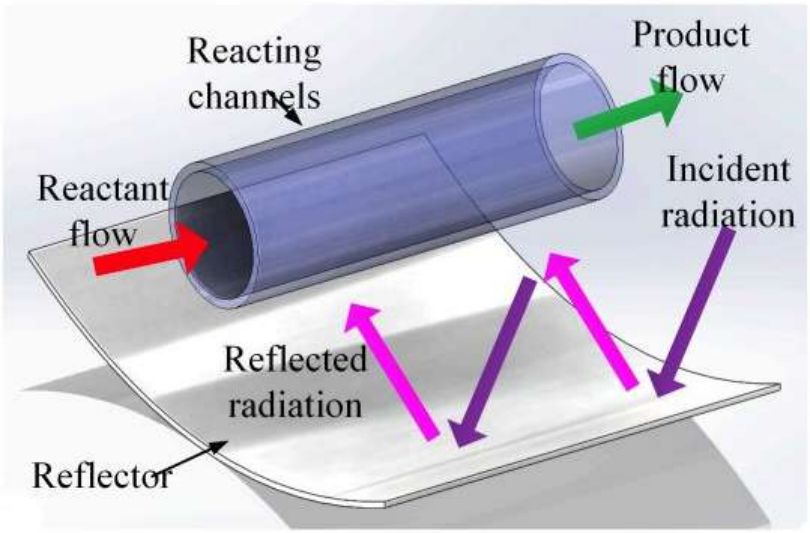

(**a**)

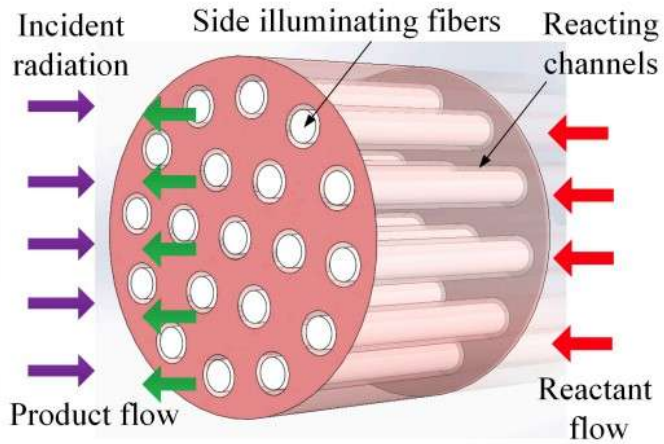

(**b**)

Figure 25. *Cont.*

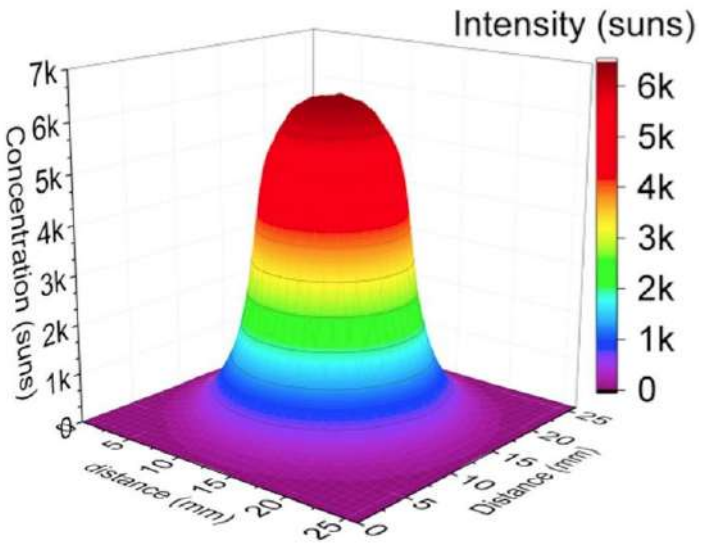

(**c**)

(**d**)

Figure 25. Schematics of (**a**) a continuous reactor integrated with a reflector and (**b**) OFMR, (**c**) a map of concentrated irradiative flux and (**d**) melted optical fibres in a point concentrating system. Readapted from [68,160] and reproduced under the Creative Commons licence from [68].

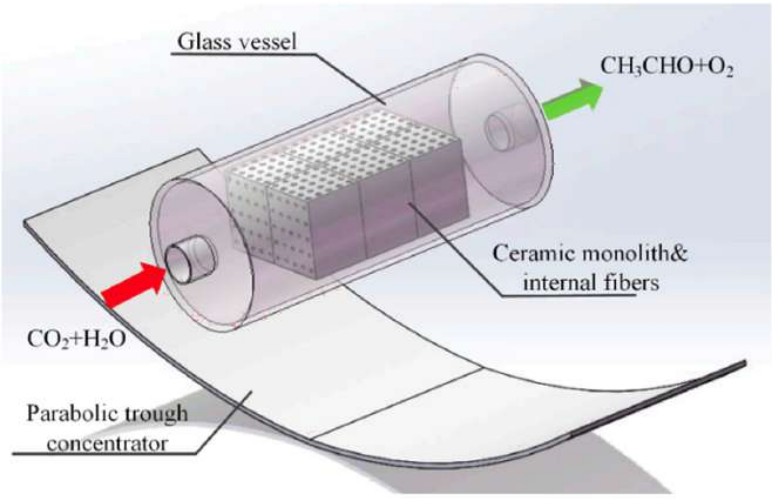

Figure 26. Schematics of OFMR (optical fibre monolith reactor) coupled with PTC system. Reproduced under the Creative Commons licence from [68].

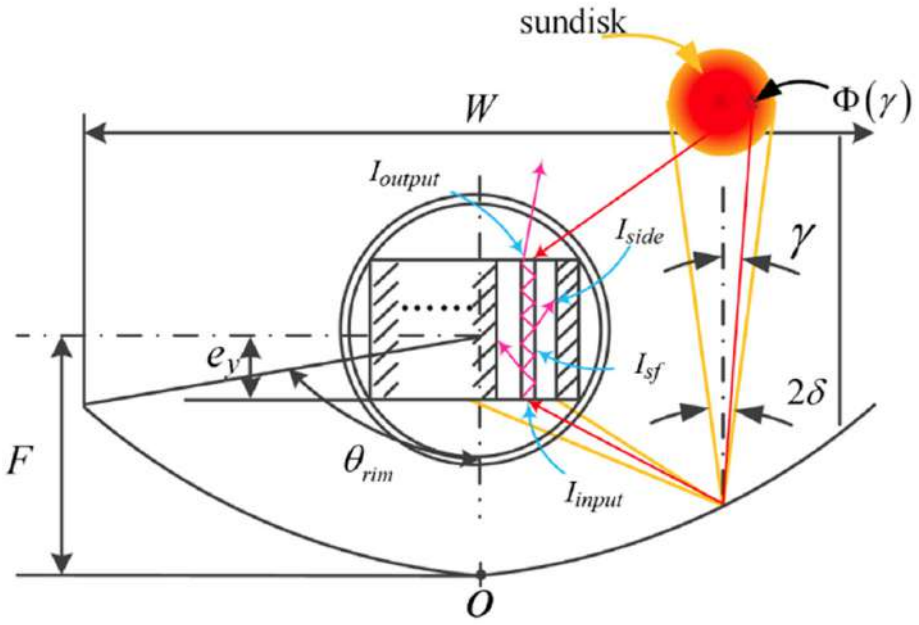

Figure 27. A diagram illustrating the transmission of rays through the optical fibre in a monolith channel. Reproduced under the Creative Commons licence from [68].

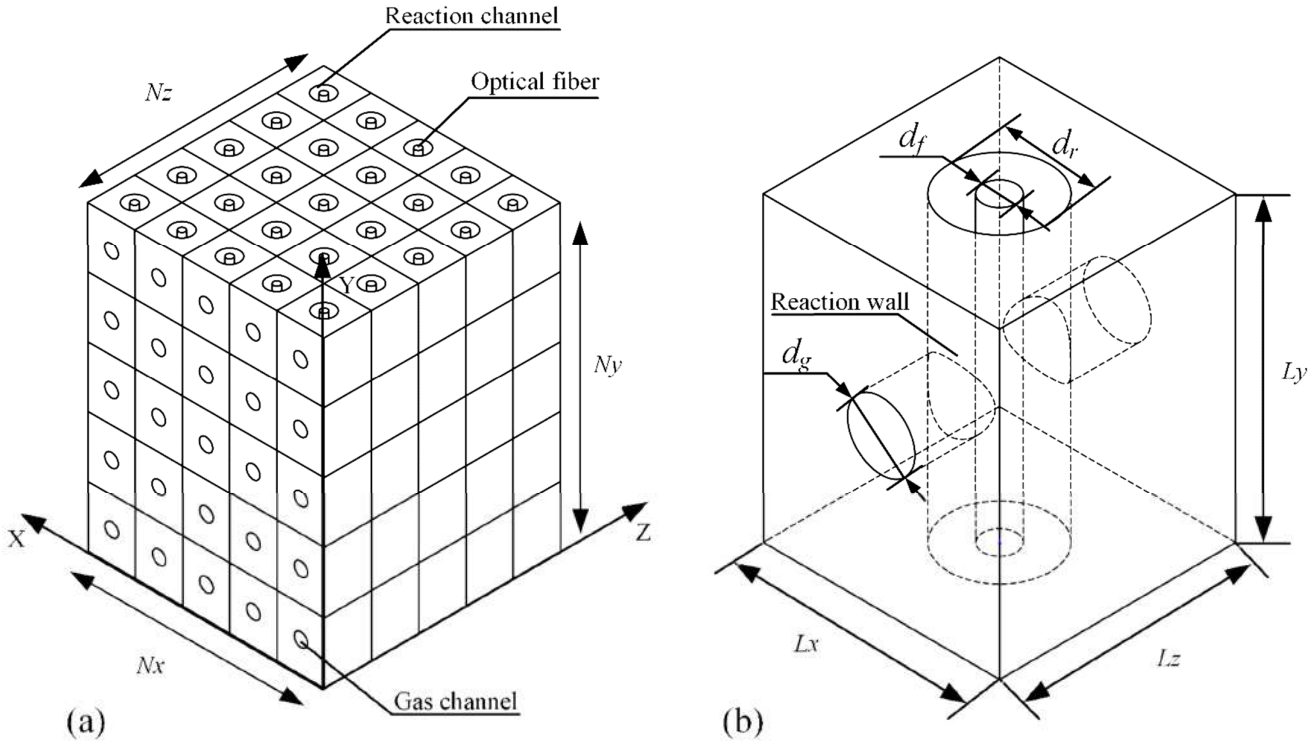

Figure 28. Schematics of the (**a**) monolith area partition and (**b**) fundamental element. Reproduced under the Creative Commons licence from [68].

Martin-Sómer et al. [161] studied to enhance the efficiency of utilising solar light for different UV-based photochemical water treatment processes. A comparative analysis was conducted between utilising sunlight directly in advanced compound parabolic collector (CPC) photoreactors and employing solar energy for generating electricity to power LED lighting sources. Seven different solar processes (CPC, PV-UVA LED, PV-UVC LED, CPC + TiO_2, CPC + H_2O_2, LED + TiO_2 and PV-UVC LED + H_2O_2) were examined, for their efficacy in both chemical oxidation and bacterial deactivation. UVC photons are more efficient

photochemically compared to UVA and solar irradiation, particularly in antibacterial and the oxidation processes. However, the low electrical efficiency of current UVC LED sources leads to a limited global efficiency in the use of solar light by its integration with PV power systems. The CPC + TiO_2 process showed a higher efficiency for the oxidation of chemicals while PV-UVC LED + H_2O_2 was found as the most efficient for the bacterial inactivation.

In addition to these, Muñoz-Flores et al. [162] investigated the photocatalytic activity at a laboratory scale by using a slurry photoreactor and also a pilot scale by using a compound parabolic trough reactor (CPC). Carbon-containing Cu-based materials were employed as a photocatalyst for the degradation of an azo-dye (tartrazine, also known as Y5), commonly employed in the food industry. The photocatalytic studies for the degradation of tartrazine were performed in a slurry photoreactor (Pyrex, total volume ca. 250 mL) under artificial solar light provided by a solar simulator (1950 W m^{-2}) with 7 h of irradiation at a laboratory scale. Furthermore, they were conducted in a pilot plant that is featured with a concentrating parabolic collector (CPC) exposed to natural solar irradiation for 10 h. A catalyst exhibited a strong photocatalytic activity compared to other metallic semiconductors presented in the existing literature. The optimisation of important operating factors in the slurry reactor under artificial solar light revealed an enhanced activity at low initial dye concentrations and low catalyst loadings. The catalyst demonstrated superior photocatalytic activity in a CPC photoreactor under moderate photon flux from natural sunlight. The results indicated that the photon flux plays a crucial role in the photodegradation process of Y5. The high irradiation levels of the solar simulator compared to the natural light in the CPC resulted in lower catalytic activity, possibly due to increased charge carrier recombination and catalyst degradation under varying irradiation conditions.

Reyes-García [163] studied radiation absorption and hydrodynamic analyses of monolithic photocatalysts used in water treatment within a CPC solar reactor. The study involved examining radiative transfer and hydrodynamic analyses to obtain the performance of solid macroscopic materials that are TiO_2 monoliths, in a CPC solar reactor. Monte Carlo simulations were used to calculate the absorbed photonic flux distribution for various monolith geometries: including asterisk and flower shapes. Various numbers of arms are considered for asterisk structure. It was observed that a five-lobe asterisk shape demonstrates the greater result: 9.6% higher power absorption, 40% larger surface area for interaction with water and 78% lower friction. In addition, it indicated that the optical activity was not significantly influenced by the level of specularity of the catalyst surface and was only minimally impacted by the positioning of the piece.

3.6.3. Linear Fresnel Reflector (LFR)

Another linear concentrating technology that is competitive with a parabolic trough collector is the linear Fresnel reflector. Due to similar working temperatures and similar concentration ratios between these two technologies, an LFR can be employed in areas where a PTC is currently being used. LFR technology is based on the use of primary segmented reflectors, which focus the incoming solar irradiation onto a receiver that is positioned several meters above the ground. These reflectors can be flat or curved [164]. In order to capture as much of the reflected solar rays as possible and redirect them to the absorbing area, a secondary reflector (or cavity) surrounds the absorber (which consists of one or more tubes, especially in the case of the evacuated tube). An LFR has some benefits and drawbacks compared to the PTC due to the different design that they have.

The primary drawback of an LFR is its lower efficiency in comparison to the PTC due to high optical losses. Especially, the segmented primary receivers, in particular, contribute to additional optical losses due to blocking and shadowing effects [165,166]. Additionally, the necessity of having a secondary reflector results in some additional losses to the system. Nevertheless, the greater separation between the receiver and the ground in an LFR, compared to the distance (receiver-down parabola) in the PTC, leads to increased optical losses for an LFR. There are some appealing approaches to handle this

problem in the literature, such as the displacement of the receiver or the inclination of the primary reflectors. Also, innovative tracking techniques can be applied to improve optical performance in a small-scale LFR.

Conversely, an LFR has some benefits for making itself a compelling technology. The primary benefit is the reduced investment cost in comparison to the PTC. According to the research, the LFR must have an investment cost that is up to 67% lower than the PTC investment cost in order to be an economically suitable option. Additionally, because the primary reflectors are positioned close to the ground, the LFR is subjected to lower wind loads. Another benefit stems from using a stable receiver that remains stationary, like in the PTC. Having this advantage, system complexity decreases, and thus minimises the risk of working fluid leakage [167].

Fang, et al. [168] proved that the reaction rate is significantly increased by large Fresnel lens (diameter = 1 m) concentrating solar light technology. As shown in Figure 29, CO_2 photoreduction with H_2O was performed in a self-made concentrating light reactor system. The automated tracing mechanism comprises a motor, a controller and a sensor, ensuring that the solar light is perpendicular to both the lens and the catalyst. Approximately 0.05 g of a catalyst was used. The catalyst preparation presented as a disc shape and was inserted into the reactor. A k-type thermocouple was inserted in a hole in the reactor wall to show the temperature, making contact with the upper surface of the catalyst.

Figure 29. The concentrating reactor system. 1. Concentrating mirror; 2. Reactor; 3. Sensor for tracing sun; 4. Controller; 5. Motor. Reproduced by kind permission of Elsevier from [168].

At the end of the reaction, for the photoreduction of CO_2, the CH_4 production rate reached 3.2 mol kg^{-1} h^{-1}, the C_2H_4 rate reached 0.51 mol kg^{-1} h^{-1} and the C_2H_6 rate reached 1.3 mol kg^{-1} h^{-1} and the CO_2 conversion achieved 3.94%. The overall solar-to-chemical energy conversion efficiency was 0.15%. The light intensity calculated based on Hangzhou light intensity on experimental days was 60 mW/cm^2 [168].

On the other hand, Zhang et al. [169] studied the design of a novel solar energy controllable linear Fresnel photoreactor (LFP) for achieving higher efficiency photocatalytic wastewater treatment under real weather conditions. The LFP could successfully adjust sunlight by controlling 6 mirrors considering solar position and weather conditions. In the

comparative experiments between the LFP and Inclined Plate Collector (IPC) as a control reactor, which passively receives sunlight, the Rhodamine B degradation efficiencies in the LFP were 2.19-fold, 1.5-fold and 2.28-fold higher than a control under the temporarily overcast, totally overcast to slightly overcast and sunny conditions, respectively. Moreover, yearly estimates suggest that the LFP can optimise light irradiance and temperature in densely populated areas, leading to high-efficiency wastewater treatment. These results demonstrate the potential of the LFP as an effective, energy-controllable reactor for green wastewater treatment, thereby enhancing the global public health.

3.6.4. Solar Towers

A solar tower, also known as a central system, is a type of concentrating technology that is primarily used in high-temperature power generating applications [167]. Typically, it is used in systems with relatively high-power capacity, where it is necessary to have a significant land extension available. Additionally, it is noteworthy that the technology is able to function with a quite high concentration ratio, up to 1000, and this fact explains the capability of operation at high temperature [170]. In the presence of primary segmented reflectors, it is possible to track the sun in two directions to follow its apparent path properly. The incident beam irradiation is concentrated by all of the primary mirrors at the solar tower into an area at the solar tower, where high temperature is created. Primary reflector choice is essential since they account for 40–50% of the system investment cost [171]. In addition to this, having small heliostats gives the benefit of high optical performance due to minimal shading and blocking effects, while also moderating wind loads to a certain extent. Typically, vertical pipes that serve as heat exchangers are inserted inside tubular receivers. Practically, heat exchangers are in charge of transferring the absorbed solar energy to the heat transfer fluid in order to valorise heat [171]. It is important to state that the tower can reach heights of 100–300 m [172]. The solar tower functions at extremely high temperatures and so it needs to use proper fluids. For operating up to 550 °C and integrating the system with a Rankine cycle, molten salts or water/steam working fluids are typically used. In the case of higher temperatures, gas working fluids or particle-based systems should be chosen and so Brayton cycles can be employed in the power generation unit. Currently, operating commercial tower plants utilise either direct steam generation or, more commonly, molten salts. These concentrating towers can reach high temperatures, enhancing the efficiency of converting heat into electricity and lowering the costs associated with thermal energy storage [133].

No direct application of solar tower concentrators to photoreactors has been reported until now. Nevertheless, the production of renewable electricity can be coupled with traditionally irradiated photoreactors with UV-Vis lamps in order to erogate the power supply.

3.6.5. Solar Dish

The focal point configuration of a solar dish concentrator allows for very high concentration ratios of up to 1000 or more [173]. To produce a comparatively uniform heat flux distribution, they consist of a concentrator with a receiver positioned either higher or lower than the focal point. For power production, solar dishes are typically coupled with a concentrator with a highly effective Stirling engine [174]. Additionally, there are several alternative uses for solar dishes that employ cavity receivers for the generation of heat. The goal of a cavity receiver is to gather solar irradiation and then reroute it into the receiver through multiple reflections. In addition, they maintain high temperatures in the area near to the receiver, which lowers thermal losses. In order to keep the heat energy inside, the outside is typically insulated. The cavity receiver also enhances the uniform distribution of heat flux across the absorber. Cavity receivers are appropriately constructed with optimised geometries, leading to various designs named hemispherical [175], cylindrical [176], conical [177], rectangular [178], hetero-conical [179], cylindro-conical [180], etc. Coil tubes with small diameters are installed inside the cavity receivers. These receivers have been studied for various applications such as power production, solar cooling, heating

production and desalination as documented in the literature [181–184]. A solar concentrator dish is illustrated, e.g., in Figure 30 [185].

Figure 30. Solar dish concentrator. Reproduced by kind permission of Elsevier from [185].

Critical issues for the application of concentration technology to photoreactors is that high-concentration factors bring about a significant increase in temperature. This is typically detrimental to photocatalysis due to the enhancement in dissipative effects while increasing temperature, even though this point has been explored in classical photocatalytic applications, only in a very narrow temperature range just over room temperature. Therefore, the effect of higher temperature still needs a considerable deepened understanding. Overall, it could be interesting to decouple the heating effects and the ones of enhanced irradiance (i.e., photons' availability over the photoactive material).

A study [186] focused on the geometry of solar farms, and tried to achieve an optimum configuration to cool down the solar panels naturally. Each solar plant was individually designed to maximise solar exposure and adapt to its surroundings. As an example, the angle of solar panels adjusts according to the latitude and their height is tailored to the local vegetation. The spacing between rows is typically determined by suitable land area. These factors influence how wind flows over the solar farm, affecting heat dissipation from the panels. The authors performed wind tunnel tests and simulations and analysed operating data to validate their model. Additionally, they also studied how varying the height, row spacing and angle of the panels affected the photovoltaic heating and cooling system. Enhancing the height of solar cells and the spacing between rows led to a 2% to 3% increase in power input. The study highlights the importance of considering the unique configuration of solar farms for estimating cooling and enhancing their efficiency.

3.6.6. Solar Light Concentrator

The types of the solar concentrators that can be adapted to photoreactors are

- Parabolic concentrator.
- Hyperboloid concentrator.
- Fresnel lens concentrator.
- Compound parabolic concentrator (CPC).
- Dielectric totally internally reflecting concentrator (DTIRC).
- Flat high concentration devices.
- Quantum dot concentrator (QDC).

These concentrators can also be categorised according to their optical properties as is shown in Table 4.

Table 4. Types of solar concentrators applied to boost photovoltaic cell devices and applicable to photoreactors [187].

Type	Description
Reflector	Upon hitting the concentrator, the sun rays will be reflected to the PV cell. Example: Parabolic Trough, Parabolic Dish, CPC Trough, Hyperboloid Concentrator.
Refractor	Upon hitting the concentrator, the sun rays will be refracted to the PV cell. Example: Fresnel Lens Concentrator.
Hybrid	Upon hitting the concentrator, the sun rays can experience both reflection and refraction before hitting the PV cell. Example: DTIRC, Flat High Concentration Devices.
Luminescent	The photons will experience total internal reflection and be guided to the PV cell. Example: QDC.

The solar irradiation power and solar spectrum could be highly variable depending on latitude, longitude, date, time, pollution and meteorological conditions. The wavelength should be set under the range of the solar spectrum if there is artificial/stimulating solar irradiation usage [7]. Mirrors, reflectors, collectors and windows are usually used as implements to harvest solar radiation. The aim of their usage is to transform solar light irradiation into usable energy. A photochemical solar collector is demonstrated in Figure 31. It was used to test the photoreduction of CO_2 under solar light and led to the formation of HCOOH, HCHO, CH_3OH, CH_3CHO and C_2H_5OH [188]. However, the overall solar-to-chemical (STC) efficiency was low because of the reverse reactions catalysed by oxide semiconductors. The schematic diagram demonstrating the solar photoreduction of CO_2 using (a) direct sunlight, (b) flat sheet reflectors, (c) a compound parabola and (d) Fresnel lens is also summarised. CO_2 photoreduction has enhanced about 0.15% as the total STC efficiency in the presence of Fresnel lens [168].

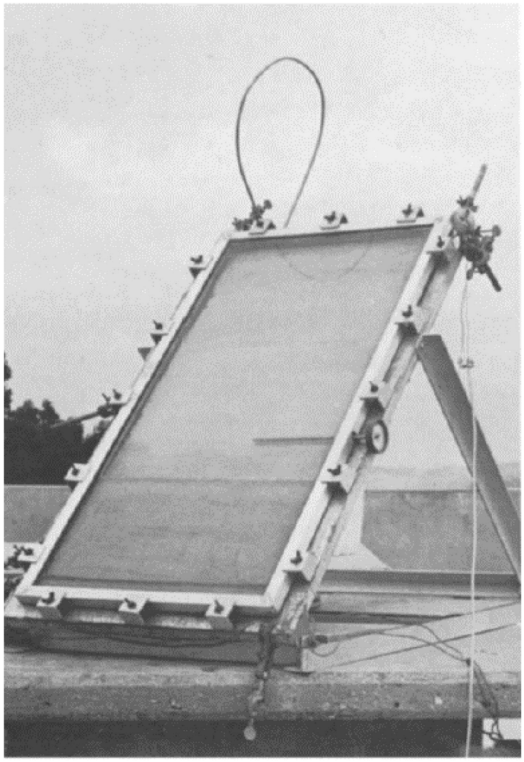

Figure 31. Photochemical solar collector. Reproduced by kind permission of Elsevier from [7,188].

A study reported in [61] used CdS nanosheets decorated with Mn_2O_3 nanoparticles as a photocatalyst in a solar photocatalytic reactor with a Fresnel lens concentrator in an area of 560 cm^2; formic acid was found as the primary product with a production rate of 1392.3 $\mu molg_{cat}^{-1}$ h^{-1}. The increase in CO_2 conversion efficiency (CCE) (%) varies with reflectors and the concentrator demonstrates that the design of the reactor plays a significant role in maximising light harvesting for this process, aside from the chemical properties of the catalysts (Figure 32).

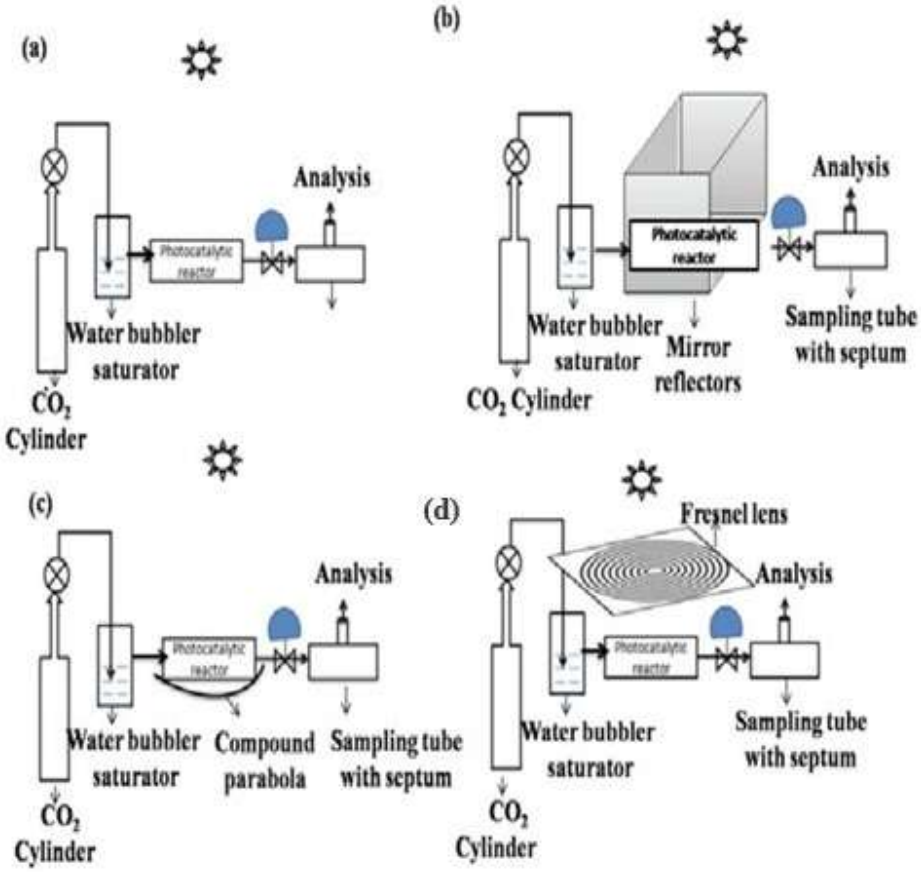

Figure 32. Solar photoreduction of CO_2; (**a**) direct sunlight, (**b**) flat sheet mirror reflectors, (**c**) compound parabola, (**d**) Fresnel lens. Reproduced by kind permission of Elsevier from [61].

Table 5 summarises how different parameters affect the performance of a solar photoreactor. It should be considered that the yield achieved significantly depends on different reaction conditions. The radiant energy transfer along with the photocatalyst site efficiently utilise radiant energy, prolong the lifetime of electrons and holes and use an effective photocatalyst; appropriate interaction between reactants, photoreactor geometry and operating conditions should be optimised to achieve a high formation rate of products. The light harvesting efficiency, termed as photocatalytic efficiency, PCE (%), and CO_2 conversion efficiency, CCE (%), were exhibited based on 1 g of the catalyst for 1 h of the reaction and they are evaluated by using the equations below [61]:

$$\mathrm{PCE}(\%) = \frac{\text{Energy value of organic produced}}{\text{Energy incident on the reactor}} * 100 \quad (13)$$

$$\text{Energy value of organics produced} = \mathrm{DG0} * \text{moles of fuels produced} \quad (14)$$

$$\mathrm{CCE}(\%) = \frac{\text{Moles of C} - \text{products obtained}}{\text{Moles of } CO_2 \text{ passed into the reactor}} * 100 \quad (15)$$

Table 5. Summary of the effect of parameters on the performance of solar photoreactor. Readapted from [7].

Influencing Parameter	Solar Photoreactor	Parameter and Photocatalyst	Product and Yield	Comments	Reference
Reactor configuration	Photoreactor	T = 23 °C, 0.5 g catalyst/300 mL solution; photolyte depth—36.7 mm	Traces of H_2	The catalyst got attached to the reactor windows, which blocked the light irradiation and resulted in low hydrogen production	[128]
	Modified photoreactor	T = 23 °C, 0.5 g catalyst/300 mL solution; photolyte depth—36.7 mm	H_2 = 58 mL/h	Increased H_2 production due to the high degree of mixing, avoiding formation of dead zones, particle settlement, and accumulation in the modified photoreactor	[128]
	Fresnel lens concentrated solar light photoreactor	T = 659.6 °C, P = 1.1 MPa, CR: −800; 250 mg TiO_2	CH_4 = 3157.2 μmol g^{-1} h^{-1}, C_2H_4 = 511.5 μmol g^{-1} h^{-1}; C_2H_6 = 1346 μmol g^{-1} h^{-1}; CH_3OH = 14.5 μmol g^{-1}	Incrementing the temperature and pressure of carbon dioxide along with water was enhanced to achieve a 3.94% CO_2 reduction	[168]
	Twin photoreactor	pH = 2.5; T = 333 K, P = 20 atm	CH_3OH = 14.5 μmol g^{-1}	An increment in the temperature, as well as pressure, is responsible for the gradual rise in the methanol production	[189]
	Photoreactor	Irradiance: 40 W m^{-2}; reaction time: 4 h; T = 40 °C	CH_4 = 28.5 μmol g^{-1}	Using low irradiance reaction time and temperature significantly affected methane production	[190]
Operating condition	Solar photoelectrochemical	T = 298 K; pH = 2.5; reaction time: 6 h	HCOOH = 1.55 μM; HCOH = 0.62 μM; CH_3OH = 2.02 μM; CH_4 = 2.16 μM	Product concentration increased with reaction time	[191]
	High-pressure photoreactor	T = 85 °C; P= 20 bar	H_2 = 51.2 mmol $h^{-1}kg_{cat}{}^{-1}$; CH_4 = 1.73 mmol $h^{-1}kg_{cat}{}^{-1}$; HCOOH&CH_3OH = 110 g C $h^{-1}kg_{cat}{}^{-1}$	An increment in pressure favoured the production of liquid products but it showed a decrement in gaseous product formation	[120]
	High-pressure photoreactor	T = 90 °C, P = 19 bar; pH = 11.4	CH_4 = 8.5 mmol $h^{-1}kg_{cat}{}^{-1}$; HCOOH&HCHO= 110 g C. h^{-1} $kg_{cat}{}^{-1}$	An increment in pressure favoured the production of liquid products but it showed a decrement in gaseous product formation	[114]
	Concentrating solar light photoreactor	Pt/TiO_2; CR = 38.2; P = 1 MPa; 7 h irradiation	CH_4 = 20.55 μmol g^{-1}	There is a variation in the methane yield with the concentration ratio as it increased initially, followed by a reduction in the production rate	[131]
	Photochemical solar collector	Rectangular plate area = (1 m × 0.5 m); thickness = 3 mm; 40–60 g/m^2 of $SrTiO_3$	HCOOH = 0.273 μmol kJ^{-1}; HCHO = 0.0154 μmol kJ^{-1}; CH_3OH = 0.0193 μmol kJ^{-1}	The overall STC efficiency obtained was low due to the reverse reactions of catalytic oxidation of the organic products on the oxide semiconductors	[188]
	CPC photoreactor	Non-truncated type; orientation: east–west; horizontal angle: 25°, CR: 4.22	H_2 = 7.14 L.h^{-1}	0.087% of average energy conversion efficiency is reported as more diffuse as well as reflected radiation being absorbed by the CPC photoreactor	[192]

Table 5. *Cont.*

Influencing Parameter	Solar Photoreactor	Parameter and Photocatalyst	Product and Yield	Comments	Reference
Solar light concentrator	Solar photocatalytic reactor	Flat sheet mirror reflectors −30 cm × 30 cm; reactor volume: 25 cm^3; continuous; reaction time: 1 h; 1 g of CdS catalyst	C_2H_5OH = 2.6 µmol $g_{cat}{}^{-1}.h^{-1}$; HCOOH = 225.7 µmol $g_{cat}{}^{-1}$ h^{-1}	Flat sheet reflectors did not result in greater CO_2 conversion to C_2H_5OH but showed a rise in HCOOH formation rate	
				Photocatalytic efficiency (PCE) (%) = 0.0005%	
				CO_2 conversion efficiency (CCE) (%) = 3.31%	[61]
	Solar photocatalytic reactor	Compound parabola, 100 mirror strips; width: 1.5 cm; length: 45 cm; reactor volume: 25 cm^3; continuous; reaction time: 1 h; 1 g of CdS catalyst	C_2H_5OH = 24.5 µmol $g_{cat}{}^{-1}$ h^{-1}; HCOOH = 777.8 µmol $g_{cat}{}^{-1}$ h^{-1}	Using CPC has increased the temperature in the photoreactor, which has increased product yield, PCE = 0.0024%; CCE = 11.99%	[61]
	Solar photocatalytic reactor	Fresnel lens diameter = 8 cm; 560 cm^2 area; reactor: 25 cm^3; continuous; reaction time: 1 h; 1 g of CdS/MnO_3 catalyst	C_2H_5OH = 52.2 µmol $g_{cat}{}^{-1}$ h^{-1}; HCOOH = 1392.3 µmol $g_{cat}{}^{-1}$ h^{-1}; H_2 = 2766 µmol $gcat^{-1}$ h^{-1}	High product yield, PCE = 0.195%; CCE = 23.08%	[61]

3.7. New Solar Concentrating Technologies

In recent years, the average levelized cost of electricity (LCOE) for concentrating solar power (CSP) has sharply decreased from EUR 0.36 to 0.11 kWh^{-1}, appearing as a 68% reduction [193]. Still, when comparing CSP to other renewable sources such as PV, which has an LCOE of approximately EUR 0.05 kWh^{-1}, and onshore wind energy at EUR 0.03 kWh^{-1}, it is not the optimum choice from an economical point of view. Cost reduction is therefore essential for an improvement in CSP. An alternative approach for further enhancement in CSP involves producing solar fuels such as hydrogen production. This method enables various seasonal storage, by being converted to solar fuels in summer and used throughout the year.

Moreover, the key considerations for the new design include minimising material usage, enhancing performance, reducing wind loads, mitigating thermal stresses that could lead to component failure, increasing safety by reducing different risks (such as fire, leakage, etc.) and developing innovative and efficient storage methods for long-term operation.

A possible solution for those critical challenges can be met with the configuration of the BD-CSP. The concept behind this technology comes from the old technology of the "Gassegrain reflector" that has an application in a telescope [194]. In the configuration, there are two or three reflecting surfaces redirecting the solar beam irradiation to a ground-based receiver. This approach can be integrated into current solar concentrating technologies to develop new-generation CSP. Moreover, it has considerable potential in concentrating photovoltaics (CPV), particularly when combined with solar filtering.

The beam-down (BD) design concentrates the solar irradiation onto the ground, ensuring that the heat transfer fluid remains in a stable arrangement near the ground. This enhances safety standards and can result in a reliable and cost-effective design. Moreover, the working fluid remains near the ground and does not need to be carried to significant height. It does not have the need to be transferred to a great height, so pumping duty is reduced, which makes the process advantageous considering the design and the economics [195]. Furthermore, the overall height of the system is reduced, resulting in a more compact solar unit. This reduction in material usage such as a decreased need for construction support contributes to lower total system costs. Reduced height also reduces wind

loads, allowing for the use of lightweight construction that has high reliability. In addition, the beam-down concept facilitates a more uniform heat flux distribution over the absorber through multiple reflections and the proper design. Another potential improvement in the technology involves utilising fluidised beds and chemical reactors in the receiver location to produce solar fuels.

The most representative example is under construction in China, called "Yumen Xinneng/Xinchen 50 MW BD-CSP" (Figure 33) [196].

Figure 33. The beam-down CSP in Yumen Xinneng/Xinchen. Reproduced by kind permission of Elsevier from [196].

This unit uses molten salt at 570 °C for feeding a water/steam Rankine cycle of 50 MW_{el} nominal electrical power. It was assessed that the LCOE is going to be approximately EUR 0.11 kWh^{-1}, which is a remarkable value for the first real plant in this category. An alternative instance is the beam-down solar platform of 100 kW at the Masdar Institute of Science and Technology [197,198]. This plant utilises molten salt at 250–550 °C and it is possible to reach up to a concentration ratio of 600 suns. In addition, another plant is located at the University of Miyazaki [199] and it is a BD technology incorporated with a thermochemical water splitting reactor; the solar heat flux on the absorber can achieve up to 110 kW_{th} at noon, while it is capable of approximately 90 kW_{th} for 3 h per day.

3.8. Beam-Down Concentrating Systems

Rabl [200] originally proposed the concept of beam-down solar concentrating technology in 1976. He emphasised the fundamental geometrical aspects of utilising an upper reflector for redirecting the solar rays into the ground. He coined to this concept a "tower reflector", noting its advantage in facilitating heat transfer by placing the receiver near the ground, thus restricting the need to move the working fluid to great heights as in the conventional solar tower design. Subsequent developments in the literature expanded upon the beam-down concept in various solar concentrating categories, leading to the evolution of CSP. This section presents different geometric designs of the beam-down configurations based on (a) the solar tower, (b) the disc concentrators, (c) the PTC and (d) the LFR.

One of the most common solar concentrating technologies for power production is the solar tower and it has a wide application in the concept of BD technology. The main benefit of the concept is the solar tower height decrement, which has an important value

for the sustainability of the system. Additionally, the location of the absorber is close to the ground and that provides a crucial opportunity of dramatically reducing the piping length and the pressure losses, while raising safety standards. Additionally, the BD configurations can achieve high concentration ratios, enabling the operation at elevated temperature levels [201].

The key point that was focused on is the performance comparison between the conventional and beam-down technology towers. A study reported in [202] makes the comparison of conventional and beam-down technology towers and reached the conclusion that in larger solar fields, the beam-down technology is more efficient. In addition, Kribus [203] conducted one of the initial investigations into the optical analysis of BD solar units. It was observed that the tower height is a crucial factor that might have some problem about dimensioning. Also, they highlighted the necessity for extra optimisation parameters due to the complexity of the beam-down design.

Another consideration is the configuration of the BD-ST, regarding the structure of the "upper reflector" or "tower reflector". The ellipsoidal and the hyperboloidal patterns are the most comparable ones.

A study [204] demonstrated that the hyperboloid design offers several benefits including the ability to use a reduced system height and smaller primary reflectors. In addition, it is noted that in the hyperboloid design, the proper location of the optical axis is indicated southward, whereas in elliptical design, it is indicated northward. Therefore, the next step involves determining the appropriate design for the receiver cavity located near the ground. This cavity is crucial for maximising the capture of solar rays and redirecting them to the receiver while reducing thermal losses. However, several key design considerations should be taken into account for optimising the system. Especially, reducing the height of the reflector tower increases the apparent size of the sun image on the receiver, requiring a larger cavity aperture [205]. Nonetheless, increasing the cavity aperture raises costs and reduces final concentration on the receiver.

In the ultimate configuration of the system, two crucial factors need to be addressed. The primary consideration is the optimal shaping of the cavity, typically a compound parabolic (CPC) shape with a minor sacrifice in efficiency. A study has shown that a 10% reduction in the area of the tower reflector leads to a 2.7% decrease in absorbed energy, whereas a 37% reduction in the area of the cavity reflector (CPC) results in a 1.1% reduction in absorbed energy by the receiver [206]. Therefore, it is more effective to decrease the CPC area for achieving a relatively small decrease in energy absorption. This is particularly relevant due to the significantly higher cost of CPCs, which is about 4–5 times greater than heliostat costs [206], partly because active cooling is required for the mirror surface [207]. To achieve the most cost-effective and geometrically optimised BD system, it is essential to conduct a thorough optimisation of the absorber area. Another important aspect of this configuration is the position of the CPC in comparison to the focal point of the incident sun rays. The CPC inlet was traditionally placed near the focal point; however, it was suggested that optimising its position in the CPC could result in greater energy absorption of 20% [208] to 26% [209]. Considering heliostat size, using less heliostats with larger apertures allows for the design of a hyperboloid reflector with lower eccentricity. This improves the concentrating ratio and reduces the system height [210].

There are some other studies that have been focused on alternative designs aiming to have the optical optimisation of BD-ST. As an example, the use of flat tower reflectors could be a different alternative to decrease the spread of solar irradiation. Cannavaro et al. [211] focused on the designing of the tower reflector geometry by using an etendue-matched strategy. This arrangement aims to redirect the solar rays efficiently to the absorber with minimal re-reflections. It has been identified as a favourable choice for low-latitude locations, achieving yearly optical efficiency up to 52%. Li et al. [212] suggested to use a rotating tower reflector. The system can achieve an immediate optical efficiency of 51%, with an optical efficiency ranging from 37% to 46% based on the tilt angle of the tower reflector (Figure 34).

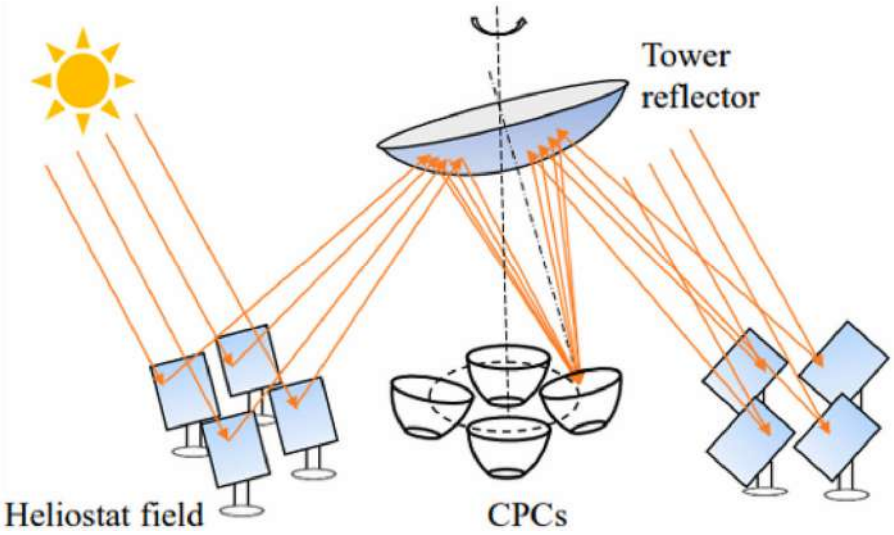

Figure 34. A beam-down solar tower configuration with a rotating tower reflector and four absorbers with a CPC cavity. Reproduced under the Creative Commons licence by Optica Publishing Group from [212].

Figure 35 demonstrates an example of a receiver with a CPC cavity. It is designed to operate with molten salt, incorporating insulation and suitable channelling for the molten salt flow. This arrangement was developed in the Solar Hybrid Fuel Project of Japan [213], where the receiver efficiency was calculated as 90%, which is a notable achievement. Typically, molten salt operation involves two temperature levels, at 280 and 550 °C. The design for the salt receiver includes a thermal mixing element, and an innovative approach is the use of an origami-inspired design as suggested in the literature [214].

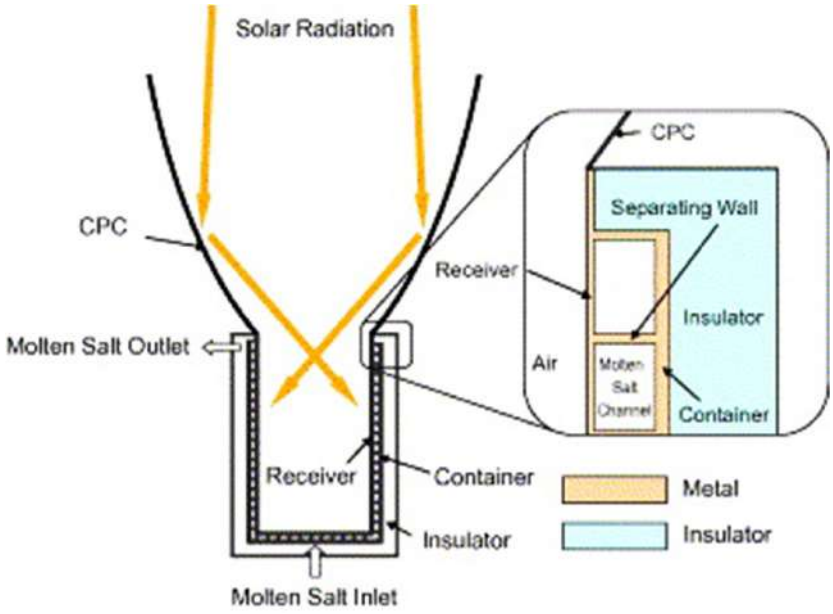

Figure 35. Typical insulated receiver with CPC cavity for operation with molten salt [191].

Another design that might be a good choice is the hexagon CPC receiver [193,194]. This design can be useful for a system with lower capacity (e.g., 30 MWth) and height up to 50 m. It is able to function with an optical efficiency of 57% and solar-to-electrical efficiency of 20% when paired with a supercritical CO_2 power cycle [193]. But still, the conventional configurations have higher optical efficiency compared to a hexagon CPC [176].

Other seminal works in the literature focus on the thermal performance of a beam-down solar system. A study reported in [195] tested a 100 kWth BD-ST incorporated with thermal energy storage functioning by the use of molten salt. They found that their setup achieves a thermal efficiency of 66.4% that is satisfactory for processes around 450 °C. Mokhtar et al. [196] focused on a 100 kWth system, employed by using a model with experimental data. They determined that the daily collector thermal efficiency is 28% for operation at 300 °C, but it reduces to 24% for operation at 600 °C.

This structure combines the beam-down reflector with a dish (hyperboloid) concentrator. The most common designs considering the secondary upper reflector are with hyperbolic or elliptic geometries. This is shown in Figure 36 [197].

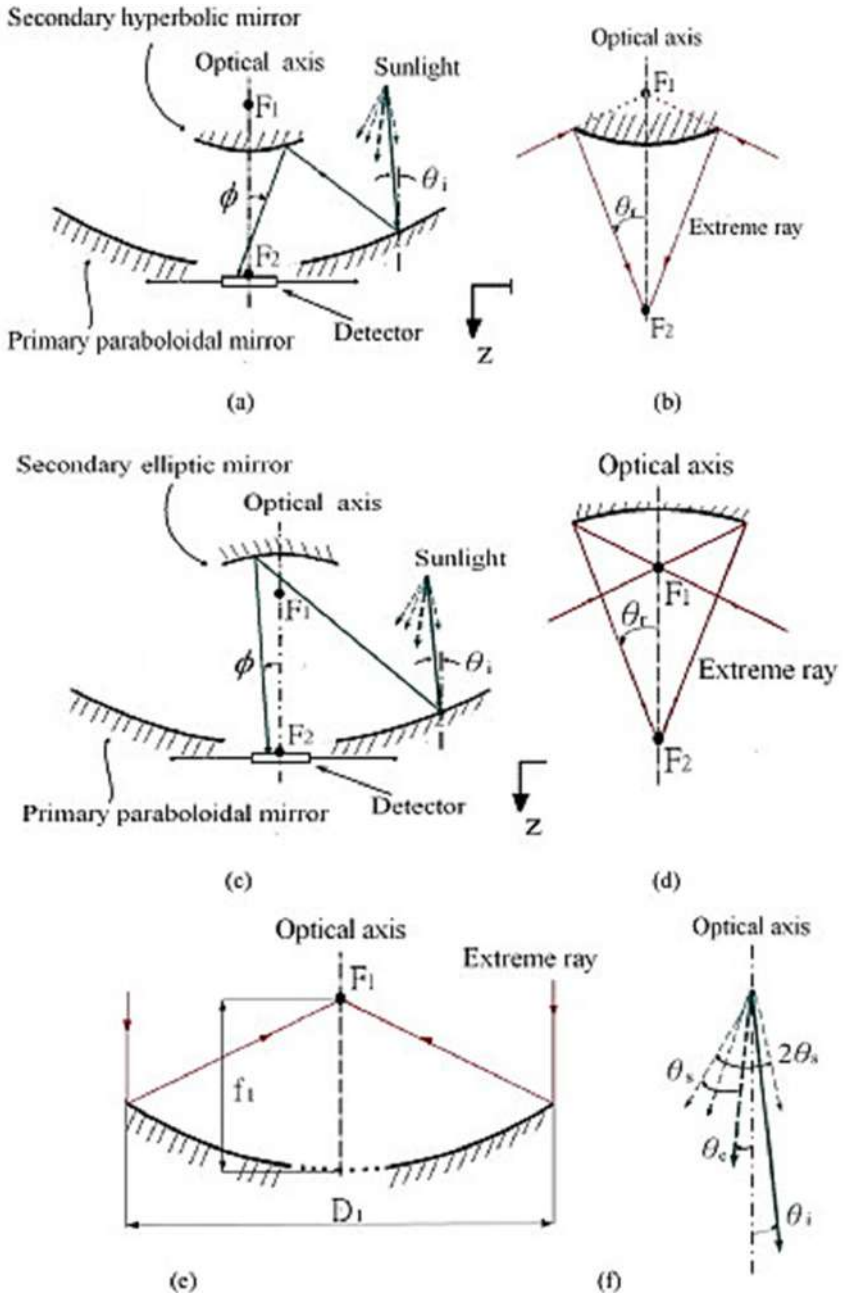

Figure 36. Schematic diagrams of (**a**) the concentrator module with a hyperboloidal pattern, (**b**) the secondary hyperboloidal part, (**c**) the concentrator module with an ellipsoidal pattern, (**d**) the secondary ellipsoidal part, (**e**) the primary paraboloidal part and (**f**) the sunlight distribution for the solar concentrator. Reproduced by kind permission of Elsevier from [215].

According to the literature, the optimum configuration is the hyperbolic shape [216] and the use of convex reflectors. In the study by Cheng et al. [217], it is found that both convex (hyperbolic) and concave (elliptic) geometries could result in relatively even heat flux distribution across a flat absorbing area. Also, they claimed that the enhancement in the concentration ratio is a parameter that has a negative impact on the uniformity due to a spillage effect. Another study [218] worked on the proper arrangement of a symmetrical two-stage flat reflected concentrator (STFC) and evaluated its concentrating energy transfer using the Monte Carlo ray tracing method (MCRTM). It consisted of two symmetrical off-axis concentrators and inclined flat reflectors. The temperature was measured without considering convection cooling and it was found that the GCR must not exceed 4.0. The adjustment of the tilt angle of the two-stage mirrors affects the concentrating ratio and the uniform irradiance, which was measured with the aid of geometric optics. Afterwards, the optimised structure parameters for a space solar power station (SSPC) were computed and the ECR distributions on the solar panel were simulated by the MCRTM. In this range, the symmetrical structure makes both sides, 'focal spots', and their gradient distribution overlap with each other and the nonuniformity of the spot could be below 5%, which results in a considerable flux distribution for a concentrator photovoltaic (CPV) system. Generally, the nonuniformity of a concentrator photovoltaic (CPV) system should not surpass 20%. It can be described as

$$\omega = \frac{\xi_{max} - \xi_{min}}{\xi_{avr}} * 100\% \quad (16)$$

where ξ_{avr} is the average flux distribution, ξ_{max} represents the maximum energy concentration ratio (ECR) and ξ_{min} is set as the minimum ECR.

Due to the requirement for expansive space, the parabolic concentrator must be assembled by combining multiple individual curved mirror facets. In the work, 24-dish structures were designed and the results were acceptable and could be used as a reference for the future, considering the precision of arrangements for multi-mirrors.

Additionally, the design of the receiver with a cavity is crucial to have the optimum arrangement. A cavity has remarkable benefits and most importantly, it is able to enhance the concentration ratio, decrease thermal losses and enhance the uniform heat flux over the absorbing area. A study employing a cavity to act as a homogeniser demonstrated that the system can maintain adequate performance levels with misalignment angles up to 1.5, but at a significant cost to nominal efficiency. Additionally, testing significantly revealed much lower performance than theoretical simulations, attributed to non-ideal manufacturing. Moreover, it was suggested to exercise critical care during the manufacturing process of reflecting surfaces.

Zhang et al. [219] showed a design as a possible solution for the "dark image" problem over the receiver. Another original study conducted by Xu et al. [220] presents the use of a BD dish arrangement with a fixed focus as seen in Figure 37. It relies on a new tracking method that involves rotating the primary reflector platform. This approach can achieve an optical efficiency of approximately 79%, resulting in a power production of around 8 kW.

Another issue regarding the operation and design of the BD dish system involves the tracking mechanism and system control. A study proved that for double-dish primary reflector design, the system exhibited greater stability to errors than conventional designs [221]. New components acting as robotic arms were added to the system. This design [222] was based on the use of a genetic algorithm and made it possible to operate with optical efficiency around 80%.

A PTC collector can be easily coupled with the beam-down idea; in this direction, some studies have been conducted in the literature, but these are limited and therefore further investigations must be conducted in the future. Uzahir and Rehman [223] made an arrangement by the use of a tubular absorber placed in the middle of the parabolic trough as seen in Figure 38.

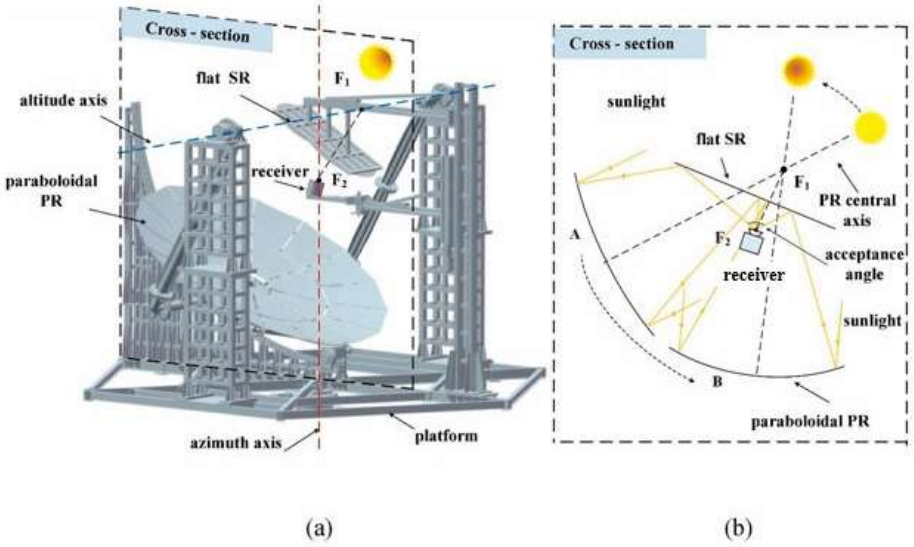

Figure 37. The fixed-focus beam-down design. (**a**) The detailed configuration, (**b**) 2D depiction of the suggested design. Reproduced by kind permission of Elsevier from [196,220].

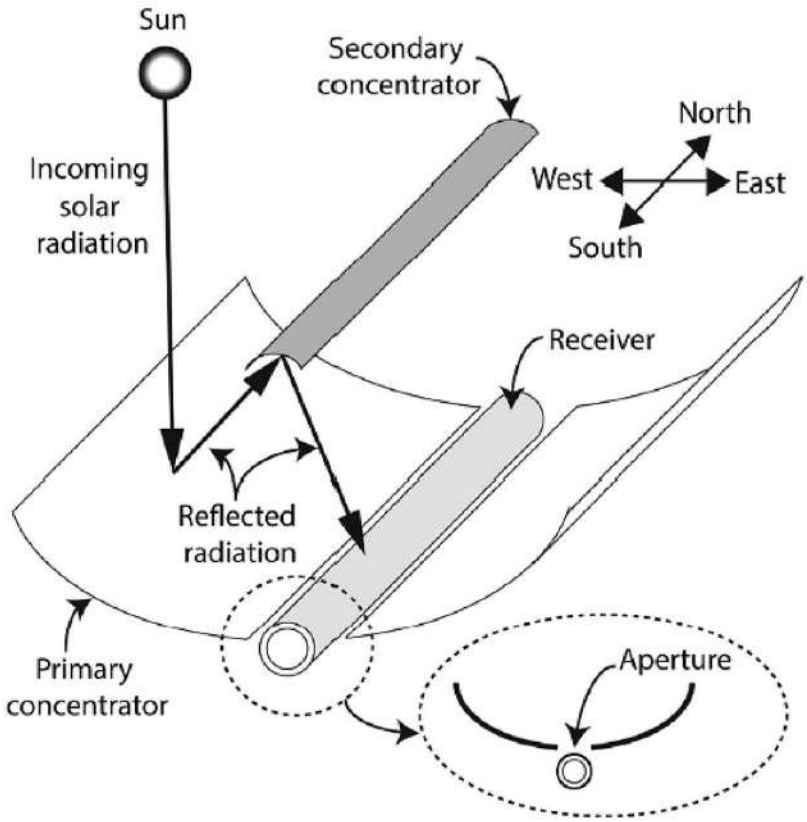

Figure 38. Beam-down PTC design with a tubular receiver with two primary parabolic reflectors. Reproduced by kind permission of Elsevier from [196,223].

This design has significantly reduced concentration ratios, compared to focal point configurations. The intercept factor, which is the proportion of the absorbed rays by the receiver to the reflected rays from the reflector, expresses the optical performance. In this configuration, the intercept factors were calculated as 90%, 89% and 77% for concentration ratios of 10, 50 and 100.

Wu et al. [224] suggested that a beam-down PTC is put on the location of a flat receiver between the primary and the secondary reflectors: Figure 39 demonstrates the

arrangement, which was tested for four different secondary reflector arrangements called flat, hyperbolic, elliptic and parabolic. The most efficient option was the parabolic-shaped secondary reflector. However, these applications did not consider any input considering thermal performance of the PTC-based systems; then, further studies regarding this point must be conducted in the future.

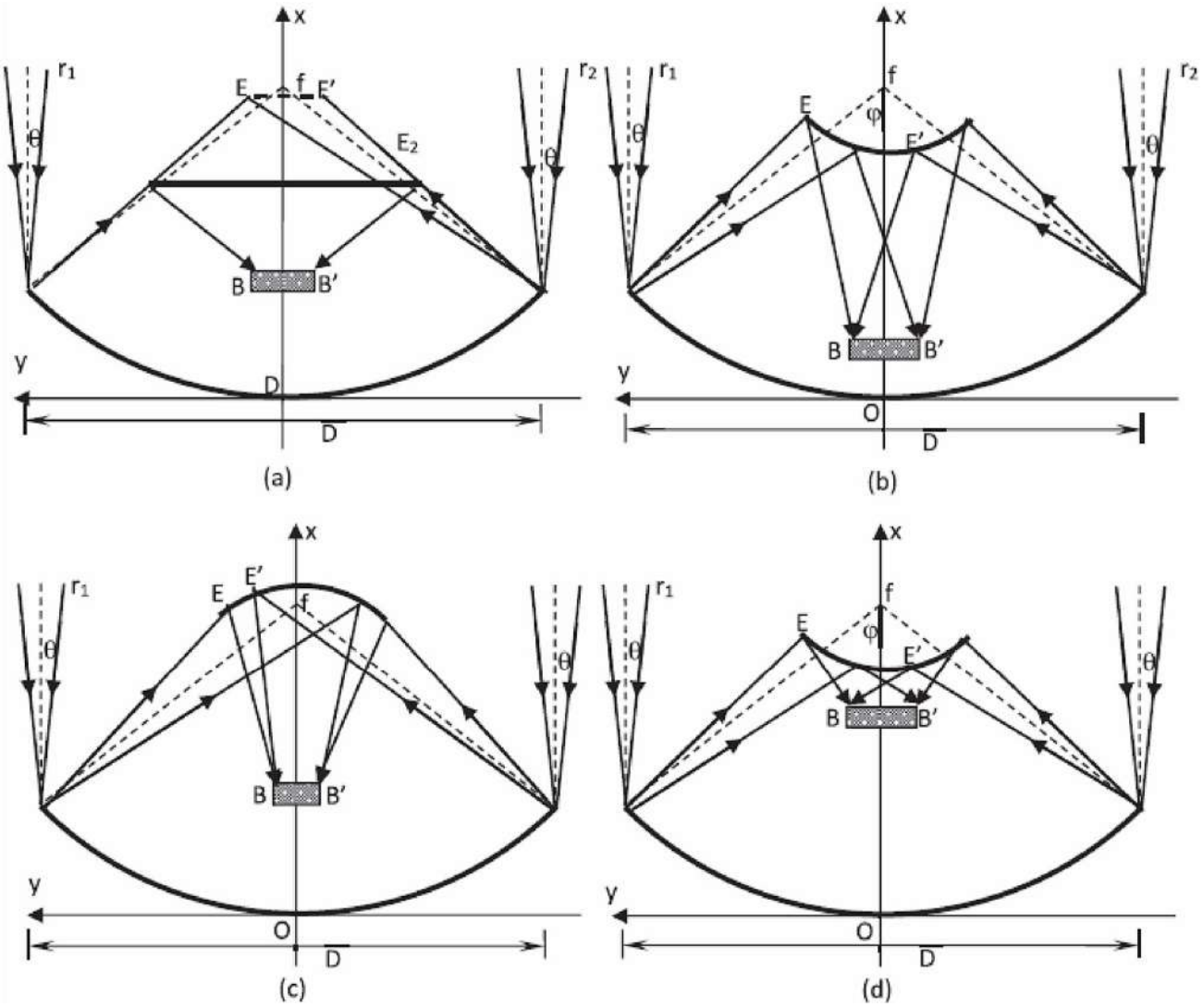

Figure 39. The beam-down PTC design with the receiver between the two reflectors. The secondary reflector has the following possible shapes: (**a**) flat, (**b**) hyperbolic, (**c**) elliptic and (**d**) parabolic. Reproduced by kind permission of Elsevier from [224].

Combining the BD concept with a linear Fresnel reflector can be a beneficial approach, as both seek to simplify the overall configuration by positioning key components close to the ground. In the BD-LFR concept, both the primary-moving reflectors and the receiver are situated on the ground, while the upper-stable reflector is positioned several meters above the ground.

Another possibility involves using a hyperbolic-shaped upper reflector along with a CPC cavity, which was shown to enhance the concentration factor up to 84 [225]. The system's height depends on the primary mirror design, and it is generally in the range of 30–40 m, with a maximum optical efficiency close to 70%. Another study [226] showed that flat upper reflector shape is better than a hyperbolic one. Specifically, the flat design was determined to be more effective, achieving an optical efficiency of 60% with a concentration ratio of 31 suns under identical simulation conditions. However, some drawbacks were

noted, including the sun image expansion on the receiver, the mirror width enhancement due to the eccentricity, the high complexity of the geometry and the creation of shadow optical losses.

In a separate study, the hyperboloid upper reflector was deemed to be superior to the elliptic design, despite the elliptic design having a greater intercept factor [227].

Though solar concentration technologies are very rarely coupled with photocatalytic reactors, their combination with photovoltaic systems is already well proven. Therefore, some hints and suggestions may come from the analysis of these case histories.

The photovoltaics (PV) efficiency can be enhanced when it is coupled with a secondary reflector to regulate the radiation flux distribution over the PV area. The improvement in a solar irradiation profile on the cell helps prevent hot spots and overheating, leading to enhanced performance and increased lifetime.

A general configuration of beam-down concentrating photovoltaics with a dish primary reflector is shown in Figure 40 [228]. This configuration consists of a multi-leg homogeniser that enables a favourable heat flux distribution of the solar rays over the PV cells. In this approach, the system achieved a peak electrical efficiency of around 15%, with an annual average of 10.6%, under specific climate conditions in Singapore.

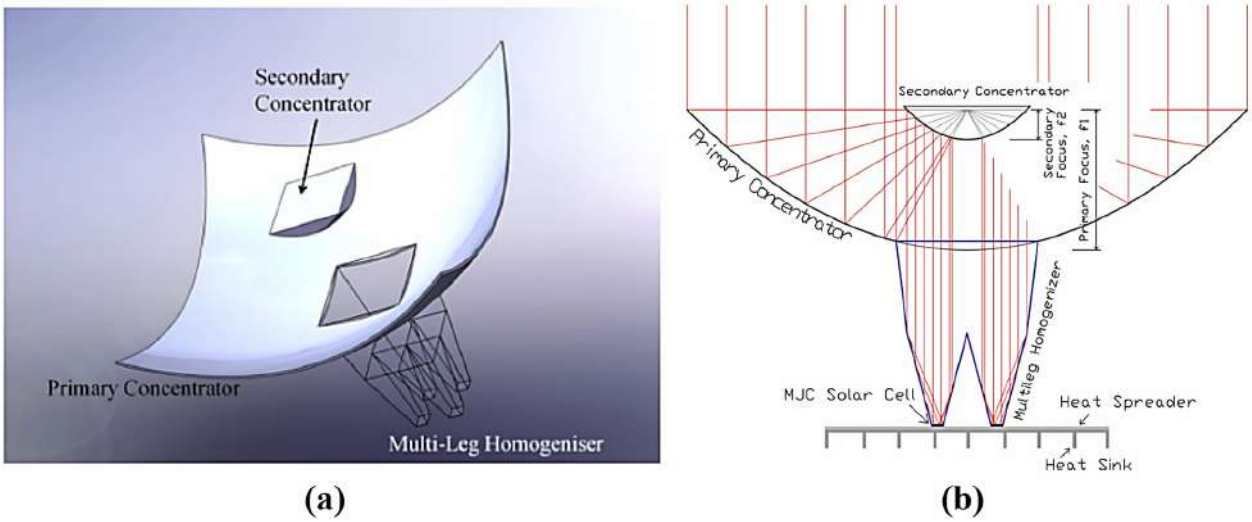

Figure 40. Typical BD-CPV with dish primary reflector and homogeniser. (**a**) Overall configuration. (**b**) Cross-section depiction. Reproduced by kind permission of Elsevier from [228].

Burhan et al. [229] combined BD-CPV with Fresnel lenses' design with a homogeniser and it was revealed that the Fresnel design was superior, achieving a yearly efficiency of 14.1%. Both designs outperformed conventional PV panels. In addition, it is beneficial to emphasise the further enhancement with the use of a conjugate refractive–reflective homogeniser that can boost the produced electricity up to 4.5% [230].

Due to the high energy concentration on concentrating PV, they reach high temperatures and this decreases the cell efficiency significantly. Indeed, approximately, the increase in the cell temperature of 1 K results in a 0.5% decrement in electrical efficiency [231]. Moreover, PV cells must be cooled properly using the natural or forced circulation of a fluid in the back side of the cell in order to overcome this problem and increase the electrical efficiency. These concepts may respond to a similar need for the cooling of photoreactors.

One solution to cool down the system is the use of nanofluids [232]. Also, there are some other configurations with fins in the back of the PV with the purpose of enhancing the cooling rate with the ambient heat sink [233].

An alternative choice is the use of appropriate filtering of the solar radiation to allow only the passage of the wavelengths that are exploited by the PV cell, so the redundant part of the solar spectrum does not heat up the cell. Figure 41 shows the wavelength that the PV and the photothermal system (PT) exploit.

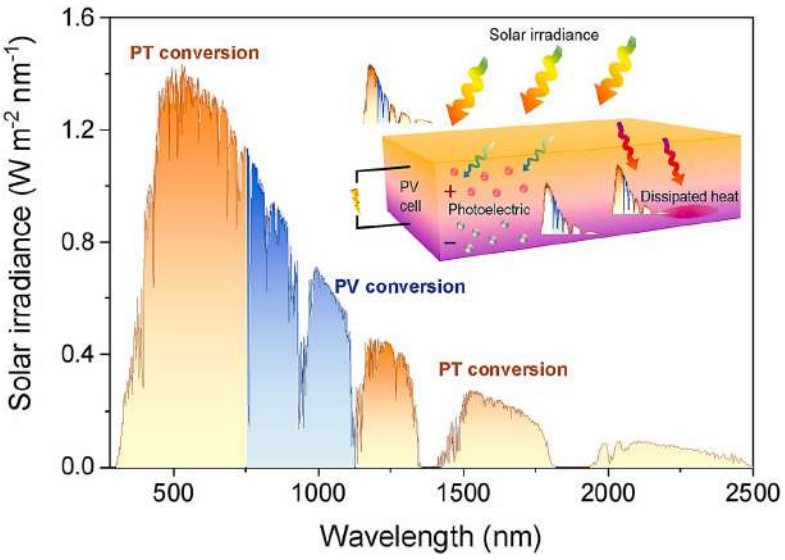

Figure 41. The depiction of the wavelengths that the PV system exploits and the photothermal (PT) system exploits for air mass to become 1.5. Reproduced by kind permission of Elsevier from [234].

The filtering can be applied by using various solutions, such as nano-filtering [235], selective absorber filtering [236], splitter reflectors [234] and thin-film wave interference filters [236]. The fundamental categories of filtering are shown in Figure 42: (a) shows nano-filtering, where solar irradiation passes through a nanofluid that absorbs certain wavelengths and permits to pass only those wavelengths exploitable by the PV; (b) demonstrates the nano-film spectral beam splitter technology, which divides sunlight into two parts, redirecting them into different directions; and (c) is the use of a semitransparent PV cell spectral beam splitter.

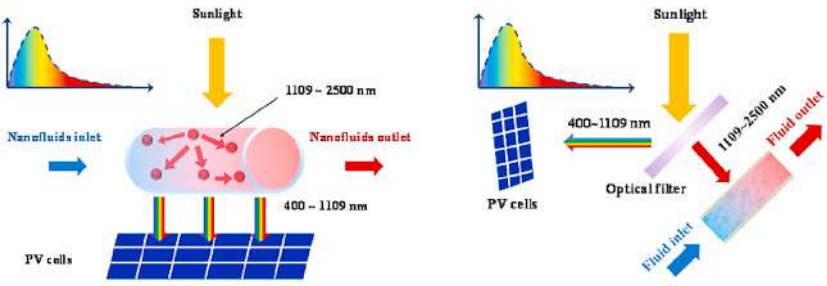

(a) Nanofluids based spectral beam splitter (b) Nano-film based spectral beam splitter

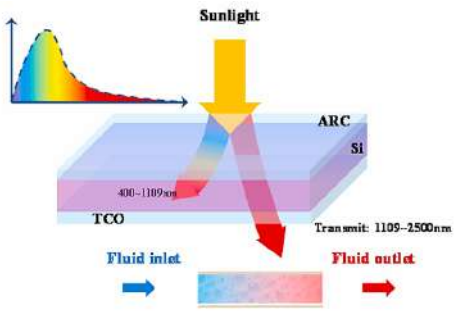

(c) Semitransparent PV cell based spectral beam splitter

Figure 42. Basic spectral beam splitting technologies. Reproduced by kind permission of Elsevier from [237].

Also, the BD systems use appropriate thin-film interference filters or dichroic mirror coatings to split the solar irradiation spectrum into two parts. The general option is the thin-film interference filters due to their flexibility to regulate the desired spectral separation [233]. The multilayer thin-film filters can be made of various materials for filtering solar rays of lower and higher wavelengths. Generally, SiO_2 is used for the lower refractive region [236] because these nanoparticles have a negligible absorbance coefficient in the visible light region [238]. Conversely, for the higher wavelength region, other materials can be chosen such as TiO_x [238], Nb_2O_3 [239], Ta_2O_5 [240] and SiN [241]. Additional to these materials, it is possible to use many materials together to achieve a gradient refractive index [242].

These ideas could be affectively applied to photoreactors' design. On one hand, the use of a solar concentrator can magnify the total radiation, impinging on the received, while proper filtering media can prevent the accumulation of useless radiation in the reactor, i.e., the spectrum could be cut for energies smaller than the band gap of the active semiconductor, which are not usable by the reacting system.

4. Conclusions and Recommendations

4.1. Conclusions

Solar energy is the most powerful natural source that can be used for electricity, chemical and fuel production. Despite the wide and abundant availability, its exploitation as a main energy source needs the deployment of appropriate energy storage technologies to overcome its intermittency and fluctuating intensity. Furthermore, locations in the world where large-scale solar energy harvesting facilities may be implemented are usually far from the utilisation points. This also calls for efficient energy distribution systems, which do not recommend storage in the electrical form, due to high losses in distribution.

On the other hand, the rise in carbon emissions with the usage of conventional fuels imposes not only valid strategies for the sequestration of CO_2, but suggests the need for utilisation of a base chemical, e.g., for the production of largely consumed C1 platform compounds. The solar photoreduction of CO_2 to regenerated fuels and chemicals, for the synthesis, e.g., of methane, methanol or formic acid, is a powerful technology to couple both needs in a convincing win–win circular approach. However, several difficulties must be overcome in order to accomplish efficient solar photoreduction to fuels. Some progress has been made in the design of photoactive materials, but photoreactors must be appropriately designed too, in order to provide a practically valid solution. Indeed, despite the considerable interest in photosynthesis and photocatalysis, scale-up examples are really limited, often due to scarce attention to the reactor engineering aspects of this application.

At a laboratory level, slurry-type reactors are the most used, followed by fixed-bed reactors, which are not very efficient due to poor light exposure for the photoactive material. High-pressure devices, optical fibre-enlightened monoliths, membrane-type photoreactors and concentrated solar photoreactors are unconventional devices under development, but they have preliminarily shown impressive results for the solar photoreduction of CO_2.

Another key point is the efficient collection and focusing of solar light on the active material, since most of the studies in the literature use UV or visible lamps, but the final aim would be the realisation of a solar-driven apparatus.

The photocatalytic process is intrinsically inefficient, because energy dissipative phenomena occur at a much higher rate and with higher sticking probability of reactive events. So, in the frame of the utilisation of solar energy for photocatalytic applications, the exploitation of solar concentration technologies can be a viable strategy to compensate, with a higher photon flux, the low material efficiency. This brings about additional issues, such as the optimisation of the configuration to focus the concentrated solar beam where needed and to avoid overheating at high magnification factors. Embryonal investigations are in progress in this frame.

The performance of solar photoreactors is significantly influenced by their configuration, and operating conditions such as the temperature, pressure and solar concentrating

ratio. A slurry photoreactor enables efficient catalyst utilisation and high-pressure operation led to some of the highest productivities reported in the literature. High selectivity and yields were also achieved with membrane photoreactors. The concentrated solar photoreactors have the benefit of high efficiency and effective light utilisation. A hybrid solar photoreactor that combines the benefits of concentrated, slurry and membrane photoreactors would increase solar CO_2 photoreduction while increasing product yield.

4.2. Recommendations

Despite some advantages, the slurry reactor design is conceptually limited to lab-scale applications due to the issues with light transmittivity and reflectivity and to the uneasy recovery of the catalyst. Therefore, for a possible improvement, a geometry of the reactor that enables better light utilisation and photon collection efficiency is compulsory for scale-up purposes. Catalyst separation issues are also important and prohibitive for continuous mode application, suggested for large-volume application. Thus, the immobilisation of a photocatalyst has to be developed and the appropriate reactor geometry to host it and focus solar light on the receiving photoactive material is needed as well. The larger area of the reactor system makes a uniform light transmission possible so that the efficiency of solar photoreduction is enhanced.

Optimum temperature control and mass transfer between the reagents and photocatalyst should be ensured by efficient stirring and mixing. To have the proper design, flow patterns should be considered.

Coupling photoreactors with solar concentration devices is a powerful strategy to achieve a boosting of productivity thanks to much higher photon flux. Unfortunately, only a few attempts have been conducted and many issues are still unsolved. According to the current technologies, costs and complexity of the solutions are still prohibitive for becoming coupled with another emerging application, such as the photoreduction of CO_2, but the incoming advantages are huge and suggest to explore the potential for this configuration.

A promising application, though never used for this application, is the solar beam-down technology that seems to offer a stimulating way to follow in this matter. However, some points should be improved. The BD-ST systems offer a key advantage in reducing system height, resulting in lower costs and complexity compared to other configurations. However, the optical design of the system must be conceived with high accuracy. The upper reflector is a fundamental component that requires attention for its design. Important aspects are the shape, the dimensions and the location of the upper reflector since it has a crucial impact on the performance of the final system. Another drawback of the BD systems is their relatively lower optical efficiency in comparison to conventional systems. The use of more than one reflecting surface results in optical losses, which can be mitigated by using highly reflective materials and designing the system to maximise intercept factors. In addition, the BD systems need an additional reflector over the receiver to be used as a homogeniser (generally with CPC geometry) to ensure a proper image of the sun in the receiver. That makes the heat flux distribution have a normalised profile; however, it results in additional optical loss in the system.

Also, the secondary reflector of the BD design faces some restrictions due to the high temperature reached that causes the reduction in its lifetime and the reflectance. Consequently, proper cooling is necessary when the temperature exceeds 150 °C. Another optical concern involved is the deposition of particles on the homogeniser over the absorber, leading to decreased efficiency at higher incident angles. Therefore, regular cleaning of the reflectors is essential to keep the system efficiency. Additionally, any concentration device imposes high temperatures on the receiver (i.e., the photoreactor) and the consequent need for cooling or radiation filtering, which should be optimised differently based on the size and geometry.

Finally, there is a need for a detailed cost analysis.

Additionally, a solar photoreduction unit can be improved, having higher sensitivity, corrosion resistance, a higher mass transfer rate and low cytotoxicity, while developing a

solar photoreactor. Energy losses, an efficiency drop, long-term stability and a cost-effective photocatalyst for the solar photoreduction of CO_2 require further investigation.

Author Contributions: Conceptualization, S.N.D. and I.R.; methodology, S.N.D. and A.G.; software, A.G.; validation, S.N.D., A.G. and M.T.; resources, I.R. and G.R.; data curation, S.N.D., A.G. and M.T.; writing—original draft preparation, S.N.D.; writing—review and editing, I.R.; visualization, M.T. and A.G.; supervision, I.R. and G.R.; project administration, I.R. and G.R.; funding acquisition, I.R. and G.R. All authors have read and agreed to the published version of the manuscript.

Funding: S.N. Degerli, A. Gramegna, I. Rossetti and G. Ramis gratefully acknowledge the financial contribution of Fondazione Cariplo through the grant 2021-0855—"SCORE—Solar Energy for Circular CO_2 Photoconversion and Chemicals Regeneration", funded in the frame of the Circular Economy call 2021. I. Rossetti and G. Ramis gratefully acknowledge the financial contribution of Next Generation EU—PIANO NAZIONALE DI RIPRESA E RESILIENZA (PNRR), Missione 4 "Istruzione e Ricerca"—Componente C2 Investimento 1.1, "Fondo per il Programma Nazionale di Ricerca e Progetti di Rilevante Interesse Nazionale (PRIN2022PNRR)" through the grant "P20227LB45—SCORE2—Solar-driven COnveRsion of CO_2 with HP-HT photoReactor".

I. Rossetti acknowledges Università degli Studi di Milano for support through the grant PSR 2021—GSA—Linea 6 "One Health Action Hub: University Task Force for the resilience of territorial ecosystems". This study was carried out within the Agritech National Research Center and received funding from the European Union Next-Generation EU (PIANO NAZIONALE DI RIPRESA E RESILIENZA (PNRR)—MISSIONE 4 COMPONENTE 2, INVESTIMENTO 1.4—D.D. 1032 17/06/2022, CN00000022). This manuscript reflects only the authors' views and opinions, neither the European Union nor the European Commission can be considered responsible for them. I. Rossetti and M. Tommasi acknowledge specifically the participation and funding of Tasks 8.2.3, 8.3.2 and 8.4.1.

Conflicts of Interest: The authors declare no conflict of interest.

References

1. Soon, W.; Baliunas, S.L.; Robinson, A.B.; Robinson, Z.W. Environmental Effects of Increased Atmospheric Carbon Dioxide. *Energy Environ.* **1999**, *10*, 439–468. [CrossRef]
2. Roy, S.C.; Varghese, O.K.; Paulose, M.; Grimes, C.A. Toward Solar Fuels: Photocatalytic Conversion of Carbon Dioxide to Hydrocarbons. *ACS Nano* **2010**, *4*, 1259–1278. [CrossRef] [PubMed]
3. Liu, J.; Li, S.; Dewil, R.; Vanierschot, M.; Baeyens, J.; Deng, Y. Water Splitting by $MnOx/Na_2CO_3$ Reversible Redox Reactions. *Sustainability* **2022**, *14*, 7597. [CrossRef]
4. Bafaqeer, A.; Tahir, M.; Amin, N.A.S. Well-designed ZnV_2O_6/g-C_3N_4 2D/2D nanosheets heterojunction with faster charges separation via pCN as mediator towards enhanced photocatalytic reduction of CO_2 to fuels. *Appl. Catal. B Environ.* **2019**, *242*, 312–326. [CrossRef]
5. Behroozi, A.H.; Xu, R. Photocatalytic CO_2 reduction: Photocatalysts, membrane reactors, and hybrid processes. *Chem. Catal.* **2023**, *3*, 100550. [CrossRef]
6. Ghoussoub, M.; Xia, M.; Duchesne, P.N.; Segal, D.; Ozin, G. Principles of photothermal gas-phase heterogeneous CO_2 catalysis. *Energy Environ. Sci.* **2019**, *12*, 1122–1142. [CrossRef]
7. Francis, A.; Kumar, H.; Sudhakar, K.; Tahir, M. A review on recent developments in solar photoreactors for carbon dioxide conversion to fuels. *J. CO2 Util.* **2021**, *47*, 101515. [CrossRef]
8. Sakakura, T.; Choi, J.-C.; Yasuda, H. Transformation of Carbon Dioxide. *Chem. Rev.* **2007**, *107*, 2365–2387. [CrossRef] [PubMed]
9. Shehzad, N.; Tahir, M.; Johari, K.; Murugesan, T.; Hussain, M. A critical review on TiO_2 based photocatalytic CO_2 reduction system: Strategies to improve efficiency. *J. CO2 Util.* **2018**, *26*, 98–122. [CrossRef]
10. Khan, A.A.; Tahir, M. Recent advancements in engineering approach towards design of photo-reactors for selective photocatalytic CO_2 reduction to renewable fuels. *J. CO2 Util.* **2019**, *29*, 205–239. [CrossRef]
11. Tahir, M.; Amin, N.S. Advances in visible light responsive titanium oxide-based photocatalysts for CO_2 conversion to hydrocarbon fuels. *Energy Convers. Manag.* **2013**, *76*, 194–214. [CrossRef]
12. Abdullah, H.; Khan, M.M.R.; Ong, H.R.; Yaakob, Z. Modified TiO_2 photocatalyst for CO_2 photocatalytic reduction: An overview. *J. CO2 Util.* **2017**, *22*, 15–32. [CrossRef]
13. Linsebigler, A.L.; Lu, G.; Yates, J.T. Photocatalysis on TiO_2 Surfaces: Principles, Mechanisms, and Selected Results. *Chem. Rev.* **1995**, *95*, 735–758. [CrossRef]

14. Ola, O.; Maroto-Valer, M.M. Review of material design and reactor engineering on TiO_2 photocatalysis for CO_2 reduction. *J. Photochem. Photobiol. C Photochem. Rev.* **2015**, *24*, 16–42. [CrossRef]
15. Wang, Y.; Bai, X.; Qin, H.; Wang, F.; Li, Y.; Li, X.; Kang, S.; Zuo, Y.; Cui, L. Facile One-Step Synthesis of Hybrid Graphitic Carbon Nitride and Carbon Composites as High-Performance Catalysts for CO_2 Photocatalytic Conversion. *ACS Appl. Mater. Interfaces* **2016**, *8*, 17212–17219. [CrossRef] [PubMed]
16. Xu, Y.; Xu, H.; Wang, L.; Yan, J.; Li, H.; Song, Y.; Huang, L.; Cai, G. The CNT modified white C_3N_4 composite photocatalyst with enhanced visible-light response photoactivity. *J. Chem. Soc. Dalt. Trans.* **2013**, *42*, 7604–7613. [CrossRef]
17. Cheng, H.; Hou, J.; Takeda, O.; Guo, X.-M.M.; Zhu, H. A unique Z-scheme 2D/2D nanosheet heterojunction design to harness charge transfer for photocatalysis. *J. Mater. Chem. A* **2015**, *3*, 11006–11013. [CrossRef]
18. Li, Z.; Zhou, Y.; Zhang, J.; Tu, W.; Liu, Q.; Yu, T.; Zou, Z. Hexagonal Nanoplate-Textured Micro-Octahedron Zn_2 SnO_4: Combined Effects toward Enhanced Efficiencies of Dye-Sensitized Solar Cell and Photoreduction of CO_2 into Hydrocarbon Fuels. *Cryst. Growth Des.* **2012**, *12*, 1476–1481. [CrossRef]
19. Sun, J.; Zhang, J.; Zhang, M.; Antonietti, M.; Fu, X.; Wang, X. Bioinspired hollow semiconductor nanospheres as photosynthetic nanoparticles. *Nat. Commun.* **2012**, *3*, 1139. [CrossRef]
20. Niu, P.; Yang, Y.; Yu, J.C.; Liu, G.; Cheng, H.-M. Switching the selectivity of the photoreduction reaction of carbon dioxide by controlling the band structure of a g-C $_3N_4$ photocatalyst. *Chem. Commun.* **2014**, *50*, 10837. [CrossRef] [PubMed]
21. Cao, S.; Low, J.; Yu, J.; Jaroniec, M.; Materials, M.J.-A. Undefined 2015 Polymeric photocatalysts based on graphitic carbon nitride. *Adv. Mater.* **2015**, *27*, 2150–2176. [CrossRef] [PubMed]
22. Zheng, Y.; Lin, L.; Wang, B.; Wang, X. Graphitic Carbon Nitride Polymers toward Sustainable Photoredox Catalysis. *Angew. Chem. Int. Ed.* **2015**, *54*, 12868–12884. [CrossRef] [PubMed]
23. Nguyen, T.-V.; Wu, J.C.S.; Chiou, C.-H. Photoreduction of CO_2 over Ruthenium dye-sensitized TiO_2-based catalysts under concentrated natural sunlight. *Catal. Commun.* **2008**, *9*, 2073–2076. [CrossRef]
24. Renz, C. Lichtreaktionen der Oxyde des Titans, Cers und der Erdsäuren. *Helv. Chim. Acta* **1921**, *4*, 961–968. [CrossRef]
25. Salgado, B.C.B.; Cardeal, R.A.; Valentini, A. Photocatalysis and Photodegradation of Pollutants. In *Nanomaterials Applications for Environmental Matrices*; do Nascimento, R.F., Ferreira, O.P., De Paula, A.J., de Oliveira Sousa Neto, V., Eds.; Advanced Nanomaterials; Elsevier: Amsterdam, The Netherlands, 2019; pp. 449–488. ISBN 978-0-12-814829-7. [CrossRef]
26. Verbruggen, S.W. TiO_2 photocatalysis for the degradation of pollutants in gas phase: From morphological design to plasmonic enhancement. *J. Photochem. Photobiol. C Photochem. Rev.* **2015**, *24*, 64–82. [CrossRef]
27. de Brito Lira, J.O.; Riella, H.G.; Padoin, N.; Soares, C. An Overview of Photoreactors and Computational Modeling for the Intensification of Photocatalytic Processes in the Gas-Phase: State-of-Art. *J. Environ. Chem. Eng.* **2021**, *9*, 105068. [CrossRef]
28. Yu, M.; Wang, J.; Tang, L.; Feng, C.; Liu, H.; Zhang, H.; Peng, B.; Chen, Z.; Xie, Q. Intimate coupling of photocatalysis and biodegradation for wastewater treatment: Mechanisms, recent advances and environmental applications. *Water Res.* **2020**, *175*, 115673. [CrossRef] [PubMed]
29. Wood, D.; Shaw, S.; Cawte, T.; Shanen, E.; Heyst, B. Van An overview of photocatalyst immobilization methods for air pollution remediation. *Chem. Eng. J.* **2020**, *391*, 123490. [CrossRef]
30. Nakata, K.; Fujishima, A. TiO_2 photocatalysis: Design and applications. *J. Photochem. Photobiol. C Photochem. Rev.* **2012**, *13*, 169–189. [CrossRef]
31. Ângelo, J.; Andrade, L.; Madeira, L.M.; Mendes, A. An overview of photocatalysis phenomena applied to NOx abatement. *J. Environ. Manag.* **2013**, *129*, 522–539. [CrossRef] [PubMed]
32. An, J.R.; Wang, Y.; Dong, W.W.; Gao, X.J.; Yang, O.Y.; Liu, Y.L.; Zhao, J.; Li, D.S. Efficient Visible-Light Photoreduction of CO_2 to CH_4 over an Fe-Based Metal-Organic Framework (PCN-250-Fe_3) in a Solid-Gas Mode. *ACS Appl. Energy Mater.* **2022**, *5*, 2384–2390. [CrossRef]
33. Yang, O.Y.; Gao, X.J.; Qi, G.D.; Wang, Y.; Dong, W.W.; Tian, Z.F.; Zhao, J.; Li, D.S.; Zhang, Q. Dye-Anchoring Strategy with a Metal-Organic Framework for a Highly Efficient Visible-Light-Driven Photocatalytic CO_2 Reduction through the Solid-Gas Mode. *ACS Appl. Energy Mater.* **2023**, *6*, 334–341. [CrossRef]
34. Dong, W.W.; Jia, J.; Wang, Y.; An, J.R.; Yang, O.Y.; Gao, X.J.; Liu, Y.L.; Zhao, J.; Li, D.S. Visible-light-driven solvent-free photocatalytic CO_2 reduction to CO by Co-MOF/Cu_2O heterojunction with superior selectivity. *Chem. Eng. J.* **2022**, *438*, 135622. [CrossRef]
35. Han, H.; Han, T.; Luo, Y.; Mushtaq, M.A.; Jia, Y.; Liu, C. Recent advances in α-Fe_2O_3-based photocatalysts for CO_2 conversion to solar fuels. *J. Ind. Eng. Chem.* **2023**, *128*, 81–94. [CrossRef]
36. Pan, Q.; Wu, Y.; Su, X.; Yin, Y.; Shi, S.; Oderinde, O.; Yui, G.; Zhang, C.; Zhang, Y. A review on the recent development of bismuth-based catalysts for CO_2 photoreduction. *J. Mol. Struct.* **2023**, *1294*, 136404. [CrossRef]
37. Anus, A.; Park, S. The synthesis and key features of 3D carbon nitrides (C_3N_4) used for CO_2 photoreduction. *Chem. Eng. J.* **2024**, *486*, 150213. [CrossRef]
38. Conte, F.; Villa, A.; Prati, L.; Pirola, C.; Bennici, S.; Ramis, G.; Rossetti, I. Effect of Metal Cocatalysts and Operating Conditions on the Product Distribution and the Productivity of the CO_2 Photoreduction. *Ind. Eng. Chem. Res.* **2022**, *61*, 2963–2972. [CrossRef] [PubMed]
39. Rossetti, I.; Bahadori, E.; Tripodi, A.; Villa, A.; Prati, L.; Ramis, G. Conceptual design and feasibility assessment of photoreactors for solar energy storage. *Sol. Energy* **2018**, *172*, 225–231. [CrossRef]

40. Conte, F.; Tripodi, A.; Rossetti, I.; Ramis, G. Feasibility Study of the Solar-Promoted Photoreduction of CO_2 to Liquid Fuels with Direct or Indirect Use of Renewable Energy Sources. *Energies* **2021**, *14*, 2804. [CrossRef]
41. Yue, P.L. Introduction to the Modelling and Design of Photoreactors. In *Photoelectrochemistry, Photocatalysis and Photoreactors*; Springer: Amsterdam, The Netherlands, 1985; pp. 527–547.
42. Nguyen, V.-H.; Wu, J.C.S. Recent developments in the design of photoreactors for solar energy conversion from water splitting and CO_2 reduction. *Appl. Catal. A Gen.* **2018**, *550*, 122–141. [CrossRef]
43. Rossetti, I.; Bahadori, E.; Tripodi, A.; Ramis, G. Modelling of photoreactors for water treatment. *Chem. Eng. Trans.* **2019**, *74*, 289–294. [CrossRef]
44. Ibhadon, A.O.; Fitzpatrick, P. Heterogeneous photocatalysis: Recent advances and applications. *Catalysts* **2013**, *3*, 189–218. [CrossRef]
45. Sayama, K.; Arakawa, H. Photocatalytic decomposition of water and photocatalytic reduction of carbon dioxide over zirconia catalyst. *J. Phys. Chem.* **1993**, *97*, 531–533. [CrossRef]
46. Zhang, Z.; Huang, Z.; Cheng, X.; Wang, Q.; Chen, Y.; Dong, P.; Zhang, X. Product selectivity of visible-light photocatalytic reduction of carbon dioxide using titanium dioxide doped by different nitrogen-sources. *Appl. Surf. Sci.* **2015**, *355*, 45–51. [CrossRef]
47. Sato, S.; Arai, T.; Morikawa, T.; Uemura, K.; Suzuki, T.M.; Tanaka, H.; Kajino, T. Selective CO_2 Conversion to Formate Conjugated with H_2O Oxidation Utilizing Semiconductor/Complex Hybrid Photocatalysts. *J. Am. Chem. Soc.* **2011**, *133*, 15240–15243. [CrossRef] [PubMed]
48. Asi, M.A.; He, C.; Su, M.; Xia, D.; Lin, L.; Deng, H.; Xiong, Y.; Qiu, R.; Li, X. Photocatalytic reduction of CO_2 to hydrocarbons using AgBr/TiO_2 nanocomposites under visible light. *Catal. Today* **2011**, *175*, 256–263. [CrossRef]
49. Wang, J.-C.J.-S.; Yao, H.-C.; Fan, Z.-Y.; Zhang, L.; Wang, J.-C.J.-S.; Zang, S.-Q.; Li, Z.-J. Indirect Z-Scheme BiOI/g-C_3N_4 Photocatalysts with Enhanced Photoreduction CO_2 Activity under Visible Light Irradiation. *ACS Appl. Mater. Interfaces* **2016**, *8*, 3765–3775. [CrossRef] [PubMed]
50. Ye, Z. *Handbook of Advanced Dielectric, Piezoelectric and Ferroelectric Materials: Synthesis, Properties and Applications*; Ye, Z.-G., Ed.; Woodhead Publishing: Sawston, UK, 2008; ISBN 978-1-84569-186-8.
51. Spadoni, G.; Bandini, E.; Santarelli, F. Scattering effects in photosensitized reactions. *Chem. Eng. Sci.* **1978**, *33*, 517–524. [CrossRef]
52. Cassano, A.E.; Alfano, O.M. Design and Analysis of Homogeneous and Heterogeneous Photoreactors. In *Chemical Engineering*; Wiley: Hoboken, NJ, USA, 2005; pp. 125–169.
53. Liu, L.; Li, Y.; He, J.; Wang, Q.; Deng, J.; Chen, X.; Yu, C. Progress on gas-solid phase photoreactor and its application in CO_2 reduction. *Green Chem. Eng.* 2023; *in press*. [CrossRef]
54. Tahir, M.; Amin, N.A.S. Indium-doped TiO_2 nanoparticles for photocatalytic CO_2 reduction with H_2O vapors to CH_4. *Appl. Catal. B Environ.* **2015**, *162*, 98–109. [CrossRef]
55. Li, X.; Bi, W.; Wang, Z.; Zhu, W.; Chu, W.; Wu, C.; Xie, Y. Surface-adsorbed ions on TiO_2 nanosheets for selective photocatalytic CO_2 reduction. *Nano Res.* **2018**, *11*, 3362–3370. [CrossRef]
56. Xin, C.; Hu, M.; Wang, K.; Wang, X. Significant Enhancement of Photocatalytic Reduction of CO_2 with H_2O over ZnO by the Formation of Basic Zinc Carbonate. *Langmuir* **2017**, *33*, 6667–6676. [CrossRef] [PubMed]
57. Tasbihi, M.; Kočí, K.; Edelmannová, M.; Troppová, I.; Reli, M.; Schomäcker, R. Pt/TiO_2 photocatalysts deposited on commercial support for photocatalytic reduction of CO_2. *J. Photochem. Photobiol. A Chem.* **2018**, *366*, 72–80. [CrossRef]
58. Lee, D.K.; Choi, J.I.; Lee, G.H.; Kim, Y.H.; Kang, J.K. Energy States of a Core-Shell Metal Oxide Photocatalyst Enabling Visible Light Absorption and Utilization in Solar-to-Fuel Conversion of Carbon Dioxide. *Adv. Energy Mater.* **2016**, *6*, 1–7. [CrossRef]
59. Razzaq, A.; Grimes, C.A.; In, S. Il Facile fabrication of a noble metal-free photocatalyst: TiO_2 nanotube arrays covered with reduced graphene oxide. *Carbon* **2016**, *98*, 537–544. [CrossRef]
60. Kim, K.H.; Kim, S.; Moon, B.C.; Choi, J.W.; Jeong, H.M.; Kwon, Y.; Kwon, S.; Choi, H.S.; Kang, J.K. Quadruple metal-based layered structure as the photocatalyst for conversion of carbon dioxide into a value added carbon monoxide with high selectivity and efficiency. *J. Mater. Chem. A* **2017**, *5*, 8274–8279. [CrossRef]
61. Kandy, M.M.; Gaikar, V.G. Enhanced photocatalytic reduction of CO_2 using CdS/Mn_2O_3 nanocomposite photocatalysts on porous anodic alumina support with solar concentrators. *Renew. Energy* **2019**, *139*, 915–923. [CrossRef]
62. Li, X.; Sun, Y.; Xu, J.; Shao, Y.; Wu, J.; Xu, X.; Pan, Y.; Ju, H.; Zhu, J.; Xie, Y. Selective visible-light-driven photocatalytic CO_2 reduction to CH_4 mediated by atomically thin CuIn5S8 layers. *Nat. Energy* **2019**, *4*, 690–699. [CrossRef]
63. Nguyen, T.-V.; Wu, J.C.S. Photoreduction of CO_2 in an optical-fiber photoreactor: Effects of metals addition and catalyst carrier. *Appl. Catal. A Gen.* **2008**, *335*, 112–120. [CrossRef]
64. Nguyen, T.-V.; Wu, J.C.S. Photoreduction of CO_2 to fuels under sunlight using optical-fiber reactor. *Sol. Energy Mater. Sol. Cells* **2008**, *92*, 864–872. [CrossRef]
65. Wu, J.C.S.; Lin, H.-M.; Lai, C.-L. Photo reduction of CO_2 to methanol using optical-fiber photoreactor. *Appl. Catal. A Gen.* **2005**, *296*, 194–200. [CrossRef]
66. Tahir, M. Photocatalytic carbon dioxide reduction to fuels in continuous flow monolith photoreactor using montmorillonite dispersed Fe/TiO_2 nanocatalyst. *J. Clean. Prod.* **2018**, *170*, 242–250. [CrossRef]
67. Tahir, M.; Amin, N.S. Photocatalytic CO_2 reduction with H_2O vapors using montmorillonite/TiO_2 supported microchannel monolith photoreactor. *Chem. Eng. J.* **2013**, *230*, 314–327. [CrossRef]

68. Tong, K.; Chen, L.; Yang, L.; Du, X.; Yang, Y. Energy transport of photocatalytic carbon dioxide reduction in optical fiber honeycomb reactor coupled with trough concentrated solar power. *Catalysts* **2021**, *11*, 829. [CrossRef]
69. Cheng, M.; Yang, S.; Chen, R.; Zhu, X.; Liao, Q.; Huang, Y. Copper-decorated TiO_2 nanorod thin films in optofluidic planar reactors for efficient photocatalytic reduction of CO_2. *Int. J. Hydrogen Energy* **2017**, *42*, 9722–9732. [CrossRef]
70. Cheng, M.; Yang, S.; Chen, R.; Zhu, X.; Liao, Q.; Huang, Y. Visible light responsive CdS sensitized TiO_2 nanorod array films for efficient photocatalytic reduction of gas phase CO_2. *Mol. Catal.* **2018**, *448*, 185–194. [CrossRef]
71. Fernández-Catalá, J.; Navlani-García, M.; Berenguer-Murcia, Á.; Cazorla-Amorós, D. Exploring CuxO-doped TiO_2 modified with carbon nanotubes for CO_2 photoreduction in a 2D-flow reactor. *J. CO2 Util.* **2021**, *54*, 101796. [CrossRef]
72. Tseng, I.-H.; Chang, W.-C.; Wu, J.C.S. Photoreduction of CO_2 using sol–gel derived titania and titania-supported copper catalysts. *Appl. Catal. B Environ.* **2002**, *37*, 37–48. [CrossRef]
73. Chen, D.; Sivakumar, M.; Ray, A.K. Heterogeneous Photocatalysis in Environmental Remediation. *Dev. Chem. Eng. Miner. Process.* **2000**, *8*, 505–550. [CrossRef]
74. Ray, A.K.; Beenackers, A.A.C.M. Development of a new photocatalytic reactor for water purification. *Catal. Today* **1998**, *40*, 73–83. [CrossRef]
75. Pozzo, R.L.; Giombi, J.L.; Baltanás, M.A.; Cassano, A.E. Performance in a fluidized bed reactor of photocatalysts immobilized onto inert supports. *Catal. Today* **2000**, *62*, 175–187. [CrossRef]
76. Kočí, K.; Obalová, L.; Matějová, L.; Plachá, D.; Lacný, Z.; Jirkovský, J.; Šolcová, O. Effect of TiO_2 particle size on the photocatalytic reduction of CO_2. *Appl. Catal. B Environ.* **2009**, *89*, 494–502. [CrossRef]
77. Braham, R.J.; Harris, A.T. A complete multi-scale simulation of light absorption within a fluidized bed photoreactor using integrated particle, fluid and photon behaviour models. *Phys. Chem. Chem. Phys.* **2013**, *15*, 12373. [CrossRef] [PubMed]
78. Ola, O.; Maroto-Valer, M.; Liu, D.; Mackintosh, S.; Lee, C.-W.; Wu, J.C.S. performance comparison of CO_2 conversion in slurry and monolith photoreactors using Pd and Rh-TiO_2 catalyst under ultraviolet irradiation. *Appl. Catal. B Environ.* **2012**, *126*, 172–179. [CrossRef]
79. Sastre, F.; Corma, A.; García, H. 185 nm Photoreduction of CO_2 to Methane by Water. Influence of the Presence of a Basic Catalyst. *J. Am. Chem. Soc.* **2012**, *134*, 14137–14141. [CrossRef] [PubMed]
80. Bafaqeer, A.; Tahir, M.; Amin, N.A.S.; Al-Bastaki, N.; Altowayti, W.A.H.; Thabit, H.A. Performance analysis of externally reflected photoreactor for CO_2 conversion to methanol using f-C_3N_4/ZnV_2O_6 S-scheme photocatalyst. *Environ. Technol. Innov.* **2023**, *30*, 103032. [CrossRef]
81. Yurdakal, S.; Loddo, V.; Ferrer, B.B.; Palmisano, G.; Augugliaro, V.; Farreras, J.G.; Palmisano, L. Optical Properties of TiO_2 Suspensions: Influence of pH and Powder Concentration on Mean Particle Size. *Ind. Eng. Chem. Res.* **2007**, *46*, 7620–7626. [CrossRef]
82. Ambrožová, N.; Reli, M.; Šihor, M.; Kuśtrowski, P.; Wu, J.C.S.; Kočí, K. Copper and platinum doped titania for photocatalytic reduction of carbon dioxide. *Appl. Surf. Sci.* **2018**, *430*, 475–487. [CrossRef]
83. Reli, M.; Huo, P.; Šihor, M.; Ambrožová, N.; Troppová, I.; Matějová, L.; Lang, J.; Svoboda, L.; Kuśtrowski, P.; Ritz, M.; et al. Novel TiO_2/C_3N_4 Photocatalysts for Photocatalytic Reduction of CO_2 and for Photocatalytic Decomposition of N_2O. *J. Phys. Chem. A* **2016**, *120*, 8564–8573. [CrossRef] [PubMed]
84. Matějová, L.; Šihor, M.; Lang, J.; Troppová, I.; Ambrožová, N.; Reli, M.; Brunátová, T.; Čapek, L.; Kotarba, A.; Kočí, K. Investigation of low Ce amount doped-TiO_2 prepared by using pressurized fluids in photocatalytic N_2O decomposition and CO_2 reduction. *J. Sol-Gel Sci. Technol.* **2017**, *84*, 158–168. [CrossRef]
85. Kočí, K.; Praus, P.; Edelmannová, M.; Ambrožová, N.; Troppová, I.; Fridrichová, D.; Słowik, G.; Ryczkowski, J. Photocatalytic Reduction of CO_2 Over CdS, ZnS and Core/Shell CdS/ZnS Nanoparticles Deposited on Montmorillonite. *J. Nanosci. Nanotechnol.* **2017**, *17*, 4041–4047. [CrossRef]
86. Asadi, A.; Larimi, A.; Jiang, Z.; Naderifar, A. Modeling and simulation of photocatalytic CO_2 reduction into methanol in a bubble slurry photoreactor. *Chem. Eng. Sci.* **2022**, *263*, 118078. [CrossRef]
87. Olivo, A.; Ghedini, E.; Pascalicchio, P.; Manzoli, M.; Cruciani, G.; Signoretto, M. Sustainable Carbon Dioxide Photoreduction by a Cooperative Effect of Reactor Design and Titania Metal Promotion. *Catalysts* **2018**, *8*, 41. [CrossRef]
88. Alexiadis, A.; Mazzarino, I. Design guidelines for fixed-bed photocatalytic reactors. *Chem. Eng. Process. Process Intensif.* **2005**, *44*, 453–459. [CrossRef]
89. Tahir, M.; Amin, N.S. Photocatalytic reduction of carbon dioxide with water vapors over montmorillonite modified TiO_2 nanocomposites. *Appl. Catal. B Environ.* **2013**, *142–143*, 512–522. [CrossRef]
90. Ozcan, O.; Yukruk, F.; Akkaya, E.U.; Uner, D. Dye sensitized CO_2 reduction over pure and platinized TiO_2. *Top. Catal.* **2007**, *44*, 523–528. [CrossRef]
91. Look, E.G.; Gafney, H.D. Photocatalyzed Conversion of CO_2 to CH_4: An Excited-State Acid–Base Mechanism. *J. Phys. Chem. A* **2013**, *117*, 12268–12279. [CrossRef] [PubMed]
92. Tan, S.S.; Zou, L.; Hu, E. Photocatalytic reduction of carbon dioxide into gaseous hydrocarbon using TiO_2 pellets. *Catal. Today* **2006**, *115*, 269–273. [CrossRef]
93. Tahir, M.; Tahir, B.; Amin, N.A.S.; Muhammad, A. Photocatalytic CO_2 methanation over NiO/In_2O_3 promoted TiO_2 nanocatalysts using H_2O and/or H_2 reductants. *Energy Convers. Manag.* **2016**, *119*, 368–378. [CrossRef]

94. Zhang, Q.-H.H.; Han, W.-D.D.; Hong, Y.-J.J.; Yu, J.-G.G. Photocatalytic reduction of CO_2 with H_2O on Pt-loaded TiO_2 catalyst. *Catal. Today* **2009**, *148*, 335–340. [CrossRef]
95. Park, M.; Kwak, B.S.; Jo, S.W.; Kang, M. Effective CH_4 production from CO_2 photoreduction using TiO_2/xmol% Cu–TiO_2 double-layered films. *Energy Convers. Manag.* **2015**, *103*, 431–438. [CrossRef]
96. Song, C.; Liu, Q.; Ji, N.; Deng, S.; Zhao, J.; Li, Y.; Song, Y.; Li, H. Alternative pathways for efficient CO_2 capture by hybrid processes—A review. *Renew. Sustain. Energy Rev.* **2018**, *82*, 215–231. [CrossRef]
97. Sharma, A.; Lee, B.-K. Photocatalytic reduction of carbon dioxide to methanol using nickel-loaded TiO_2 supported on activated carbon fiber. *Catal. Today* **2017**, *298*, 158–167. [CrossRef]
98. Tommasi, M.; Conte, F.; Alam, M.I.; Ramis, G.; Rossetti, I. Highly Efficient and Effective Process Design for High-Pressure CO_2 Photoreduction over Supported Catalysts. *Energies* **2023**, *16*, 4990. [CrossRef]
99. Wang, Z.-Y.Y.; Chou, H.-C.C.; Wu, J.C.S.S.; Ping Tsai, D.; Mul, G.; Engineering, C.; Tsai, D.P.; Mul, G. CO_2 photoreduction using NiO/$InTaO_4$in optical-fiber reactor for renewable energy. *Appl. Catal. A Gen.* **2010**, *380*, 172–177. [CrossRef]
100. Lo, C.-C.; Hung, C.-H.; Yuan, C.-S.; Wu, J.-F. Photoreduction of carbon dioxide with H_2 and H_2O over TiO_2 and ZrO_2 in a circulated photocatalytic reactor. *Sol. Energy Mater. Sol. Cells* **2007**, *91*, 1765–1774. [CrossRef]
101. Rastgaran, A.; Fatoorehchi, H.; Khallaghi, N.; Larimi, A.; Borhani, T.N. Modelling of photocatalytic CO_2 reduction into value-added products in a packed bed photoreactor using the ray tracing method. *Carbon Capture Sci. Technol.* **2023**, *8*, 100118. [CrossRef]
102. Ren, M.; Valsaraj, K. Inverse opal titania on optical fiber for the photoreduction of CO_2 to CH_3OH. *Int. J. Chem. React. Eng.* **2009**, *7*, A90. [CrossRef]
103. Walko, P.S.; Devi, R.N. Scalable optical fiber reactor for photocatalytic H_2 production: Addressing scattering issues. *Int. J. Hydrogen Energy* **2023**, *48*, 17086–17096. [CrossRef]
104. Tahir, M.; Amin, N.S. Photocatalytic CO_2 reduction and kinetic study over In/TiO_2 nanoparticles supported microchannel monolith photoreactor. *Appl. Catal. A Gen.* **2013**, *467*, 483–496. [CrossRef]
105. Yuan, K.; Yang, L.; Du, X.; Yang, Y. Performance analysis of photocatalytic CO_2 reduction in optical fiber monolith reactor with multiple inverse lights. *Energy Convers. Manag.* **2014**, *81*, 98–105. [CrossRef]
106. Liu, H.; Zhao, J.; Li, C.; Ji, S. Conceptual design and CFD simulation of a novel metal-based monolith reactor with enhanced mass transfer. *Catal. Today* **2005**, *105*, 401–406. [CrossRef]
107. Usubharatana, P.; McMartin, D.; Veawab, A.; Tontiwachwuthikul, P. Photocatalytic Process for CO_2 Emission Reduction from Industrial Flue Gas Streams. *Ind. Eng. Chem. Res.* **2006**, *45*, 2558–2568. [CrossRef]
108. Tahir, B.; Tahir, M.; Amin, N.S. Performance analysis of monolith photoreactor for CO_2 reduction with H_2. *Energy Convers. Manag.* **2015**, *90*, 272–281. [CrossRef]
109. Liou, P.-Y.; Chen, S.-C.; Wu, J.C.S.; Liu, D.; Mackintosh, S.; Maroto-Valer, M.; Linforth, R. Photocatalytic CO_2 reduction using an internally illuminated monolith photoreactor. *Energy Environ. Sci.* **2011**, *4*, 1487. [CrossRef]
110. Xiong, Z.; Lei, Z.; Ma, S.; Chen, X.; Gong, B.; Zhao, Y.; Zhang, J.; Zheng, C.; Wu, J.C.S. Photocatalytic CO_2 reduction over V and W codoped TiO_2 catalyst in an internal-illuminated honeycomb photoreactor under simulated sunlight irradiation. *Appl. Catal. B Environ.* **2017**, *219*, 412–424. [CrossRef]
111. Zheng, H.; Xu, G.; Li, W.; Zhang, X.; Wang, B.; Qin, L.; Zhou, L. Polymeric carbon nitrides/3D honeycomb poly(ionic liquid)s photoreactor with improved photo-electric property for efficient wastewater treatment. *Eur. Polym. J.* **2024**, *204*, 112710. [CrossRef]
112. Cheng, J.; Zhang, M.; Wu, G.; Wang, X.; Zhou, J.; Cen, K. Photoelectrocatalytic Reduction of CO_2 into Chemicals Using Pt-Modified Reduced Graphene Oxide Combined with Pt-Modified TiO_2 Nanotubes. *Environ. Sci. Technol.* **2014**, *48*, 7076–7084. [CrossRef] [PubMed]
113. Li, F.; Zhang, L.; Tong, J.; Liu, Y.; Xu, S.; Cao, Y.; Cao, S. Photocatalytic CO_2 conversion to methanol by Cu_2O/graphene/TNA heterostructure catalyst in a visible-light-driven dual-chamber reactor. *Nano Energy* **2016**, *27*, 320–329. [CrossRef]
114. Rossetti, I.; Villa, A.; Compagnoni, M.; Prati, L.; Ramis, G.; Pirola, C.; Bianchi, C.L.; Wang, W.; Wang, D. CO_2 photoconversion to fuels under high pressure: Effect of TiO_2 phase and of unconventional reaction conditions. *Catal. Sci. Technol.* **2015**, *5*, 4481–4487. [CrossRef]
115. Lee, W.-H.; Liao, C.-H.; Tsai, M.-F.; Huang, C.-W.; Wu, J.C.S. A novel twin reactor for CO_2 photoreduction to mimic artificial photosynthesis. *Appl. Catal. B Environ.* **2013**, *132–133*, 445–451. [CrossRef]
116. Cheng, Y.-H.; Nguyen, V.-H.; Chan, H.-Y.; Wu, J.C.S.; Wang, W.-H. Photo-enhanced hydrogenation of CO_2 to mimic photosynthesis by CO co-feed in a novel twin reactor. *Appl. Energy* **2015**, *147*, 318–324. [CrossRef]
117. Chu, F.; Li, S.; Chen, H.; Yang, L.; Ola, O.; Maroto-Valer, M.; Du, X.; Yang, Y. Modeling photocatalytic conversion of carbon dioxide in bubbling twin reactor. *Energy Convers. Manag.* **2017**, *149*, 514–525. [CrossRef]
118. Qin, G.; Zhang, Y.; Ke, X.; Tong, X.; Sun, Z.; Liang, M.; Xue, S. Photocatalytic reduction of carbon dioxide to formic acid, formaldehyde, and methanol using dye-sensitized TiO_2 film. *Appl. Catal. B Environ.* **2013**, *129*, 599–605. [CrossRef]
119. Arai, T.; Sato, S.; Kajino, T.; Morikawa, T. Solar CO_2 reduction using H_2O by a semiconductor/metal-complex hybrid photocatalyst: Enhanced efficiency and demonstration of a wireless system using $SrTiO_3$ photoanodes. *Energy Environ. Sci.* **2013**, *6*, 1274. [CrossRef]
120. Rossetti, I.; Villa, A.; Pirola, C.; Prati, L.; Ramis, G. A novel high-pressure photoreactor for CO_2 photoconversion to fuels. *RSC Adv.* **2014**, *4*, 28883–28885. [CrossRef]

121. Bahadori, E.; Tripodi, A.; Villa, A.; Pirola, C.; Prati, L.; Ramis, G.; Dimitratos, N.; Wang, D.; Rossetti, I. High pressure CO_2 photoreduction using Au/TiO_2: Unravelling the effect of co-catalysts and of titania polymorphs. *Catal. Sci. Technol.* **2019**, *9*, 2253–2265. [CrossRef]
122. Tommasi, M.; Conte, F.; Rossetti, I.; Ramis, G. Carbon Nitride-Based Catalysts for High Pressure CO_2 Photoreduction. *Mater. Proc.* **2022**, *11*, 1. [CrossRef]
123. Conte, F.; García-López, E.I.; Marcì, G.; Bianchi, C.L.M.; Ramis, G.; Rossetti, I. Carbon Nitride-Based Catalysts for High Pressure CO_2 Photoreduction. *Catalysts* **2022**, *12*, 1628. [CrossRef]
124. Bahadori, E.; Tripodi, A.; Villa, A.; Pirola, C.; Prati, L.; Ramis, G.; Rossetti, I. High pressure photoreduction of CO_2: Effect of catalyst formulation, hole scavenger addition and operating conditions. *Catalysts* **2018**, *8*, 430. [CrossRef]
125. Conte, F.; Rossetti, I.; Ramis, G.; Vaulot, C.; Hajjar-Garreau, S.; Bennici, S. Low Metal Loading (Au, Ag, Pt, Pd) Photo-Catalysts Supported on TiO_2 for Renewable Processes. *Materials* **2022**, *15*, 2915. [CrossRef]
126. Ramis, G.; Bahadori, E.; Rossetti, I. Design of efficient photocatalytic processes for the production of hydrogen from biomass derived substrates. *Int. J. Hydrogen Energy* **2021**, *46*, 12105–12116. [CrossRef]
127. Galli, F.; Compagnoni, M.; Vitali, D.; Pirola, C.; Bianchi, C.L.; Villa, A.; Prati, L.; Rossetti, I. CO_2 photoreduction at high pressure to both gas and liquid products over titanium dioxide. *Appl. Catal. B Environ.* **2017**, *200*, 386–391. [CrossRef]
128. Huang, C.; Yao, W.; T-Raissi, A.; Muradov, N. Development of efficient photoreactors for solar hydrogen production. *Sol. Energy* **2011**, *85*, 19–27. [CrossRef]
129. Sacco, O.; Vaiano, V.; Sannino, D. Main parameters influencing the design of photocatalytic reactors for wastewater treatment: A mini review. *J. Chem. Technol. Biotechnol.* **2020**, *95*, 2608–2618. [CrossRef]
130. Vasumathi, K.K.; Premalatha, M.; Subramanian, P. Parameters influencing the design of photobioreactor for the growth of microalgae. *Renew. Sustain. Energy Rev.* **2012**, *16*, 5443–5450. [CrossRef]
131. Han, S.; Chen, Y.; Abanades, S.; Zhang, Z. Improving photoreduction of CO_2 with water to CH_4 in a novel concentrated solar reactor. *J. Energy Chem.* **2017**, *26*, 743–749. [CrossRef]
132. Rani, S.; Bao, N.; Roy, S.C. Solar Spectrum Photocatalytic Conversion of CO_2 and Water Vapor Into Hydrocarbons Using TiO_2 Nanoparticle Membranes. *Appl. Surf. Sci.* **2014**, *289*, 203–208. [CrossRef]
133. Flamant, G.; Grange, B.; Wheeldon, J.; Siros, F.; Valentin, B.; Bataille, F.; Zhang, H.; Deng, Y.; Baeyens, J. Opportunities and challenges in using particle circulation loops for concentrated solar power applications. *Prog. Energy Combust. Sci.* **2023**, *94*, 101056. [CrossRef]
134. Bellos, E.; Tzivanidis, C. Alternative designs of parabolic trough solar collectors. *Prog. Energy Combust. Sci.* **2019**, *71*, 81–117. [CrossRef]
135. Bejan, A.; Kearney, D.W.; Kreith, F. Second Law Analysis and Synthesis of Solar Collector Systems. *J. Sol. Energy Eng.* **1981**, *103*, 23–28. [CrossRef]
136. Bellos, E.; Tzivanidis, C. A Realistic Approach of the Maximum Work Extraction from Solar Thermal Collectors. *Appl. Syst. Innov.* **2018**, *1*, 6. [CrossRef]
137. Bellos, E.; Tzivanidis, C. Solar concentrating systems and applications in Greece—A critical review. *J. Clean. Prod.* **2020**, *272*, 122855. [CrossRef]
138. Morin, G.; Dersch, J.; Platzer, W.; Eck, M.; Häberle, A. Comparison of Linear Fresnel and Parabolic Trough Collector power plants. *Sol. Energy* **2012**, *86*, 1–12. [CrossRef]
139. Kalogirou, S.A. Solar thermal collectors and applications. *Prog. Energy Combust. Sci.* **2004**, *30*, 231–295. [CrossRef]
140. Meißner, T.M.; Oskay, C.; Bonk, A.; Grégoire, B.; Donchev, A.; Solimani, A.; Galetz, M.C. Improving the corrosion resistance of ferritic-martensitic steels at 600 °C in molten solar salt via diffusion coatings. *Sol. Energy Mater. Sol. Cells* **2021**, *227*, 111105. [CrossRef]
141. Chen, J.; Xiao, G.; Xu, H.; Zhou, X.; Yang, J.; Ni, M.; Cen, K. Experiment and dynamic simulation of a solar tower collector system for power generation. *Renew. Energy* **2022**, *196*, 946–958. [CrossRef]
142. Zhang, H.L.; Baeyens, J.; Degrève, J.; Cacères, G. Concentrated solar power plants: Review and design methodology. *Renew. Sustain. Energy Rev.* **2013**, *22*, 466–481. [CrossRef]
143. Fuqiang, W.; Ziming, C.; Jianyu, T.; Yuan, Y.; Yong, S.; Linhua, L. Progress in concentrated solar power technology with parabolic trough collector system: A comprehensive review. *Renew. Sustain. Energy Rev.* **2017**, *79*, 1314–1328. [CrossRef]
144. Ali, M.F.; Ghani, M.R.A.; Gan, C.K.; Othman, S.; Jano, Z.; Sutikno, T. A Review on Solar Secondary Concentrator. *TELKOMNIKA* **2018**, *16*, 2365. [CrossRef]
145. Bushra, N.; Hartmann, T. A review of state-of-the-art reflective two-stage solar concentrators: Technology categorization and research trends. *Renew. Sustain. Energy Rev.* **2019**, *114*, 109307. [CrossRef]
146. Bellos, E.; Tzivanidis, C. Development of analytical expressions for the incident angle modifiers of a linear Fresnel reflector. *Sol. Energy* **2018**, *173*, 769–779. [CrossRef]
147. Balasubramanian, K.R.; Jinshah, B.S.; Ravikumar, K.; Divakar, S. Thermal and hydraulic characteristics of a parabolic trough collector based on an open natural circulation loop: The effect of fluctuations in solar irradiance. *Sustain. Energy Technol. Assess.* **2022**, *52*, 102290. [CrossRef]
148. Praveen, R.P.; Mouli, K.V.V.C. Performance enhancement of parabolic trough collector solar thermal power plants with thermal energy storage capability. *Ain Shams Eng. J.* **2022**, *13*, 101716. [CrossRef]

149. Arabkoohsar, A.; Sadi, M. A solar PTC powered absorption chiller design for Co-supply of district heating and cooling systems in Denmark. *Energy* **2020**, *193*, 116789. [CrossRef]
150. Ziyaei, M.; Jalili, M.; Chitsaz, A.; Nazari, M.A. Dynamic simulation and life cycle cost analysis of a MSF desalination system driven by solar parabolic trough collectors using TRNSYS software: A comparative study in different world regions. *Energy Convers. Manag.* **2021**, *243*, 114412. [CrossRef]
151. Immonen, J.; Mohammadi, K.; Powell, K.M. Simulating a solar parabolic trough collector plant used for industrial process heat using an optimized operating scheme that utilizes flexible heat integration. *Sol. Energy* **2022**, *236*, 756–771. [CrossRef]
152. Ouagued, M.; Khellaf, A.; Loukarfi, L. Performance analyses of Cu–Cl hydrogen production integrated solar parabolic trough collector system under Algerian climate. *Int. J. Hydrogen Energy* **2018**, *43*, 3451–3465. [CrossRef]
153. Said, Z.; Ghodbane, M.; Boumeddane, B.; Tiwari, A.K.; Sundar, L.S.; Li, C.; Aslfattahi, N.; Bellos, E. Energy, exergy, economic and environmental (4E) analysis of a parabolic trough solar collector using MXene based silicone oil nanofluids. *Sol. Energy Mater. Sol. Cells* **2022**, *239*, 111633. [CrossRef]
154. Minero, C.; Pelizzetti, E.; Malato, S.; Blanco, J. Large solar plant photocatalytic water decontamination: Degradation of pentachlorophenol. *Chemosphere* **1993**, *26*, 2103–2119. [CrossRef]
155. Minero, C. Kinetic analysis of photoinduced reactions at the water semiconductor interface. *Catal. Today* **1999**, *54*, 205–216. [CrossRef]
156. Zhang, N.; Hou, H.; Yu, G.; Hu, E.; Duan, L.; Zhao, J. Simulated performance analysis of a solar aided power generation plant in fuel saving operation mode. *Energy* **2019**, *166*, 918–928. [CrossRef]
157. Tian, M.; Su, Y.; Zheng, H.; Pei, G.; Li, G.; Riffat, S. A review on the recent research progress in the compound parabolic concentrator (CPC) for solar energy applications. *Renew. Sustain. Energy Rev.* **2018**, *82*, 1272–1296. [CrossRef]
158. Sedki, L.; Maaroufi, M. Design of parabolic solar daylighting systems based on fiber optic wires: A new heat filtering device. *Energy Build.* **2017**, *152*, 434–441. [CrossRef]
159. Yuan, K.; Yang, L.; Du, X.; Yang, Y. Numerical analysis of photocatalytic CO_2 reduction in optical fiber monolith reactor with optimized structures. *Energy Convers. Manag.* **2014**, *87*, 258–266. [CrossRef]
160. Yang, Z.; Li, L.; Wang, J.T.; Wang, W.; Song, J. Realization of high flux daylighting via optical fibers using large Fresnel lens. *Sol. Energy* **2019**, *183*, 204–211. [CrossRef]
161. Martín-Sómer, M.; Molina-Ramírez, M.D.; Perez-Araujo, M.L.; Van Grieken, R.; Marugán, J. Comparing the efficiency of solar water treatment: Photovoltaic-LED vs compound parabolic collector photoreactors. *J. Environ. Chem. Eng.* **2023**, *11*, 109332. [CrossRef]
162. Muñoz-Flores, P.; Poon, P.S.; Ania, C.O.; Matos, J. Performance of a C-containing Cu-based photocatalyst for the degradation of tartrazine: Comparison of performance in a slurry and CPC photoreactor under artificial and natural solar light. *J. Colloid Interface Sci.* **2022**, *623*, 646–659. [CrossRef] [PubMed]
163. Reyes-García, J.L.; Arancibia-Bulnes, C.A.; Méndez-Arriaga, F.; Valadés-Pelayo, P.J.; Cabrera, M.A.R. Optical and hydrodynamic performance of photocatalytic monoliths of different shapes in a solar photoreactor with compound parabolic collector. *Catal. Today* **2024**, *429*, 114498. [CrossRef]
164. Benyakhlef, S.; Al Mers, A.; Merroun, O.; Bouatem, A.; Boutammachte, N.; El Alj, S.; Ajdad, H.; Erregueragui, Z.; Zemmouri, E. Impact of heliostat curvature on optical performance of Linear Fresnel solar concentrators. *Renew. Energy* **2016**, *89*, 463–474. [CrossRef]
165. Hongn, M.; Larsen, S.F.; Gea, M.; Altamirano, M. Least square based method for the estimation of the optical end loss of linear Fresnel concentrators. *Sol. Energy* **2015**, *111*, 264–276. [CrossRef]
166. Nixon, J.D.; Dey, P.K.; Davies, P.A. Design of a novel solar thermal collector using a multi-criteria decision-making methodology. *J. Clean. Prod.* **2013**, *59*, 150–159. [CrossRef]
167. Li, Q.; Erqi, E.; Qiu, Y. Triple-objective optimization of He Brayton cycles for ultra-high-temperature solar power tower. *Energy Convers. Manag.* **2022**, *270*, 116210. [CrossRef]
168. Fang, X.; Gao, Z.; Lu, H.; Zhang, Z. Boosting CO_2 photoreduction activity by large Fresnel lens concentrated solar light. *Catal. Commun.* **2019**, *125*, 48–51. [CrossRef]
169. Zhang, C.; Liu, N.; Ming, J.; Sharma, A.; Ma, Q.; Liu, Z.; Chen, G.; Yang, Y. Development of a novel solar energy controllable Linear fresnel photoreactor (LFP) for high-efficiency photocatalytic wastewater treatment under actual weather. *Water Res.* **2022**, *208*, 117880. [CrossRef] [PubMed]
170. Xiao, G.; Nie, J.; Xu, H.; Zhang, C.; Zhu, P. Performance analysis of a solar power tower plant integrated with trough collectors. *Appl. Therm. Eng.* **2022**, *214*, 118853. [CrossRef]
171. Merchán, R.P.; Santos, M.J.; Medina, A.; Hernández, A.C. High temperature central tower plants for concentrated solar power: 2021 overview. *Renew. Sustain. Energy Rev.* **2022**, *155*, 111828. [CrossRef]
172. Aseri, T.K.; Sharma, C.; Kandpal, T.C. A techno-economic appraisal of parabolic trough collector and central tower receiver based solar thermal power plants in India: Effect of nominal capacity and hours of thermal energy storage. *J. Energy Storage* **2022**, *48*, 103976. [CrossRef]
173. Coventry, J.; Andraka, C. Dish systems for CSP. *Sol. Energy* **2017**, *152*, 140–170. [CrossRef]

174. Malik, M.Z.; Shaikh, P.H.; Zhang, S.; Lashari, A.A.; Leghari, Z.H.; Baloch, M.H.; Memon, Z.A.; Caiming, C. A review on design parameters and specifications of parabolic solar dish Stirling systems and their applications. *Energy Rep.* **2022**, *8*, 4128–4154. [CrossRef]
175. Loni, R.; Asli-Ardeh, E.A.; Ghobadian, B.; Kasaeian, A.B.; Bellos, E. Energy and exergy investigation of alumina/oil and silica/oil nanofluids in hemispherical cavity receiver: Experimental Study. *Energy* **2018**, *164*, 275–287. [CrossRef]
176. Karimi, R.; Gheinani, T.T.; Avargani, V.M. A detailed mathematical model for thermal performance analysis of a cylindrical cavity receiver in a solar parabolic dish collector system. *Renew. Energy* **2018**, *125*, 768–782. [CrossRef]
177. Hassan, A.; Quanfang, C.; Abbas, S.; Lu, W.; Youming, L. An experimental investigation on thermal and optical analysis of cylindrical and conical cavity copper tube receivers design for solar dish concentrator. *Renew. Energy* **2021**, *179*, 1849–1864. [CrossRef]
178. Loni, R.; Kasaeian, A.B.; Asli-Ardeh, E.A.; Ghobadian, B.; Roux, W.G. Le Performance study of a solar-assisted organic Rankine cycle using a dish-mounted rectangular-cavity tubular solar receiver. *Appl. Therm. Eng.* **2016**, *108*, 1298–1309. [CrossRef]
179. Pye, J.; Hughes, G.; Abbasi, E.; Asselineau, C.-A.; Burgess, G.; Coventry, J.; Logie, W.; Venn, F.; Zapata, J. Development of a higher-efficiency tubular cavity receiver for direct steam generation on a dish concentrator. In *AIP Conference Proceedings*; AIP Publishing: Melville, NY, USA, 2016; p. 30029.
180. Bellos, E.; Bousi, E.; Tzivanidis, C.; Pavlovic, S. Optical and thermal analysis of different cavity receiver designs for solar dish concentrators. *Energy Convers. Manag. X* **2019**, *2*, 100013. [CrossRef]
181. Piadehrouhi, F.; Ghorbani, B.; Miansari, M.; Mehrpooya, M. Development of a new integrated structure for simultaneous generation of power and liquid carbon dioxide using solar dish collectors. *Energy* **2019**, *179*, 938–959. [CrossRef]
182. Figaj, R.; Szubel, M.; Przenzak, E.; Filipowicz, M. Feasibility of a small-scale hybrid dish/flat-plate solar collector system as a heat source for an absorption cooling unit. *Appl. Therm. Eng.* **2019**, *163*, 114399. [CrossRef]
183. Subramani, J.; Nagarajan, P.K.; Subramaniyan, C.; Anbuselvan, N. Performance studies on solar parabolic dish collector using conical cavity receiver for community heating applications. *Mater. Today Proc.* **2021**, *45*, 1862–1866. [CrossRef]
184. Aboelmaaref, M.M.; Zayed, M.E.; Zhao, J.; Li, W.; Askalany, A.A.; Ahmed, M.S.; Ali, E.S. Hybrid solar desalination systems driven by parabolic trough and parabolic dish CSP technologies: Technology categorization, thermodynamic performance and economical assessment. *Energy Convers. Manag.* **2020**, *220*, 113103. [CrossRef]
185. Deng, Y.; Li, S.; Appels, L.; Zhang, H.; Sweygers, N.; Baeyens, J.; Dewil, R. Steam reforming of ethanol by non-noble metal catalysts. *Renew. Sustain. Energy Rev.* **2023**, *175*, 113184. [CrossRef]
186. Smith, S.E.; Stanislawski, B.J.; Eng, B.K.; Ali, N.; Silverman, T.J.; Calaf, M.; Cal, R.B. Viewing convection as a solar farm phenomenon broadens modern power predictions for solar photovoltaics. *J. Renew. Sustain. Energy* **2022**, *14*, 063502. [CrossRef]
187. Madhugiri, G.A.; Karale, S.R. High solar energy concentration with a Fresnel lens: A Review. *Int. J. Mod. Eng. Res.* **2012**, *2*, 1381–1385.
188. Halmann, M.; Ulman, M.; Aurian-Blajeni, B. Photochemical solar collector for the photoassisted reduction of aqueous carbon dioxide. *Sol. Energy* **1983**, *31*, 429–431. [CrossRef]
189. Zhu, S.; Liang, S.; Wang, Y.; Zhang, X.; Li, F.; Lin, H.; Zhang, Z.; Wang, X. Ultrathin nanosheets of molecular sieve SAPO-5: A new photocatalyst for efficient photocatalytic reduction of CO_2 with H_2O to methane. *Appl. Catal. B Environ.* **2016**, *187*, 11–18. [CrossRef]
190. Olivo, A.; Thompson, W.A.; Bay, E.R.B.; Ghedini, E.; Menegazzo, F.; Maroto-Valer, M.; Signoretto, M. Investigation of process parameters assessment via design of experiments for CO_2 photoreduction in two photoreactors. *J. CO2 Util.* **2020**, *36*, 25–32. [CrossRef]
191. Peng, Y.P.; Yeh, Y.T.; Wang, P.Y.; Huang, C.P. A solar cell driven electrochemical process for the concurrent reduction of carbon dioxide and degradation of azo dye in dilute $KHCO_3$ electrolyte. *Sep. Purif. Technol.* **2013**, *117*, 3–11. [CrossRef]
192. Wei, Q.; Yang, Y.; Hou, J.; Liu, H.; Cao, F.; Zhao, L. Direct solar photocatalytic hydrogen generation with CPC photoreactors: System development. *Sol. Energy* **2017**, *153*, 215–223. [CrossRef]
193. IRNEA. *Renewable Power Generation Costs in 2021*; International Renewable Energy Agency: Abu Dhabi, United Arab Emirates, 2022; 160p. Available online: https://www.irena.org/-/media/Files/IRENA/Agency/Publication/2018/Jan/IRENA_2017_Power_Costs_2018.pdf (accessed on 15 November 2023).
194. Willson, R.N. *Reflecting Telescope Optics I*; Springer: Berlin/Heidelberg, Germany, 2004; ISBN 978-3-540-40106-3.
195. Thalange, V.C.; Pal, E.; Minocha, N.; Nayak, A.K.; Mahajani, S.M.; Panse, S.V.; Joshi, J.B. Thermal hydraulics of natural circulation loop in beam-down solar power tower. *Energy* **2018**, *159*, 1088–1101. [CrossRef]
196. Bellos, E. Progress in beam-down solar concentrating systems. *Prog. Energy Combust. Sci.* **2023**, *97*, 101085. [CrossRef]
197. Calvet, N.; Martins, M.; Grange, B.; Perez, V.G.; Belasri, D.; Ali, M.T.; Armstrong, P.R. The Masdar Institute solar platform: A new research facility in the UAE for development of CSP components and thermal energy storage systems. In *AIP Conference Proceedings*; AIP Publishing: Melville, NY, USA, 2016; p. 100003.
198. Grange, B.; Kumar, V.; Gil, A.; Armstrong, P.R.; Codd, D.S.; Slocum, A.; Calvet, N. Preliminary Optical, Thermal and Structural Design of a 100 kWth CSPonD Beam-down On-sun Demonstration Plant. *Energy Procedia* **2015**, *75*, 2163–2168. [CrossRef]
199. Kodama, T.; Gokon, N.; Matsubara, K.; Yoshida, K.; Koikari, S.; Nagase, Y.; Nakamura, K. Flux Measurement of a New Beam-down Solar Concentrating System in Miyazaki for Demonstration of Thermochemical Water Splitting Reactors. *Energy Procedia* **2014**, *49*, 1990–1998. [CrossRef]

200. Rabl, A. Tower reflector for solar power plant. *Sol. Energy* **1976**, *18*, 269–271. [CrossRef]
201. Wei, X.; Lu, Z.; Yu, W.; Xu, W. Ray tracing and simulation for the beam-down solar concentrator. *Renew. Energy* **2013**, *50*, 161–167. [CrossRef]
202. Segal, A.; Epstein, M. Comparative Performances of 'Tower-Top' and 'Tower-Reflector' Central Solar Receivers. *Sol. Energy* **1999**, *65*, 207–226. [CrossRef]
203. Kribus, A.; Zaibel, R.; Segal, A. Extension of the Hermite Expansion Method for Cassegrainian Solar Central Receiver Systems. *Sol. Energy* **1998**, *63*, 337–343. [CrossRef]
204. Segal, A.; Epstein, M. The optics of the solar tower reflector. *Sol. Energy* **2001**, *69*, 229–241. [CrossRef]
205. Segal, A.; Epstein, M. Practical Considerations in Designing Large Scale "Beam Down" Optical Systems. *J. Sol. Energy Eng.* **2008**, *130*, 011009. [CrossRef]
206. Segal, A.; Epstein, M. Truncation of the Secondary Concentrator (CPC) as Means to Cost Effective Beam-Down System. *J. Sol. Energy Eng.* **2010**, *132*, 031004. [CrossRef]
207. Lahlou, R.; Armstrong, P.R.; Calvet, N.; Slocum, A.H.; Shamim, T. Testing of a secondary concentrator integrated with a beam-down tower system under non-liquid cooling strategies. In *AIP Conference Proceedings*; AIP Publishing: Melville, NY, USA, 2018; p. 170007.
208. Diago, M.; Calvet, N.; Armstrong, P.R. Net power maximization from a faceted beam-down solar concentrator. *Sol. Energy* **2020**, *204*, 476–488. [CrossRef]
209. Diago, M.; Armstrong, P.R.; Slocum, A.H.; Calvet, N. Where should beam down heliostat central rays intersect the final optical element axis? In *AIP Conference Proceedings*; AIP Publishing: Melville, NY, USA, 2018; Volume 2033. [CrossRef]
210. Leonardi, E. Detailed analysis of the solar power collected in a beam-down central receiver system. *Sol. Energy* **2012**, *86*, 734–745. [CrossRef]
211. Canavarro, D.; Delgado, G.; Patil, V.; Blanco, M.; Horta, P. Etendue-matched solar tower beam-down system for high-temperature industrial processes. In *AIP Conference Proceedings*; AIP Publishing: Melville, NY, USA, 2022; p. 120005.
212. Li, L.; Yang, S.; Wang, B.; Pye, J.; Lipiński, W. Optical analysis of a solar thermochemical system with a rotating tower reflector and a receiver–reactor array. *Opt. Express* **2020**, *28*, 19429. [CrossRef] [PubMed]
213. Hasuike, H.; Yoshizawa, Y.; Suzuki, A.; Tamaura, Y. Study on design of molten salt solar receivers for beam-down solar concentrator. *Sol. Energy* **2006**, *80*, 1255–1262. [CrossRef]
214. Hamer, T.T.; Zhou, L.; Trumper, D.L.; Slocum, A.H.; Calvet, N. An Origami-Inspired Design of a Thermal Mixing Element within a Concentrated Solar Power System. In *Proceedings of the Volume 5B: 41st Mechanisms and Robotics Conference*; American Society of Mechanical Engineers: New York, NY, USA, 2017.
215. Chen, C.-F.; Lin, C.-H.; Jan, H.-T. A solar concentrator with two reflection mirrors designed by using a ray tracing method. *Optik* **2010**, *121*, 1042–1051. [CrossRef]
216. Chen, C.-F.; Lin, C.-H.; Jan, H.-T.; Yang, Y.-L. Design of a solar concentrator combining paraboloidal and hyperbolic mirrors using ray tracing method. *Opt. Commun.* **2009**, *282*, 360–366. [CrossRef]
217. Cheng, Q.; Chai, J.; Zhou, Z.; Song, J.; Su, Y. Tailored non-imaging secondary reflectors designed for solar concentration systems. *Sol. Energy* **2014**, *110*, 160–167. [CrossRef]
218. Meng, X.; Xia, X.; Sun, C.; Dai, G. Optimal design of symmetrical two-stage flat reflected concentrator. *Sol. Energy* **2013**, *93*, 334–344. [CrossRef]
219. Zhang, Y.; Yang, H.; Jiang, P.; Mao, S.; Yu, M. Research on a square Cassegrain-type solar concentrating reflector with a double pyramid. *Opt. Appl.* **2016**, *46*, 461–471. [CrossRef]
220. Xu, H.; Xu, C.; Li, S.; Zhang, Z.; Liu, Y.; Xin, T.; Yang, Y. A beam-down solar concentrator with a fixed focus—Design and performance analysis. *Sol. Energy* **2022**, *241*, 428–436. [CrossRef]
221. Yang, S.; Wang, J.; Lund, P.D.; Jiang, C.; Liu, D. Assessing the impact of optical errors in a novel 2-stage dish concentrator using Monte-Carlo ray-tracing simulation. *Renew. Energy* **2018**, *123*, 603–615. [CrossRef]
222. Wardhana, A.S.; Ashari, M.; Suryoatmojo, H. Designing and modeling a novel dual parabolic concentrator with three degree of freedom (DOF) robotic arm. *Sol. Energy* **2019**, *194*, 436–449. [CrossRef]
223. Uzair, M.; ur Rehman, N. Intercept Factor for a Beam-Down Parabolic Trough Collector. *J. Sol. Energy Eng.* **2021**, *143*, 061002. [CrossRef]
224. Wu, S.; Tang, R.; Wang, C. Numerical calculation of the intercept factor for parabolic trough solar collector with secondary mirror. *Energy* **2021**, *233*, 121175. [CrossRef]
225. Sánchez-González, A.; Gómez-Hernández, J. Beam-down linear Fresnel reflector: BDLFR. *Renew. Energy* **2020**, *146*, 802–815. [CrossRef]
226. Taramona, S.; González-Gómez, P.Á.; Briongos, J.V.; Gómez-Hernández, J. Designing a flat beam-down linear Fresnel reflector. *Renew. Energy* **2022**, *187*, 484–499. [CrossRef]
227. Li, X.; Lin, M.; Dai, Y.; Wang, C.-H. Comparison-Based Optical Assessment of Hyperboloid and Ellipsoid Reflectors in a Beam-Down Solar Tower System with Linear Fresnel Heliostats. *J. Sol. Energy Eng.* **2017**, *139*, 061003. [CrossRef]
228. Burhan, M.; Chua, K.J.E.; Ng, K.C. Simulation and development of a multi-leg homogeniser concentrating assembly for concentrated photovoltaic (CPV) system with electrical rating analysis. *Energy Convers. Manag.* **2016**, *116*, 58–71. [CrossRef]

229. Burhan, M.; Shahzad, M.W.; Ng, K.C. Long-term performance potential of concentrated photovoltaic (CPV) systems. *Energy Convers. Manag.* **2017**, *148*, 90–99. [CrossRef]
230. Shanks, K.; Baig, H.; Singh, N.P.; Senthilarasu, S.; Reddy, K.S.; Mallick, T.K. Prototype fabrication and experimental investigation of a conjugate refractive reflective homogeniser in a cassegrain concentrator. *Sol. Energy* **2017**, *142*, 97–108. [CrossRef]
231. Ansari, E.; Akhtar, M.N.; Othman, W.A.F.W.; Abu Bakar, E.; Alhady, S.S.N. Numerical Investigation of Thermal Efficiency of a Solar Cell. *Appl. Sci.* **2022**, *12*, 10887. [CrossRef]
232. Said, Z.; Arora, S.; Bellos, E. A review on performance and environmental effects of conventional and nanofluid-based thermal photovoltaics. *Renew. Sustain. Energy Rev.* **2018**, *94*, 302–316. [CrossRef]
233. Atkin, P.; Farid, M.M. Improving the efficiency of photovoltaic cells using PCM infused graphite and aluminium fins. *Sol. Energy* **2015**, *114*, 217–228. [CrossRef]
234. Hong, W.; Li, B.; Li, H.; Niu, X.; Li, Y.; Lan, J. Recent progress in thermal energy recovery from the decoupled photovoltaic/thermal system equipped with spectral splitters. *Renew. Sustain. Energy Rev.* **2022**, *167*, 112824. [CrossRef]
235. Kumar, S.; Thakur, R.; Singhy, A.; Tripathi, R.K.; Sethi, M. A review of heat removal mechanism in concentrated PVT systems using beam splitter. *Mater. Today Proc.* **2022**, *50*, 952–961. [CrossRef]
236. Mojiri, A.; Taylor, R.; Thomsen, E.; Rosengarten, G. Spectral beam splitting for efficient conversion of solar energy—A review. *Renew. Sustain. Energy Rev.* **2013**, *28*, 654–663. [CrossRef]
237. Liang, H.; Wang, F.; Yang, L.; Cheng, Z.; Shuai, Y.; Tan, H. Progress in full spectrum solar energy utilization by spectral beam splitting hybrid PV/T system. *Renew. Sustain. Energy Rev.* **2021**, *141*, 110785. [CrossRef]
238. Liang, H.; Han, H.; Wang, F.; Cheng, Z.; Lin, B.; Pan, Y.; Tan, J. Experimental investigation on spectral splitting of photovoltaic/thermal hybrid system with two-axis sun tracking based on SiO_2/TiO_2 interference thin film. *Energy Convers. Manag.* **2019**, *188*, 230–240. [CrossRef]
239. Hu, P.; Zhang, Q.; Liu, Y.; Sheng, C.; Cheng, X.; Chen, Z. Optical analysis of a hybrid solar concentrating Photovoltaic/Thermal (CPV/T) system with beam splitting technique. *Sci. China Technol. Sci.* **2013**, *56*, 1387–1394. [CrossRef]
240. Terui, H.; Kobayashi, M. Refractive-index-adjustable SiO_2-Ta_2O_5 films for integrated optical circuits. *Appl. Phys. Lett.* **1978**, *32*, 666–668. [CrossRef]
241. Crisostomo, F.; Taylor, R.A.; Surjadi, D.; Mojiri, A.; Rosengarten, G.; Hawkes, E.R. Spectral splitting strategy and optical model for the development of a concentrating hybrid PV/T collector. *Appl. Energy* **2015**, *141*, 238–246. [CrossRef]
242. Wang, G.; Yao, Y.; Chen, Z.; Hu, P. Thermodynamic and optical analyses of a hybrid solar CPV/T system with high solar concentrating uniformity based on spectral beam splitting technology. *Energy* **2019**, *166*, 256–266. [CrossRef]